Review Article

Slimane Merouani*, Aissa Dehane and Oualid Hamdaoui

Cutting-edge techniques in low-temperature electrochemical water splitting: advancements in hydrogen production

https://doi.org/10.1515/revic-2024-0057 Received July 8, 2024; accepted September 30, 2024; published online October 21, 2024

Abstract: This review provides a comprehensive examination of strategies aimed at advancing low-temperature electrolysis for sustainable hydrogen production. It begins by exploring the significance and challenges associated with water splitting, followed by an in-depth discussion on the fundamentals of electrochemical water splitting and crucial performance indicators, including reversible hydrogen electrode potential, specific and mass activities, overpotential, Tafel slope, stability and durability, and Faradaic and energy efficiencies. The article then extensively discusses various emerging strategies, such as decoupled water electrolysis, hybrid water electrolysis (including reagentsacrificing, pollutant-degrading, and value-added types), tandem water electrolysis, microbial electrolysis cells (covering reactor configurations, electrode materials, microbial populations, and substrates), and the application of external stimuli like ultrasonic, magnetic, and super gravity fields. Additionally, the challenges and advancements in seawater electrolysis are reviewed, with a focus on electrocatalysts, seawater electrolyzers, and future directions. Furthermore, the article addresses current challenges in electrolysis and electrolyzer development, offering perspectives on the future of these techniques. By delving into these strategies, this review aims to contribute to the advancement of clean energy technologies and the transition towards a hydrogen-based economy.

*Corresponding author: Slimane Merouani, Department of Chemical Engineering, Faculty of Process Engineering, University Constantine 3 Salah Boubnider, P.O. Box 72, 25000 Constantine, Algeria,

E-mail: s.merouani@yahoo.fr

Aissa Dehane, Department of Chemical Engineering, Faculty of Process Engineering, University Constantine 3 Salah Boubnider, P.O. Box 72, 25000 Constantine, Algeria

Oualid Hamdaoui, Chemical Engineering Department, College of Engineering, King Saud University, P.O. Box 800, 11421 Riyadh, Saudi Arabia

Keywords: electrochemical water/seawater splitting; hydrogen production; decoupled electrolysis; hybrid electrolysis; tandem electrolysis; microbial electrolysis cells

1 Introduction

Shifting towards carbon-neutral energy sources is crucial for sustainable progress. While renewable sources like wind, solar, and tidal power show potential, their intermittent nature presents challenges for consistent energy supply. Hydrogen gas emerges as a promising alternative due to its carbon-neutral properties and flexible production methods. Unlike renewables, hydrogen production offers diverse pathways and convenient storage and transport options. However, the primary method of hydrogen production involves extracting it from fossil fuels, resulting in carbon dioxide emissions. To fully harness the potential of environmentally friendly hydrogen energy, it's essential to develop sustainable and cost-effective methods for green hydrogen production. 2,3

Electrochemical water splitting stands out as a promising avenue for converting electricity sourced from renewable energy into high-purity hydrogen fuel.⁴ This process involves driving the electrochemical water splitting reaction, wherein the electricity generated from renewable sources is utilized to produce high-purity hydrogen.^{5,6} This hydrogen can then be stored, transported, and utilized through hydrogen/oxygen fuel cells, which efficiently convert the chemical energy of hydrogen into electricity, with water being the sole by-product.^{7,8} As a result, electrochemical water electrolysis is recognized as a pivotal technology for clean energy storage and conversion, facilitating the realization of the hydrogen economy. 4 This technology encompasses two main routes: low- and high-temperature water electrolysis.8 Low-temperature electrolysis generally refers to processes operating below 200 °C. While this includes ambient temperatures, it also encompasses slightly elevated temperatures that are used to enhance efficiency. This is in contrast to high-temperature electrolysis, which typically occurs between 500 °C and 1,000 °C, such as in solid

oxide electrolysis. Among the current low-temperature technologies are alkaline water electrolysis (AWE), proton exchange membrane water electrolysis (PEMWE), and anion exchange membrane water electrolysis (AEMWE). 9 Each of these methods offers unique advantages and applications in the context of hydrogen production and utilization.^{8,10}

Water splitting involves two crucial half-reactions: the hydrogen evolution reaction (HER) occurring at the cathode and the oxygen evolution reaction (OER) at the anode. Unfortunately, both the HER and the OER exhibit sluggish kinetics and significant energy barriers, necessitating voltage inputs much higher than the theoretical thermodynamic voltage for substantial H2 production rates. This results in relatively low energy efficiencies. 11 Consequently, electrocatalysts are indispensable to expedite kinetics and reduce voltage inputs. 12-14 Currently, precious metals like Pt and noble metal oxides such as RuO2 and IrO2 serve as the advanced electrocatalysts for HER and OER, respectively.8 However, the high cost, limited durability, and scarcity of these noble metal catalysts severely hamper their extensive adoption in large-scale H₂ production. Rapid ongoing research took place in the last decade to discover new electrocatalysts for efficient performance of both HER and OER, with reduced energy (overpotential). Among these catalysts, doped materials such as transition metal phosphides, oxides, and nitrides have shown promise due to their abundance and tunable electronic properties. 15 Nanostructured catalysts, such as metal nanoparticles supported on conductive substrates, offer high surface area and active sites for catalytic reactions.¹⁶ Porous materials, including metal-organic frameworks (MOFs) and covalent organic frameworks (COFs), provide excellent mass transport properties and catalytic activity. 17,18 Additionally, earthabundant elements like iron, cobalt, and nickel have been extensively studied for their potential as low-cost alternatives to noble metals.4 These advancements in catalyst design hold significant potential for overcoming the limitations of noble metal catalysts and enabling the widespread adoption of water electrolysis for hydrogen production. Furthermore, the integration of novel membrane materials, including proton exchange membranes (PEMs) and ionconducting polymers, has enabled precise control of ion transport and minimized crossover effects, leading to improved electrolyzer efficiency. ¹⁶ Additionally, advancements in reactor design, such as flow-through and flow-by configurations, have optimized mass transport and electrolyte distribution, enhancing overall system performance. 19,20

Moreover, ongoing research efforts have also focused on exploring new strategies in electrolysis technologies to enhance durability, efficiency, and stability.⁴ These include

decoupled,²¹ hybrid,^{22,23} acid/alkaline asymmetric electrolyte, 24 and tandem 18 electrolysis approaches, which integrate multiple electrochemical processes to improve overall system performance and resource utilization. Additionally, microbial electrolysis cells (MECs) have garnered attention for their ability to produce hydrogen from organic matter using microorganisms as biocatalysts.²⁵ Furthermore, seawater electrolysis has emerged as a promising avenue for sustainable hydrogen production, leveraging abundant seawater resources for large-scale electrolysis operations.^{26–29}

This chapter serves as a comprehensive exploration of cutting-edge strategies for low-temperature electrolysis aimed at hydrogen production. We embark on a journey through the fundamental principles of electrochemical water splitting, elucidating the underlying mechanisms and performance indicators that govern the efficiency of electrolysis systems. Building upon this foundation, we delve into emerging strategies and advancements in electrolysis technology, spanning decoupled, hybrid, and tandem electrolysis approaches, as well as microbial electrolysis cells and seawater electrolysis.

2 Electrochemical water splitting

In the realm of low-temperature electrochemical water splitting, a common setup involves immersing two electrodes in an aqueous electrolyte and applying a voltage sufficient to trigger the separation of water into hydrogen (H_2) and oxygen (O_2) , Eq. (1). To prevent the potentially explosive mixing of these product gases, a membrane separator is typically employed. These cell configurations have undergone extensive research over the years and demonstrate effective performance under both acidic and alkaline conditions, particularly when a stable power source is available. They can achieve current densities for hydrogen and oxygen production around 1 A/cm² for acidic regime electrolysis and 0.2–0.5 A/cm² for alkaline regime electrolysis.13

$$2H_2O \rightarrow 2H_2 + O_2$$
 (1)

The process of water electrolysis is the sum of two halfreactions: the HER and the OER. These half-equations exhibit slight variations depending on the pH level at which the electrolysis occurs (Figure 1a). At standard conditions (1 atm, 25 °C) and acidic electrolytes (pH 0), the HER and OER proceed as follows (all potentials are referenced against the standard hydrogen electrode, SHE):⁴

$$HER: 2H^+ + 2e^- \rightarrow H_2 \qquad (E^0 = 0V)$$
 (2)

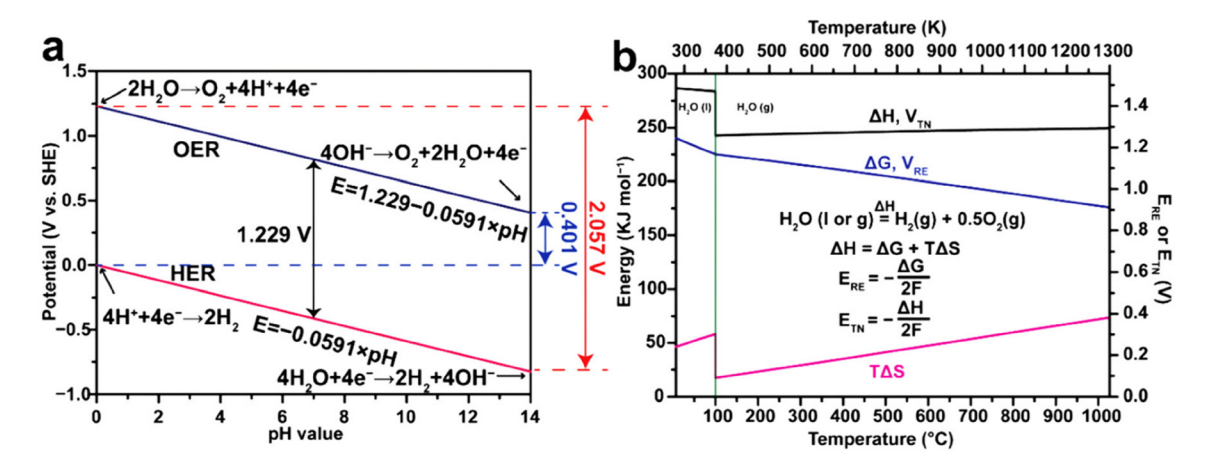


Figure 1: Electrochemical water electrolysis. (a) Thermodynamic potentials of HER and OER in aqueous electrolytes at various pH values under standard conditions (25 °C, 1 atm). (b) Thermodynamics of water splitting in relation to temperature at 0.1 MPa. From. ⁴

OER:
$$2H_2O \rightarrow O_2 + 4H^+ + 4e^- \quad (E^0 = 1.229V)$$
 (3)

in neutral electrolytes (pH 7),

HER:
$$2H_2O + 2e^- \rightarrow H_2 + 2OH^-$$
 (E⁰ = -0.414V) (4)

OER:
$$2H_2O \rightarrow O_2 + 4H^+ + 4e^- \quad (E^0 = 0.815V)$$
 (5)

in alkaline electrolytes (pH 14),

HER:
$$2H_2O + 2e^- \rightarrow H_2 + 2OH^- \qquad (E^0 = -0.828V)$$
 (6)

OER:
$$4OH^- \rightarrow O_2 + 2H_2O + 4e^- \quad (E^0 = 0.401V)$$
 (7)

The water splitting reaction (Eq. (1)) is an endothermic process, described by $\Delta H_0 = \Delta G_0 + T \Delta S_0$, [ΔG_0 : change in Gibbs free energy (237.1 kJ/mol), ΔH_0 : enthalpy change (285.8 kJ/mol), and $T\Delta S_0$ (ΔQ) thermal energy (48.7 kJ/mol) under standard conditions (25 °C, 1 atm)]. Enthalpy, comprising both electrical and thermal components, signifies the total energy involved. Thus, under standard conditions, the water splitting reaction can be simplified as:4

$$H_2O_{liquid}$$
 + 237.1 kJ/mol electricity + 48.7 kJ/mol heat
 \rightarrow $H_{2,\,gas}$ + 1/2 $O_{2,\,gas}$ (8)

In low-temperature water electrolysis, heat can come from external sources or Joule heating through ionic and electric currents. Under standard conditions, the theoretical minimum cell voltage of electrolysis operation, i.e., the reversible cell voltage (E_{RE}), is 1.23 V, calculated using $E_{RE} = \Delta G_0/(nF)$, where n is the number of electrons transferred per reaction, i.e., n = 2 for reaction (1), and F is Faraday's constant (96,485 C/mol). Nevertheless, E_{RE} decreases as temperature increases. Within the temperature range of 0–1,000 °C, E_{RE} ranges from 1.25 to 0.91 V (Figure 1b).

The thermoneutral cell voltage (E_{TN}) represents the minimum voltage required for electrolysis to occur in an ideal cell without heat integration. It is s 1.48 V under standard conditions, as calculated using $E_{TN} = \Delta H_0/(nF)$. In the case of high-temperature electrolysis, water is supplied as steam, necessitating external evaporation. This indicates that the total energy demand (*AH*) for the electrolysis reaction (including thermal energy, $T\Delta S_0$) is supplied electrically. According to Figure 1b, for liquid water below 100 °C, the E_{TN} is approximately 1.47-1.48 V (284-286 kJ/mol_{H2}). In the temperature range of 100-1,000 °C, when steam is supplied, it reduces to 1.26–1.29 V (243–249 kJ/mol_{H2}). This implies that the minimum electrical energy consumption for steam electrolysis compared to liquid water electrolysis can be reduced by the heat of evaporation, which is 41.0 kJ/mol at ambient pressure.³⁰ The total energy consumption, including water evaporation, remains almost constant from 0 to 1,000 °C.

The exploration of water electrolysis technologies encompasses three primary methods: Alkaline Electrolysis Cells (AEC), Proton Exchange Membrane Electrolysis Cells (PEMEC), and Solid Oxide Electrolysis Cells (SOEC). The setup for each technology is depicted in Figure 2, with Table 1 offering a concise overview of component materials, performance indicators, and cost parameters.

AEC, the long-standing water electrolysis technology adopted since 1920, is extensively employed in large-scale industrial environments.31 These systems are known for their accessibility, durability, and relatively lower capital costs, attributed to the absence of noble metals and the maturity of stack components. 5,11,32 Nonetheless, challenges like low current density, operating pressure limitations, and constraints on dynamic operation adversely impact system scalability and hydrogen production costs. Ongoing

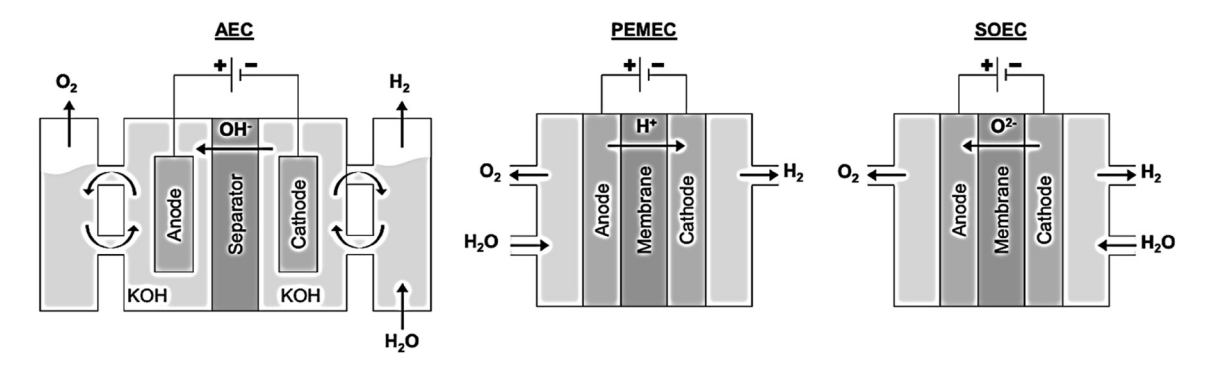


Figure 2: Schematic representation of three electrolysis cell technologies. Reproduced with permission from.³¹

Table 1: Key characteristics of AEC, PEMEC; and SOEC.31

	AEC	PEMEC	SOEC
Reactions	Cathode:	Cathode:	Cathode:
	$2H_2O + 2e^- \rightarrow H_2 + 2OH^-$	$2H^+ + 2e^- \rightarrow H_2$	$H_2O+2e^- \rightarrow H_2 + O^{2-}$
	Anode:	Anode:	Anode:
	$2H_2O \rightarrow O_2 + 4H^+ + 4e^-$	$2H_2O \rightarrow O_2 + 4H^+ + 4e^-$	$0^{2-} \rightarrow \frac{1}{2}0_2 + 2e^-$
Electrolyte	Aqueous potassium hydroxide (20–40 wt%	Polymer membrane (e.g.,	Yttria stabilised Zirconia
	KOH) ^{11,227}	Nafion) ^{13,227}	(YSZ) ^{34,228}
Cathode material	Ni, Ni–Mo alloys ^{11,227}	Pt, Pt–Pd ¹³	Ni/YSZ ^{34,228}
Anode material	Ni, Ni–Co alloys ^{11,227}	RuO ₂ , IrO ₂ ¹³	LSM/YSZ ^{34,228}
Current density (A/cm ²)	0.2-0.4 ¹³	$0.6-2.0^{13}$	0.3-2.0 ³⁴
Cell voltage (V)	1.8-2.4 ¹³	1.8-2.2 ¹³	0.7–1.5 ³⁴
oltage efficiency (%HHV)	62-82 ¹³	67-82 ¹³	<110 ²²⁷
Cell area (m²)	<4 ²²⁷	<0.3 ²²⁷	<0.01 ²²⁷
Operating temp. (°C)	60-80 ¹³	50-80 ¹³	650-1,000 ^{34,228}
Operating pressure (bar)	<30 ²²⁷	<200 ²²⁷	<25 ²²⁷
Production rate (m ³ H2/h)	<760 ²²⁷	<40 ²²⁷	<40 ²²⁷
Stack energy (kWh _{el} /m ³ _{H2})	4.2-5.9 ¹³	4.2-5.5 ¹³	>3.2 ²²⁷
System energy (kWh _{el} / m ³ _{H2})	4.5-6.6 ³⁶	4.2-6.6 ³⁶	>3.7 (>47) _{kWh_energy}
II H2) Gas purity (%)	> 99.5 ¹¹	99.99 ²²⁷	99.9
Lower dynamic range (%)	10-40 ^{13,227}	0-10 ¹³	>30
System response	Seconds ²²⁷	Milliseconds ²²⁷	Seconds
Cold-start time (min)	<60 ³⁶	<20 ³⁶	<60
Stack lifetime (h)	60,000-90,000 ³⁶	20,000-60,000 ³⁶	<10,000
Maturity	Mature	Commercial	Demonstration
Capital cost (€ kW _{el} ⁻¹)	1,000-1,200 ³⁶	1,860-2,320 ³⁶	>2,000 ³⁶

endeavors aim to improve current density, operating pressure, and system design to enable dynamic operation, thereby fostering compatibility with intermittent renewable sources. ^{11,32}

PEMEC systems, originating from the solid polymer electrolyte (SPE) concept in the 1960s, were introduced to mitigate limitations associated with AEC.³³ Despite being less established than AEC, PEMEC boasts advantages such as high power density, efficiency, and operational flexibility, rendering it suitable for small-scale applications.^{11,32} However, challenges persist, including the expense of platinum

catalysts and fluorinated membrane materials, complexity arising from high-pressure operation, water purity prerequisites, and shorter lifetimes compared to AEC. Ongoing advancements focus on simplifying systems, cost reduction, and enhancing stack manufacturing processes.^{11,32}

SOEC, considered the least mature technology, has had limited commercial adoption, mainly showcased in laboratory-scale trials.³¹ Utilizing solid ion-conducting ceramics as electrolytes, it enables operation at elevated temperatures. Noteworthy advantages encompass high electrical efficiency, reduced material expenses, and the capacity for

reverse operation or syngas production. Nevertheless, material degradation at elevated temperatures presents a significant obstacle. Present research concentrates on stabilizing existing materials, innovating new ones, and reducing operating temperatures to facilitate commercial viability.³⁴

The capital costs for AEC and PEMEC systems are estimated at approximately 1000 V/kWel, and 2000 V/kWel, respectively, while SOEC systems, being less prevalent commercially, surpass 2000 V/kW_{el}.31 AEC systems are generally cited as being two to three times more costly than steam methane reformers (SMR), the dominant hydrogen production technology relying on methane gas reformation.³⁵

To effectively utilize intermittent power sources, Electrolyzers necessitate prompt responses from system components, operation within a narrower dynamic range without compromising gas purity, and efficient cold-start capabilities or standby operation.³¹ Although PEMEC Electrolyzers appear most adept at meeting these criteria, AEC and SOEC can also be modified, with their components tailored for intermittent power provision.^{36,37}

3 Performance indicators

Various performance and metrics indicators are widely utilized to assess the electrocatalytic performance of HER and OER electrocatalysts. These include the reversible hydrogen electrode (RHE) potential, mass and specific activities, Tafel slope, overpotential, catalytic stability, and faradaic and energy efficiencies. These metrics are pivotal in designing efficient electrocatalysts and facilitating comparisons across different materials, offering valuable insights into intrinsic activity and redox reaction kinetics.

3.1 Reversible hydrogen electrode potential

To standardize the evaluation and comparison of electrocatalytic performance across different pH conditions, it's recommended to reference all potentials for HER and OER to the Reversible Hydrogen Electrode (RHE).⁴ This reference is expressed by equation (4):

$$E_{RHE} = E_{SHE} + pH\left(\frac{2.303RT}{F}\right) \tag{9}$$

E_{SHE} represents the measured potential of the designated reference electrode with respect to SHE, pH is the actual electrolyte pH value, R is the universal ideal gas constant, T is the absolute temperature, and F is the Faraday constant. At 298 K, the term 2.303 R T/F approximately equals 0.059 V.4 By incorporating pH dependence, the RHE ensures that the equilibrium potentials of the ${\rm O_2}$ and ${\rm H_2}$ redox reactions are fixed at 1.23 and 0 V versus RHE at 298 K, respectively. Standardizing potential values with respect to RHE facilitates direct comparison of electrocatalyst performance across electrolytes with changeable pH. This approach enables researchers to accurately assess and compare electrocatalytic efficiencies under different environmental conditions.

Two prevalent methods are employed to convert the measured potentials of working electrodes referenced to a particular reference electrode to potentials referenced to the RHE. ⁴ The first method involves determining the actual pH of the electrolyte and using the formula:³⁸

E (vs. RHE) =
$$E_{measured}$$
 (vs. reference electrode)
+ E_{Ref}^{0} (vs. RHE) + 0.059pH (10)

where, E_{measured} represents the measured potential of the working electrode with respect to the reference electrode, E_{Ref}^{0} (vs. SHE) is the standard thermodynamic potential of the reference electrode.

The alternative recommended method involves experimental calibration of the reference electrode against the RHE in the actual electrolyte during the hydrogen redox reaction.³⁹ This calibration process entails using two platinum electrodes as both the working and counter electrodes alongside the reference electrode in the same electrolyte conditions as those used for electrocatalytic characterization. In the protocol, the electrolyte could be pre-saturated with high-purity H₂ before calibration. Cyclic voltammetry is then conducted at a low scan rate in the reversible hydrogen evolution and hydrogen oxidation potential range, and the average value of the two voltage intercepts for two branch curves at zero current yields the experimentally determined conversion factor (E_{offset}). Subsequently, the E_{measured} (vs. reference electrode) used in the test can be converted to RHE potential using equation (4):

$$E$$
 (vs. RHE) = $E_{measured}$ (vs. reference electrode) - E_{offset} (11)

Reference 38 have detailed these procedures and established the calibration curves for various reference electrodes (Ag/AgCl, Hg/HgO and Hg/Hg2Cl2) in different electrolytes.38

3.2 Specific and mass activities

The ration of current density (j) and electrocatalyst area, at a given potential, is known as the specific activity of an electrocatalyst. Typically, three types of areas are utilized to calculate (j): the geometrical electrode area (GEA), the electrochemically active surface area (ECSA), and the BET specific surface area. 40 ECSA is commonly measured through double layer capacitance (C_{dl}) in a non-faradaic potential window, preferably in aprotic electrolytes. 41 For electrodes with flat and smooth surfaces, current density can be normalized with GEA. However, for porous electrodes and powder electrocatalysts, it's advisable to assess specific activity by dividing (i) with BET surface area or ECSA.4

On the other hand, the mass activity (in A/mg_{catalyst}) represents the current density normalized by the mass of the active electrocatalyst at a specific potential. An ideal electrocatalyst exhibits high specific activity and mass activity. 42,43 In practical applications, achieving optimal mass loading involves maximizing coverage of the conductive substrate with the electrocatalyst and optimizing the thickness of the electrocatalyst layer to enhance electron and mass transfer processes.4

3.3 Overpotential

Overpotential (n) is the additional voltage needed to drive an electrochemical reaction beyond its thermodynamic potential. It represents the surplus voltage required to overcome energy barriers and resistances within the electrolytic cell, enabling the desired reactions. These barriers include electrical resistance in wiring and electrodes, activation energies of reactions (for the OER and HER), bubble overpotential (where gas bubbles hinder reaction access), and ionic conductivity overpotential.4

Determining η typically involves electrochemical measurements, often using techniques like linear sweep voltammetry at low sweep rates to minimize capacitance current.¹⁴ Under standard conditions, the reversible thermodynamic potentials for the HER and OER are 0 V and 1.23 V, respectively. Overpotential at an anticipated current density without iR recompense is given by: $\eta_{HER} = E_{RHE} - 0 \text{ V}$ and $\eta_{OER} = E_{RHE} - 1.23 \text{ V}$. At j = 10 mA/cm², overpotential (η_{10}) is indeed a crucial parameter for assessing electrodes' electrocatalytic activity.44

The choice of electrode material significantly influences overpotential. Electrodes themselves can act as catalysts, reducing the activation energy of electrochemical reactions. Hence, electrode design often involves doping or coating with more stable and active layers. The primary effect of an electrocatalyst is to reduce the overpotential of either the HER or OER.¹¹ Table 2 listing various electrocatalysts helpful for reducing overpotential or stabilizing electrodes in industrial water electrolysis further illustrate this point.

Table 2: Hydrogen and oxygen overpotentials of different electrode

Electrode composition	Temp. (°C)	Electrolyte	C (M)	<i>j</i> (A/m²)	η (mV)	Ref
HER						_
Ni-Fe-Mo-Zn	80	кон	6	1,350	83	229
Ni-S-Co	80	NaOH	28 wt%	1,500	70	230
Ni50 %-Zn	N/A	NaOH	6.25	1,000	168	231
MnNi _{3·6} Co _{0·75}	70	NaOH	30 wt%	1,000	39	232
$Mn_{0.4}Al_{0.27}$						
Ti ₂ Ni	70	NaOH	30 wt%	1,000	16	233
Ni50 %Al	25	NaOH	1	1,000	114	234
Ni75 %	80	KOH	6	3,000	185	235
Mo25 %						
Ni80 %Fe18 %	80	кон	6	3,000	270	235
Ni73 %W25 %	80	кон	6	3,000	280	235
Ni60 %	80	KOH	6	3,000	225	235
Zn40 %						
Ni90 %Cr10 %	80	кон	6	3,000	445	235
OER						
Ni + spinel	25	КОН	1	1,000	235 ± 7	236
type Co₃O₄						
Ni + La doped	25	кон	1	1,000	224 ± 8	236
Co_3O_4						
MnO _x modi-	25	кон	0.5	100	300	237
fied Au						
Li10 % doped	RT^a	кон	1	10	550	238
Co_3O_4						
Ni	90	КОН	50 wt%	1,000	300	239
La _{0.5} Sr _{0.5} CoO ₃	90	KOH	50 wt%	1,000	250	239
$Ni_{0\cdot 2}Co_{0\cdot 8}LaO_3$	90	КОН	50 wt%	1,000	270	239

a, room temperature.

3.4 Tafel slope

The Tafel equation (Eq. (12)) represents the connection between the overpotential (at each electrode) and the current density's logarithm:¹¹

$$\eta = a + b \times \log(j) \tag{12}$$

where a = $(2.3 \text{ R T})/(\alpha F)\log(j_0)$ and b = $(-2.3 \text{ R T})/(\alpha F)$, T is the absolute temperature (in K), α is the symmetry factor variable, and F is the Faraday constant. "b" is referred to as the 'Tafel slope', it helps to define the rate determining step by examining the sensitivity of the current response to the applied potential.⁴ A lower Tafel slope indicates greater electrocatalytic kinetics. Some electrocatalysts exhibit Tafel slope values that do not conform to linear fitting of the plot of log(i) versus overpotential (η) across a wide potential range. 45–47 This leads to overpotential-dependent Tafel slopes. 4,48

Table 3 presents a comparison of kinetic parameters, including current density and Tafel slope, for HER and OER

Table 3: Tafel slope of HER and OER on different electrode metals. 11

Metal	Electrolyte	Temp.	I_0 (A/m 2)	Tafel	Ref.
		(°C)		slope (mV)	
HER					
Ni	1 M NaOH	20	1.1×10^{-2}	121	240
Fe	2 M NaOH	20	9.1×10^{-2}	133	241
Pb	6 M NaOH	25	4.0×10^{-2}	121	242
Zn	6 M NaOH	25	8.5×10^{-6}	124	242
Co	0.5 M NaOH	25	4.0×10^{-3}	118	243
Pt	0.1 M NaOH	22	4.0	105	244
Au	0.1 M NaOH	25	4.0×10^{-2}	120	244
OER					
Pt	30 % KOH	80	1.2×10^{-5}	46	245
Ir	1 M NaOH	N/A	1.0×10^{-7}	40	246
Rh	1 M NaOH	N/A	6.0×10^{-8}	42	246
Ni	50 % KOH	90	4.2×10^{-2}	95	247
Co	30 % KOH	80	3.3×10^{-2}	126	245
Fe	30 % KOH	80	1.7×10^{-1}	191	245

on various metal electrode materials. If hydrogen adsorption on the cathode is the rate-determining step, electrode materials with more boundaries and cavities in their surface structure will create more electrolysis centers for hydrogen adsorption. 11 Conversely, if hydrogen desorption is the ratedetermining step, physical properties such as surface perforation or roughness could increase electron transfer by providing extra reaction area or preventing bubbles growing, thereby enhancing the rate of electrolysis. 11 It is important to note that both the Tafel slope and n10 are significantly influenced by the loading mass of the electrocatalyst, as demonstrated in the comprehensive study by Anantharaj Kundu. 49 This research confirmed that increasing the mass of the electrocatalyst leads to a notable decrease in both the Tafel slope and n10. In the study, five NiO/CC electrodes with incrementally increasing catalyst loadings of 0.205, 0.310, 0.410, 0.615, and 0.820 mg cm⁻² were prepared using the conventional drop-casting method. These electrodes were then evaluated for OER performance in 1 M KOH, where the dependency of overpotentials and Tafel slope on catalyst loading was investigated. The results clearly showed that both $\eta 10$ and the Tafel slope decreased as the catalyst loading increased.

3.5 Stability and durability

The stability of direct water splitting involves efficiently producing hydrogen and oxygen through electrochemical processes over time. Various factors, like the corrosive nature of electrolytes, influence stability in electrochemical cells. Electrode materials must exhibit high corrosion resistance to ensure prolonged stability, while membrane

stability is crucial for effectively separating HER and OER.44 Catalyst stability is equally important for sustained high performance, and maintaining selective ion transport across membranes is essential to prevent unintended crossovers and instability. Controlling operating conditions is imperative to mitigate adverse stability effects. Large-scale systems often face scaling issues, impacting efficiency and stability. Regular monitoring, maintenance, and ongoing research in material science, catalyst, and system engineering enhance long-term stability.

Meanwhile, evaluating the stability of electrocatalysts and two-electrode electrolyzers involves techniques like cyclic voltammetry or chronopotentiometry. Durability tests typically last from tens to thousands of hours, conducted at a current density of 10 mA/cm². In^{4,48} industrially relevant hydrogen production, electrolyzers must operate at higher current densities, usually ranging from 0.5 to 2 A/cm², while demonstrating extreme stability and a lifespan of thousands of hours to years. 4 Monitoring dissolved metal cation concentrations and other ions in electrolytes, along with quantifying the percentage of weight loss of active metal centers after long-term stability tests, is advisable.

3.6 Faradaic and energy efficiencies

The Faradaic efficiency (FE) measures the actual amount of produced H₂ or O₂ compared to the theoretically calculated amount, assuming all the passed charge contributes solely to forming H₂ or O₂. The FE is calculated using the formula:⁴

$$FE = \frac{n_{\text{gas, measured}}}{n_{\text{gas, theortical}}} = \frac{n_{\text{gas, measured}}}{I \times (nF)^{-1}} \times 100 \%$$
 (13)

where I is the current (A), n = 2 for H₂ and 4 for O₂, is the number of electrons transferred to produce 1 mol gas, and F = 96,485.3 C/mol is Faraday's constant. Water-gas displacement method or Gas chromatography (GC) are typically used to measure the amount of H_2 or O_2 produced, while an electrochemical workstation monitors the passed charge. Ideally, an electrocatalyst should exhibit 100% faradaic efficiency, while losses occur in water electrolyzers when electrons and ions contribute in undesirable reactions at the electrodes and/or in the electrolytes systems.

Energy efficiency (also called electrical efficiency or electricity-to-hydrogen energy conversion efficiency) is another crucial factor for assessing the effectiveness of water electrolysis cells or systems. Cell-level energy efficiency is commonly evaluated by considering only the electricity energy input for the electrolysis cell, excluding other energy inputs such as heat sources and auxiliaries. The energy efficiency (EE) is calculated using the formula:⁴

$$EE = \frac{\Delta H_{H2} \times n_{H2,\,measured}}{P_{dc}} = \frac{\Delta H_{H2} \times \frac{FE \times I}{nF}}{I \times U} = \frac{E_{TN} \times FE}{U} \tag{14}$$

where n_{H2} ,measuredn is in mole/s, P_{dc} is the power supplied by the external direct-current power supply (W), U is the voltage applied (V), FE is the faradaic efficiency, ΔH_{H2} is the reaction enthalpy (heat of reaction), and E_{TN} is the thermoneutral voltage derived from ΔH_{H2} ($E_{TN} = \Delta H^0/nF$, where $\Delta H^0 = 285.8$ kJ/mol under standard conditions⁴). Numerous factors need to be considered when calculating EE. A detailed examination of these factors can be found in the review authored by Li et al.⁴

4 Emerging strategies for electrochemical water splitting

To overcome a range of technical challenges in water electrolysis, such as overcoming energy barriers, integrating incompatible electrocatalysts, and managing reactant mass transfer, several strategies have been invented. These include decoupled, hybrid, and tandem water electrolysis, as well as biological electrolysis cell approaches. Additionally, seawater electrolysis stands as a separate technique due to its distinct characteristics and potential. In the next sections, we'll explore each of these techniques, detailing their principles and accomplishments.

4.1 Decoupled water electrolysis

4.1.1 The concept

The decoupled water electrolysis concept was proposed to overcome several disadvantages of classical cell electrolyzers, where the HER and OER happened simultaneously (Figure 3a), possibly lead to $\rm H_2/O_2$ crossover, even if an ostensibly gas impermeable membrane (or diaphragm). Thus, scenario is particularly high probable at low current densities or under high gas pressure electrolysis. This problem could touch the

 $\rm H_2$ purity, in addition to the risk of creating of an extremely explosive or oxidative environment due to the coexistence $\rm H_2$, $\rm O_2$ and electrocatalysts under favorable electrocatalytic conditions, which pose safety concerns, degrade the electrolyzer and shorten its operation lifespan. Hese issues call for alternative electrolyzer designs, not only avoiding the crossover of $\rm H_2/\rm O_2$ gases but also allowing suppleness in controlling electrolysis products.

Figure 3b and c presents schematic illustrations of a decoupled water electrolyzer. In this system, during the HER at the cathode, a redox mediator (dissolved in the electrolyte) undergoes oxidation at the anode instead of the OER. This oxidized redox mediator is then reduced back to its initial state at the same electrode, while the OER is coupled to another working electrode. Through the alternation of these steps, hydrogen and oxygen are generated sequentially. This method allows for the temporal and/or spatial separation of HER and OER, facilitated by redox mediators. Essentially, the redox mediator serves as a reversible electron and/or proton donor/acceptor. When the redox mediator can simultaneously accept or donate both protons and electrons, it can act as a pH buffer during electrolysis and is referred to as an electron coupled-proton buffer, ECPB. Sa

Mediators can be categorized into three main types: soluble, dispersed, and solid-state decoupling agents.⁵⁴ An example of a dissolved mediator is the polyoxometalate $\text{Li}_{6}[P_{2}W_{18}O_{62}]$, which has the remarkable capacity to reversibly accept up to 18 electrons in water media. Transition metal salts, such as those involving the V(III)/V(II) and Ce(III)/Ce(IV) redox couples, 55 as well as complexes like Fe(CN)₆ 3-/Fe(CN)₆ 4-56 are also commonly used in this category. Additionally, organic systems like hydroquinone sulfonate and anthraguinone-2,7disulfonic acid serve as dissolved mediators. 57,58 Dispersed mediators, on the other hand, involve particulate systems dispersed in a solution containing a redox couple. For instance, Zhao et al.⁵⁹ utilized BiVO₄ particles dispersed in an aqueous medium comprising the Fe(III)/Fe(II) redox pair. Upon solar light radiation, BiVO₄ particles oxidize water to generate O2 while reducing Fe(III) to Fe(II) at the same time.

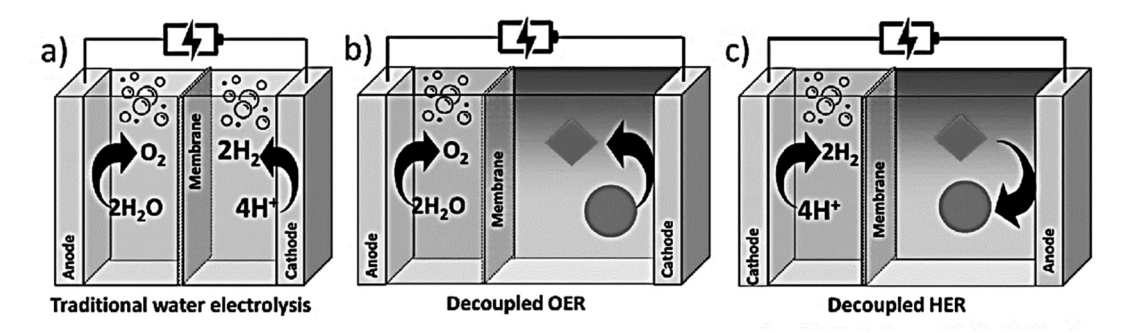


Figure 3: Comparison of traditional 'coupled' electrolysis and decoupled electrolysis for water splitting: (a) Conventional water electrolysis in acidic conditions. (b) Decoupled oxygen generation and mediator reduction. (c) Decoupled mediator reoxidation and hydrogen evolution. In panels (b) and (c), the circle denotes the oxidized form of the decoupling agent "medaitor", while the diamond represents the reduced form of this decoupling agent. From. ⁵⁴

Solid-state mediators, exemplified by NiOOH/Ni(OH)₂, ⁶⁰ are integrated with electrodes and operate without the need for solubilization. These solid mediators facilitate electron transfer reactions directly at the electrode surface. The choice of mediator phase significantly influences the physical components and operation of the system. Indeed, soluble redox mediator systems can operate under static or flow conditions, as the mediator can be pumped between chambers. Conversely, in systems with solid-state mediators, the decoupling agent is typically integrated with an electrode that can be moved between cells to interact with either the HER or OER. Detailed analysis of key studies in this area will be discussed further.

The success of redox mediator-assisted decoupled water electrolysis hinges largely on the electrochemical properties of the redox mediator. Several crucial criteria must be considered when selecting suitable candidates for redox mediators:61

- (i) High solubility in aqueous media (of soluble mediators),
- (ii) Rapid and reversible electron transfer between the redox mediator and the inert electrode, ensuring that the pH of the reaction medium remains unchanged throughout both the OER and HER steps.
- (iii) Well-positioned redox potential between the onset HER and OER potentials,

- (iv) Excellent durability over a large number of redox cvcles.
- (v) Economical composition and synthesis.

4.1.2 Decoupling water splitting systems

Several innovative strategies for nonconventional water splitting have been summarized by You and Sun, 18 wherein H₂ production from water splitting is integrated with other oxidation reactions of greater utility than O2 evolution. Additionally, Liu et al. 61 Paul and Symes, 54 Wallace and Symes⁶² have provided valuable mini-reviews on decoupled water splitting agents, highlighting recent progress in the field. More recently, McHugh et al.²¹ reported a comprehensive review article focusing on redox mediators for water splitting. Table 4 provides an overview of various decoupling agents along with their key performance metrics, demonstrating their effectiveness in electrochemical water splitting. Readers interested in more detailed information are encouraged to refer to the provided references for further insights.

Symes and Cronin achieved the initial practical implementation of decoupled oxygen and hydrogen evolution through electrolytic water splitting in 2013.⁵³ They employed

Table 4: Overview of select decoupling agents utilized for electrochemical water splitting. 21,54

Decoupling agent	Redox potential (V vs SHE)	pH for redox potential	Maximum operation	Best Farad	ic efficiency	Ref.
				HER	OER	
H ₃ PMo ₁₂ O ₄₀	+0.50, +0.65	0.3	5 cycles	100 %	100 %	53,248,249
H ₄ [SiW ₁₂ O ₄₀]	0.0, -0.22	0.5	9 cycles	$75 \pm 7 \%$	100 %	64,250,251
H ₃ PW ₁₂ O ₄₀	+0.237, -0.036	0.42	-	46.6 %	_	63
H ₄ SiO ₄ ·12MoO ₃	+0.509	0.69	_	_	_	63
$H_6ZnW_{12}O_{40}$	-0.078, -0.198	0.4	200 cycles	95.5 %	_	252
$[P_2W_{18}O_{62}]^{6-}$	+ 0.3, + 0.1, 0 to -0.5	1	100 cycles	_	_	253
V(III)/V(II)	-0.26	0	-	$96 \pm 4 \%$	_	55,254
Ce(IV)/Ce(III)	+ 1.48	0	_	_	78.8 %	254
Fe(CN) ₆ ^{3-/} Fe(CN) ₆ ⁴⁻	+ 0.77	7.2	_	99.88 %	_	56,255
FcNCl	+ 0.6	6.5	20 cycles	100 %	100 %	50
Hydroquinone sulfonate	+ 0.65	0.7	20 cycles	$98 \pm 7 \%$	91 ± 5 %	57
AQDS	+ 0.214	0	100 cycles	100 %	100 %	58
NiOOH/Ni(OH) ₂	+ 0.55	14	100 cycles	100 %	100 %	60,65,66
FeOx	+ 0.8 to + 1.5	14	50 cycles	>90 %	>90 %	256
MnO ₂ /MnOOH	+ 0.15	14	10 cycles	100 %	_	257
Fe ₃ O ₄ /FeOOH	-	_	-	100 %	_	258
CoO	-	_	_	100 %	_	259
PTPAn	+ 0.789 + 0.689	0.3	120 cycles	98.7 %	98.7 %	67
PTO	+ 0.46 + 0.589	0.3	300 cycles	_	_	260
PANI	+ 0.45 + 0.91	0.3	40 cycles	_	_	261

j, current density; FcNCl, (ferrocenylmethyl)trimethylammonium chloride; AQDS, anthroquinone-2,7-disulfonic acid; PTPAn, polytriphenylamine; PTO, pyrene-4,5,9,10-tetraone; PANI, polyaniline.

the polyoxometalate phosphomolybdic acid (H₃PMo₁₂O₄₀) to separate the OER from the HER under acidic conditions, as described by the following equations:

$$H_3PMo_{12}O_{40} + H_2O \rightarrow H_5PMo_{12}O_{40} + \frac{1}{2}O_2$$
 (15)

$$H_5PMo_{12}O_{40} \rightarrow H_3PMo_{12}O_{40} + H_2$$
 (16)

Therefore, during the oxidation of water to produce O₂, protons, and electrons, the polyoxometalate underwent reduction, forming H₅PMo₁₂O₄₀. Upon subsequent reoxidation, H₅PMo₁₂O₄₀ was converted back to H₃PMo₁₂O₄₀, releasing protons and electrons which were utilized to generate hydrogen at the cathode. Subsequently, the same researchers established a range of mediators (organic redox), such as 1,4hydroguinone derivatives and anthraguinone-2.7-disulfonic acid. 57,58 Additionally, Symes's and Cronin's groups investigated other inorganic polyoxometalate complexes, including phosphotungstic acid (PTA) and silicotungstic acid (STA), as alternative redox mediators with more negative redox potentials than the HER onset potentials of the catalysts. 63,64 Unlike previous redox mediator systems, which required two electrochemically driven steps, PTA and STA mediators are initially reduced (electrochemically) and accept protons during the OER. In the subsequent non-electrochemical step, the reduced PTA or STA evolve hydrogen spontaneously when making contact with Pt, Ni₂P, Ni₅P4, or Mo₂C catalysts without additional energy input, regenerating the oxidized PTA or STA, as the HER onset potentials (on those catalysts) are more positive than the redox potentials of the reduced from of STA and PTA. 62,63 This approach also accomplished decoupled HER and OER.

After Symes's and Cronin's works, various types of decoupled systems/setups were proposed.²¹ In 2014, Amstutz et al.⁵⁵ introduced a novel vanadium- and ceriumbased anolyte system for decoupled electrolysis. The adopted device configuration (Figure 4a) allowed for both conventional operation as a redox flow battery and the conversion of energy to hydrogen, offering large flexibility for renewable energy usage. They utilized a V(III) salt in sulfuric acid, in which V(III) is reduced to V(II) on a graphite felt electrode:

$$2V(II) + 2H^{+} \rightarrow H_{2} + 2V(III)$$
 (17)

The position of the V(III)/V(II) redox couple (-0.26 V vs SHE) is more negative than the proton reduction couple, allowing for spontaneous hydrogen generation when the V(II) solution is exposed to hydrogen evolution catalysts. The HER was achieved over an Mo₂C catalyst with a Faradaic yield of up to 96 %. At the anode, the oxidation of an acidic solution of Ce(III) to Ce(IV) took place:

$$4Ce(IV) + 2H_2O \rightarrow 4Ce(III) + 4H^+ + O_2$$
 (18)

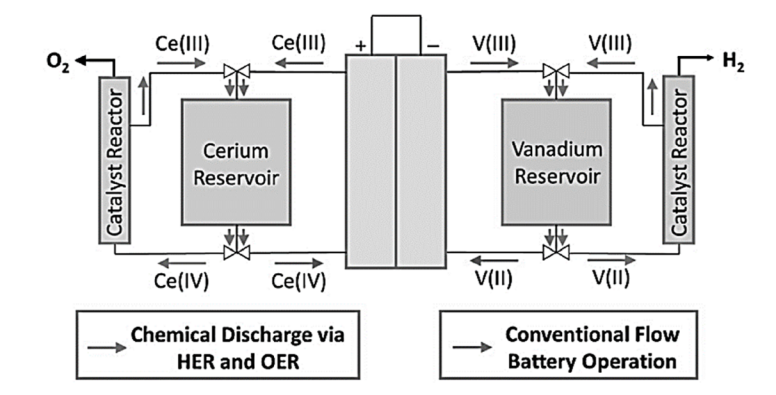
The position of Ce(III)/Ce(IV) redox under these circumstances is more anodic than that for water oxidation. This means that Ce(IV) can oxidize water to generate oxygen, becoming reduced back to Ce(III) in the process. This catalytic water oxidation reaction was achieved over RuO2 nanoparticles, although the Faradaic yield for the OER was somewhat less than optimal (78 % \pm 8 %) due to a side reaction involving degradation of the RuO₂ catalyst by Ce(IV). The authors suggested transitioning to an all-vanadium system to mitigate this issue, where the reduction of V(V) to V(IV) would mediate the OER.

Ho et al.⁵⁵ introduced a similar combined chemical/ electrochemical system for hydrogen production (Figure 4b). A photoelectrochemical cell was employed to reduce V(III) to V(II) while performing OER at the anode. The V(II) solution was directed to a flask containing a Mo₂C catalyst for ondemand H_2 evolution. A bipolar membrane maintained a significant pH differential between the anode and cathode compartments, crucial for the system's operation. The dual electrolyte system comprised an anodic compartment with a Ni mesh oxygen evolution electrode in KOH concentrated solution and a cathodic compartment with a Pt foil electrode in sulfuric acid. At the Ni anode, OH was oxidized, producing electrons, water, and oxygen. These electrons reduced V(III) ions to V(II), and the charged V(II) solution was transferred to a detached reactor for hydrogen production. The study investigated hydrogen production efficiency at various depths of charge of the vanadium solution, showing Faradaic efficiencies ranging from 83 % to 87 %. Additionally, the system demonstrated hydrogen generation under elevated pressures, with efficiencies approaching 60 % at pressures of up to ten atmospheres. Furthermore, the authors showcased the system's direct powering by renewable energy through coupling it to a photovoltaic module. Hydrogen was generated with a Faradaic efficiency of 80 %, under solar irradiation, achieving a solar-to-hydrogen energy conversion efficiency of 5.80 %.

Goodwin and Walsh⁵⁶ presented a novel method to spatially decouple the OER/HER using the Fe(CN)₆³⁻/ Fe(CN)₆⁴⁻ redox couple and a closed bipolar electrode. In their setup (Figure 4b), they utilized carbon cloths connected by a wire as the closed bipolar electrode, bridging between two separate two-compartment cells. Each cell contained a solution of K₃Fe(CN)₆/K₄Fe(CN)₆ in 0.1 m KOH, with one end of the closed bipolar electrode submerged in each solution. The device operated by facilitating water oxidation at a Pt electrode coupled with the reduction of Fe(CN)₆³⁻ at one end of the closed bipolar electrode in one cell. In the other cell,

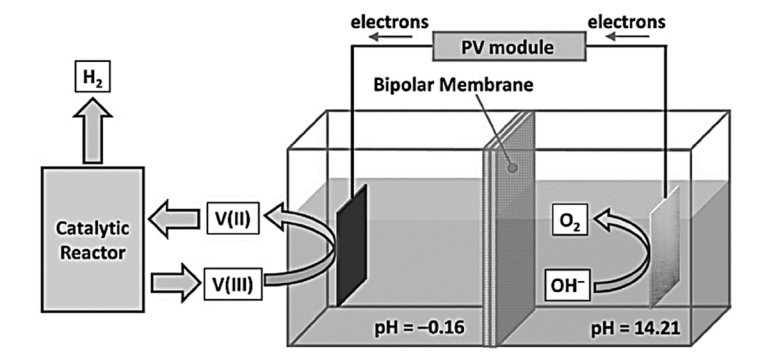
(a):

The Ce-V redox flow battery system utilized by Amstutz et al. [254].



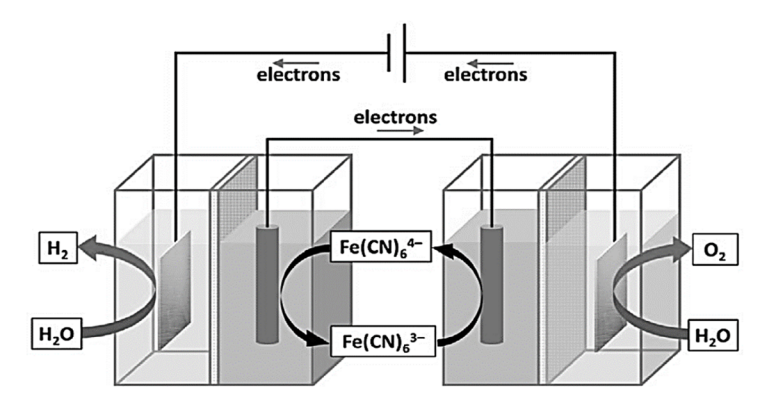
(b):

The V(III)/V(II) decoupling redox system utilized by Ho et al. [55].



(c):

The bipolar electrode cell system used by Goodwin and Walsh [56].



(d):

Li et al.'s [50] setup with (ferrocenylmethyl)trim ethylammonium chloride decoupling agent.

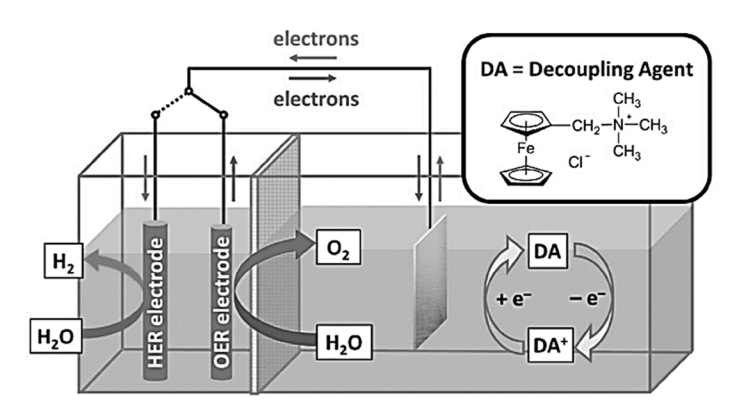


Figure 4: Schematic representation of a sample of experimental setups utilized by researchers for decoupled water electrolysis. From. 54

oxidation of $Fe(CN)_6^{4-}$ occurred at the opposite end of the closed bipolar electrode, accompanied by hydrogen evolution at the second platinum electrode.

Li et al.⁵⁰ investigated the use of ferrocene derivatives. specifically (ferrocenylmethyl)trimethylammonium chloride (FcNCl), as a decoupling agent to separate the HER and OER in a two-compartment H-cell setup (Figure 4d). One compartment contained a carbon counter electrode in a solution of FcNCl, while the other compartment housed electrodes for the HER and OER. The system enabled temporally separated HER and OER to take place, demonstrating stability over 20 redox cycles without significant pH variation. Furthermore, the study highlighted the potential for sunlight-driven hydrogen production, achieving currents of approximately 20 mA/cm² for the HER using a photovoltaic module under solar irradiation.

Zhao et al.⁵⁹ proposed a more direct decoupled solar-tohydrogen system, where sunlight activates BiVO₄ particles dispersed in an aqueous solution containing the Fe(III)/Fe(II) redox couple. Under solar irradiation, BiVO₄ particles oxidize water to produce oxygen while simultaneously reducing Fe(III) to Fe(II). The Fe(II) ions can then be re-oxidized to Fe(III) in an electrolytic cell, generating hydrogen at the cathode with 100 % Faradaic efficiency. Notably, this process operates at cell potentials significantly lower than conventional methods. Although conceptually similar to previous solar-to-hydrogen systems, Zhao et al.'s work achieved remarkable solar-to-hydrogen efficiencies of around 2%, a substantial improvement over earlier studies.

Chen et al.⁶⁰ proposed a novel approach to decoupled systems where the electrode served as the redox mediator. In their single-compartment setup, a nickel hydroxide (Ni(OH)₂) electrode underwent oxidation at the cathode, facilitating the HER. The electrode could then be regenerated through reduction coordinated with the OER at the anode. Similarly, Landman et al. 65,66 proposed a similar system but implemented it in two separate chambers using photoelectrochemistry. Ma et al.⁶⁷ also proposed a comparable system utilizing polytriphenylamine (PTPAn) as the electrode material. They demonstrated that this system achieved near quantitative Faradaic efficiencies for H₂ and O₂ production, with a photovoltaic-driven setup exhibiting an excellent overall solar-to-hydrogen conversion efficiency of 5.4%. Additionally, Dotan et al.⁶⁸ presented a decoupled system involving Ni(OH)2, where the oxidation of Ni(OH)2 was coordinated with H₂ production, and the electrode was regenerated through introducing a heated solution to the electrochemical cell.

These examples showcase the potential of decoupled water splitting systems, although they currently lack the capability to generate electricity in one of their decoupled

cycles, hindering their function as a dual-use H₂ generation/ electricity storage system. An example of such a system described by Bienvenu⁶⁹ involved the reduction of Zn²⁺ ions to Zn^0 at the cathode during OER at the anode. Upon polarity switching, the Zn⁰ electrode underwent spontaneous oxidation, resulting in the generation of both electricity and hydrogen at the cathode.

In conclusion, decoupled water electrolysis systems represent a promising solution to mitigate the challenges associated with traditional electrolyzers, offering efficient hydrogen production while avoiding gas crossover and ensuring safety. These systems, facilitated by various redox mediators and innovative configurations, demonstrate significant potential for advancing clean hydrogen generation technologies. However, further research is needed to address limitations and enhance the scalability and dual-use capabilities of decoupled systems for broader applications in renewable energy and beyond.

4.2 Hybrid water electrolysis

In parallel with the concept of decoupled water electrolysis, researchers have been exploring hybrid water electrolysis as a means to mitigate the limitations of the OER, such as high oxidation overpotential, thereby reducing the overall energy input required for hydrogen generation. This approach involves replacing the OER with alternative, thermodynamically more favorable oxidation reactions using various substrates like alcohols, 70,71 amines, 72 aldehydes,⁷³ hydrazine,^{74,75} urea,^{74,76} and more.⁷⁷ Fan et al.,⁷⁸ Kahlstorf et al., 77 Ran et al., 16 Chen et al. 22 and Du et al. 23 have extensively reviewed the progress in hybrid water electrolysis. Notably, this system holds promise for waste treatment or valorization, provided the waste stream meets certain criteria:⁷⁹

- Firstly, the substance must be soluble for efficient operation.
- Secondly, its theoretical oxidation potentials should be lower than the OER to minimize energy consumption.
- Thirdly, waste valorization should either generate economic benefits through electrochemical oxidation or, if it is not suitable for valorization, it should be transformed into less harmful byproducts.
- Lastly, a constant waste output is crucial for research value and practical availability.

Several wastes, including hydrogen sulfide, cellulose wastes, crude glycerol, and plastics, meet these criteria.⁷⁹ Hydrogen sulfide and glycerol dissolve readily, while cellulose and certain plastics can be hydrolyzed to yield

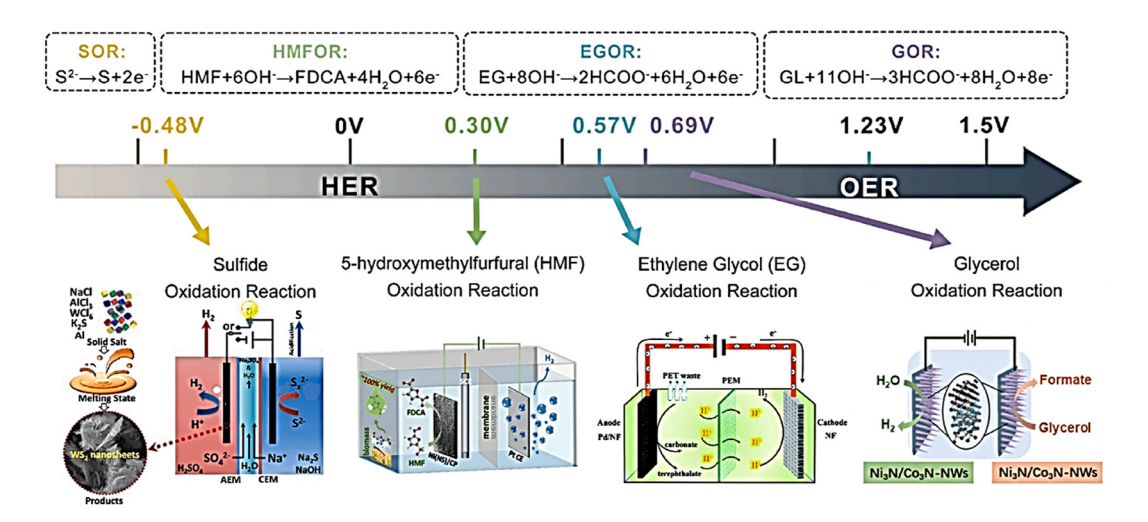


Figure 5: Schematic illustration of alternative oxidation reactions for hybrid water electrolysis systems with theoretical oxidation potentials axis. From. 79

water-soluble byproducts such as ethylene glycol and (EG) 5-hydroxymethylfurfural (HMF). Figure 5 illustrates alternative oxidation reactions for waste valorization, along with their oxidation potentials, indicating potential energy savings. Significantly, the oxidation potential of the sulfide reaction lies below the HER potential of 0 V, suggesting significant potential for energy saving⁸⁰ and, sometimes, the reaction can proceed without the need for electricity consumption.81

Due et al.²³ classified waste valorization into three main categories: (i) Reagent-sacrificing type, which enables H₂ production under low voltages while sacrificial reactants (such as ammonia and hydrazine) are oxidized to nonvaluable products; (ii) Pollutant-degradation type, where the sacrificial reactants undergoing oxidation are pollutants (e.g., organic dyes, urea ...); and (iii) value-added type, which involves upgrading organic reactants (e.g., glucaric acid, tetrahydroisoquinolines, biomass-derived chemicals) to valuable products. However, practical outcomes depend on various factors, including reaction products, conditions, and catalysts. Consequently, careful product selection and costeffective catalyst development are vital for future research in this area. A comprehensive analysis of these factors is provided in the review by Wang et al. 79

4.2.1 Reagent-sacrificing type

Hydrazine and ammonia electrooxidation are typical examples of this category.²³ This system involves the anodic conversion of hydrazine and ammonia, both commercially valuable substrates, into non valuable products like N_2 (Eqs. (19) and (20)).

$$N_2H_4 + 40H^- \rightarrow N_2 + 4H_2O + 4e^-$$
 (19)

$$2NH_3 + 6OH^- \rightarrow N_2 + 6H_2O + 6e^-$$
 (20)

Crucially, the thermodynamic potential of these reactions, i.e., -0.38 V for reaction (19), is markedly lower than that of the OER (1.23 V), resulting in a significant decrease in the overall cell voltage needed for water splitting.²³ In many cases, hydrazine oxidation reaction (HzOR) enabled the attainment of a current density of up to 500 mA/cm² at a cell voltage of 1V without generating O_2 . Additionally 75,82,83 , 10 mA/cm² could be achieved at a microvoltage level in the presence of hydrazine.²³ Bifunctional electrocatalysts have been developed to facilitate the HER coupled with hydrazine oxidation, further enhancing the efficiency of hydrogen generation, the addition of 0.02 M hydrazine to a 1 M KOH solution reduced the required voltage for reaching 15 mA/ cm² from 1.97 V to 0.63 V, utilizing the bifunctional Ni@Pd-Ni alloy nanosheets as electrodes.⁸⁴ Sun et al.⁸⁵ reported that CoS₂/TiM nanoarrays and Ni₂P/NF catalysts enable efficient hydrogen evolution at relatively low cell voltages, with the former achieving hydrogen evolution with only a cell voltage of 0.81 V to achieve 100 mA/cm² (pure water splitting required 1.89 V to achieve this current density). Furthermore, Ni₂P/NF catalysts enable H₂ production with 1.0 V at 500 mA/cm², exhibiting remarkable durability and highly Faradaic efficiency for H₂ generation.⁸² Moreover, Tang et al. 86 introduced a porous nitrogen-doped carbon material encapsulating cobalt/LaCoO_x hybrid nanoparticles (Co/ LaCoOx@N-C) as a bifunctional catalyst for both HER and HzOR. This catalyst demonstrated remarkable electrochemical activity in HzOR, achieving 69.2 mA/cm² at only 0.3 V. Moreover, the development of direct hydrazine fuel cells (DHFCs) offers a promising avenue for sustainable hydrogen generation. In these systems, hydrazine serves as the feedstock, leveraging its high energy density and utilization rate. 87,88

Durable bifunctional electrocatalysts like P,W co-doped Co₃N nanowire on NF (PW-Co₃N NWA/NF) demonstrate remarkable electrochemical performance in hydrazine splitting, facilitating efficient hydrogen production with minimal energy consumption.⁸⁷ PW-Co₃N NWA/NF achieves hydrogen evolution with an exceptionally low cell voltage of 28 mV to reach 10 mA/cm², outperforming overall water splitting.⁸⁷ The oxidation of hydrazine can sustain a current density of 200 mA/cm² over an overpotential of 607 mV, underscoring the enhanced energy efficiency of hydrazine oxidation coupled with HER for H₂ production.⁸⁷ Furthermore, the integration of direct hydrazine fuel cells with overall hydrazine-splitting units (using Fe-doped CoS₂ nanosheets as electrocatalysts for both the HER and HzOR) in a self-powered system demonstrates the feasibility of efficient hydrogen evolution without external power input, achieving an H2 evolution rate of 9.95 mmol/h, a 98 % Faradaic efficiency, and a 20-h stability (electrode:3D nanoporous NixCo1-xSe nanorod array).83

Similar to hydrazine oxidation, the oxidation of ammonia (Eg. (20)) offers a thermodynamically more favorable alternative to OER. Ammonia, being more ubiquitous and easily accessible compared to hydrazine, holds greater promise as a replacement for OER.²³ While Pt has traditionally been recognized as the most effective catalyst for ammonia oxidation, 23,89 its high cost and scarcity have spurred the exploration of non-noble metal-based alternatives. Mei et al. 90 introduced a catalyst consisting of N-doped NiZnCu layered double hydroxides (LDH) with reduced graphene oxide on nickel foam (N-LDH/rGO). In a two-electrode system utilizing the prepared NiZnCu LDH as both anode and cathode, 50 mA/ cm² was achieved at 0.769 V, surpassing the noble-metal system where Pt/C served as the cathode and IrO₂ served as the anode by 0.170 V. Furthermore, this two-electrode system maintained the current density for at least 18 h. Further studies reported in the literature highlight the advantageous use of ammonia in advancing HER using various synthesized electrocatalysts for the cathode material, such as Ni(OH)2-Cu₂O, N-NiZnCu LDH, Ni₅₀Cu₅₀/C, among others. 91-93

Overall, despite the added expense associated with sacrificial reagents, their utilization ensures stable water electrolysis at high current densities without O_2 production, rendering them an optimal choice for hybrid water electrolysis systems.

4.2.2 Pollutant-degrading type

Sacrificial reagents tend to increase the overall system cost compared to the value of the starting substrate (such as hydrazine or ammonia), despite the potential reduction in cell voltage. To address this challenge, these substrates could be substituted with environmental pollutants, offering opportunities for oxidative degradation (remediation) while also advancing HER. When integrated with water electrolysis, this process of anode oxidation, resembling waste treatment, is referred to as the pollutant-degrading type.²³

A typical example is Urea $(CO(NH_2)_2)$, commonly found in industrial wastewater and domestic sewage, although organic dyes are also viable alternatives. Combining the urea oxidation reaction (UOR) with water electrolysis can achieve ecological preservation and clean energy production by efficiently generating H_2 and purifying urea-rich wastewater or urine (Gnana Kumar et al., 2020). The UOR (Eq. (21)) coupled with HER (Eq. (6)) in alkaline electrolysis results in the overall reaction depicted in Eq. (22):⁹⁴

Anode:
$$CO(NH_2)_2 + 6OH^- \rightarrow N_2 + CO_2 + 5H_2O + 6e^-,$$

 $E^0 = -0.46 \text{ V vs. SHE}$ (21)

Overall:
$$CO(NH_2)_2 + H_2O \rightarrow N_2 + 3H_2 + CO_2$$
,
 $E = 0.37 \text{ V vs. SHE}$ (22)

Reaction (21) has undergone extensive examination across various cathode and anode materials. The overall cell potential required to attain $10\,\text{mA/cm}^2$ (V₁₀) fluctuates depending on the specific anode/cathode pairing and the concentration of urea. This variability is demonstrated below:

- V_{10} = 1.41 V for MnO₂/CoP_x couple using 1.0 M KOH with 0.5 M CO(NH₂)₂, ⁹⁵
- V₁₀ = 1.38 V for Ni₃Se₄/CoP_x couple using 1.0 M KOH with 0.1 M CO(NH₂)₂, ⁹⁶
- V_{10} = 1.305 V for N-NiZnCu LDH/N-NiZnCu LDH couple using 1.0 M KOH with 0.3 M CO(NH₂)₂,⁹⁰
- V_{10} = 1.4 V for CoP/C/CoP/C couple using 1.0 M KOH with 0.1 M CO(NH₂)₂, 97
- V_{10} = 0.89 V for N-CoP/N-CoP couple using 0.5 M H₂SO₄, 0.96 M FeSO₄/0.74 M Fe₃(SO₄)₂.⁸⁰

In all of these systems, successful degradation of urea has been accomplished. Research into the mechanism and kinetics of UOR on Ni-based electrocatalysts in an alkaline medium indicates that urea oxidation takes place subsequent to the formation of NiOOH under electrooxidation conditions.²² NiOOH then interacts with urea molecules, replenishing active sites for subsequent adsorption/desorption of intermediates.²²

In the other hand, Zhang et al. explored the combination of HER with the decomposition of methylene blue, a textile dye. They utilized FeNiP nano-sheets coated with a

carbon shell as the cathode catalyst. The oxidation was observed at approximately 1.2 V across different concentrations of methylene blue. Due to the excellent protection and conductivity supplied by the carbon shell, the catalyst exhibited an overpotential of 104 mV to achieve a current density of 10 mA/cm², which remained stable even after 1,000 cycles of CV scans. Additionally, under a constant current density of 1 mA/cm², entire degradation of methylene blue could be achieved in 53 min, where the corresponding potential remained steady for over 2,500 s.

In conclusion, considering the ongoing escalation of environmental pollution, the coupling of HER with pollutant degradation undeniably holds promising prospects for the future. However, since real-world pollutants are much more complex, further research efforts should be directed towards realizing real hybrid electrolysis under practical scenarios.

4.2.3 Value-added type

Table 5 provides an overview of recent electrooxidation of organic (EOO) reactions considered value-added. Briefly, small alcohols undergo anodic partial oxidation, yielding aldehydes/ketones in a 2e⁻ process or carboxylic acids in a 4e process, while aldehydes can be oxidized to carboxylic acids. Oxidative coupling of two alcohols enables ester production, exemplified by ethyl acetate from ethanol. Ringopening reactions, like adipic acid production from cyclohexanone/cyclohexanol, are also feasible. 99 Larger biomassderived compounds, such as 5-hydroxymethylfurfural (HMF) or glycerol, yield various products based on reaction conditions and catalysts. Glycol oxidation, for instance, vields multiple commercially relevant products, including formic acid, lactic acid, and carbon dioxide. 100,101 Alkenes enable the synthesis of epoxides, diols, and higher oxidized

Table 5: Sample of electrooxidation of organics (EOO) producing value-added chemicals within hybrid water electrolysis systems. 262

Reaction type	Anode catalyst	Organic substrate	concentrations	Product	E _{OER} (V _{RHE}) at 10 mA/cm ²	V _{EOO} (V _{RHE}) at 10 mA/cm ²	Ref.
	Co(OH)₂@HOS	Methanol	3.0 M in 1.0 M KOH	Formate	1.571	1.385	263
	Co ₃ O ₄ NSs	Ethanol	1.0 M in 1.0 M KOH	Ethyl acetate	1.50	1.445	264
	Rh nanosheets	2-Propanol	1.0 M in 1.0 M KOH	Acetone	1.61	0.233	265
	NC@CuCo ₂ N _x	Benzyl alcohol	15 mM in 1.0 M KOH	Benzaldehyde	1.46	1.25	266
	Mo-Ni alloy NP	Benzyl alcohol	10 mM in 1.0 M KOH	Benzoic acid	1.49	1.345	267
	PdAg	Ethylene glycol	1 M in 0.5 M KOH	Glycolic acid	1.55	0.57	268
	MoO _x /Pt	Glycerol	0.1 M in 1.0 M KOH	Glycerate	_	_	269
	Co-Ni alloy	Glucose	0.1 M in 1.0 M KOH	Gluconic acid/ gluconolactone	-	-	270
	Ni_3S_2	Furfuryl alcohol	10 mM in 1.0 M KOH	2-Furoic acid	ca. 1.50 (onset)	ca. 1.35 (onset)	271
Aldehyde oxidation	Ni ₂ P/Ni	FUR	30 mM in 1.0 M KOH)	2-Furoic acid	1.55 (onset)	1.34 (onset	272
	PbO ₂	FUR	10 mM in pH 1.0 H2SO4	Maleic acid	1.85 (onset)	1.60 (onset)	273
	MoO ₂ -FeP@C	HMF	10 mM in 1.0 M KOH	FDCA	1.474	1.359	274
	(FeCrCoNiCu) ₃ O ₄ NSs	HMF	50 mM in 1.0 M KOH	FDCA	1.50 (onset)	1.35 (onset)	275
Amine oxidation	NiSe	Benzylamine	1 mmol in 1.0 M KOH	Benzyl nitrile	1.48 (onset)	1.34 (onset)	72
	VP-Ni(OH) ₂ NS _s	Propylamine	10 mmol 1.0 M KOH	Propionitrile	1.53	1.36	276
Nitroalkane oxidation	NiSe nanorods	α-nitrotoluene	0.4 mmol in 1.0 M KOH	<i>E</i> -nitroethene	-	-	277
S-DHD of THIQ	Ni2P 1,2,3,4-	Tetrahydroisoquinoline	0.5 mmol in 1.0 M KOH	3,4-Dihydroisoquinoline	ca. 1.48 (onset)	ca. 1.10 (onset)	278
Sulfide oxidation	CoFe-LDH	Diphenyl sulfide	0.25 M in MeCN/ H ₂ O	Diphenyl sulfoxide	1.90 V	1.39 V	279

S-DHD of THIQ, semi-dehydrogenation of Dihydroisoguinolines; FUR, furfural; HMF, 5-hydroxymethylfurfural; FDCA, 2,5-Furandicarboxylic acid.

species, while amines can be oxidized to nitriles via dehydrogenation or coupled to form diazo compounds. Some detailed analyses oof the results were discussed in the subsequent sections.

Hydrogen sulfide (H₂S), a notorious environmental contaminant, can be recovered as elemental sulfur, which has diverse applications like pesticide manufacturing and lithium-sulfur batteries. 79 Integrating the sulfide oxidation reaction (SOR) with the HER in hybrid water electrolysis systems offers a more favorable theoretical voltage (Figure 5) and faster reaction kinetics than traditional water electrolysis, leading to reduced energy consumption.¹⁰²

$$S^{2-} \rightarrow S + 2e^-, E^0 = -0.48 \text{ V vs. SHE}$$
 (23)

Besides elemental sulfur, SOR can yield sulfites, thiosulfates, and sulfates. However, sulfur's insolubility water leads to deposition on the anode, forming a highresistivity passivating layer ($\sim 10^{15} \Omega/m$). While highly alkaline electrolytes may mitigate this, a more effective approach involves preventing sulfur deposition through interface engineering. Zhang et al. 103 introduced a "selfcleaning" concept, developing a hydrophobic NiS₂ catalyst that resists sulfur species deposition, enabling prolonged desulfurization (100 h at 20 mA/cm²). Zhang et al. 104 proposed "chainmail catalysts", constructing a grapheneencapsulated CoNi alloy catalyst (CoNi@NGs) preventing direct metal-sulfur contact. This catalyst catalyzed sulfide oxidation via graphene shell-induced electron transfer, exhibiting high activity over 500 h (30 mA/cm²). Various electrocatalysts were also developed by various researchers, showing variable stabilities (e.g., Ni-Co-C: 64 h at 100 mA/cm², ¹⁰² CoS₂@C/MXene: 180 h at 30 mA/cm², ¹⁰⁵ WS₂: 14 h at 100 mA/cm²¹⁰⁶).

Crude glycerol, a by-product constituting 10 wt% of the biodiesel production process, poses a significant oversupply issue, with global annual production surpassing 5 billion liters.⁷⁹ Anodic oxidation within hybrid water electrolysis systems not only converts glycerol into valued chemicals but also concurrently generates hydrogen at the cathode, offering notable carbon-neutral advantages. 107 Glycerol's susceptibility to nucleophilic attack, owing to its three adjacent hydroxyl groups, results in a spectrum of oxidation products ranging from C₁ to C₃, including formic acid, lactic acid, glycolic acid, and dihydroxyacetone. Oxidizing glycerol to formic acid is favored due to its potential to minimize byproduct formation. The theoretical oxidation potential for glycerol to formic acid (Eq. 24, 0.69 V) is significantly lower than that of the OER (Figure 5). However, efficient catalysts are crucial for this conversion, with nickel compounds garnering considerable attention.⁷⁹

$$C_3H_8O_3 + 110H^- + 8e^- \rightarrow 3HCOOH + 8H_2O, E^0$$

= 0.69 V vs. SHE (24)

Li et al. 108 introduced a carbon fiber cloth-supported NiMoN nanoplate catalyst, requiring only 1.36 V voltage in a hybrid water electrolysis system at 10 mA/cm² and achieving a remarkable Faradaic efficiency of 95% for formic acid production. Zhu et al. 109 proposed a Ni₂N/Co₃N heterogeneous nanowire catalyst, achieving 1 A/cm² at a voltage of 2.01 V and realizing an impressive Faradaic efficiency of 94.6 % toward formate production. Tran et al. 110 explored the performance of glycerol oxidation under various crystalline MnO₂ catalysts, i.e., α -, β -, and γ -MnO₂. The three phases showed selectivity exceeding 90 % for the C₃ product, yet y-MnO₂ demonstrated superior stability and current density compared to the other phases.

The cellulosic waste conversion into individual components, such as glucose, furfural, oligosaccharides, and 5hydroxymethylfurfural (HMF), through hydrolysis processes holds promise for waste valorization. 111 HMF serves as a crucial platform chemical facilitating the subsequent conversion of cellulose waste into several valuable products, including 2,5diformylfuran (DFF), 5-formyl-2-furancarboxylic acid (FFCA), 5-hydroxymethyl-2-furancarboxylic acid (HMFCA), and 2,5furandicarboxylic acid (FDCA).¹¹² The theoretical voltage necessary for the oxidation of HMF to FDCA is merely 0.30 V, as shown in Eq. (25), significantly lower than conventional water electrolysis (1.23 V), enabling resource recovery and hydrogen production with low energy consumption.

$$HMF + 6OH^{-} \rightarrow FDCA + 4H_{2}O + 6e^{-}E^{0} = 0.30 \text{ V vs. SHE}$$
 (25)

Grabowski et al. achieved a 71 % yield of FDCA through the HMF electrochemical oxidation in a 1.0 M NaOH solution using nickel oxide/hydroxide catalysts. 113 Nickel-based catalysts have demonstrated efficacy in oxidizing HMF through an electrochemical-chemical coupling mechanism. 113

In conclusion, the integration of the HER with anodic electrooxidation of organics significantly reduces the cell voltage required for water splitting, leading to improved hydrogen production. Despite these advantages and recent advancements, this coupling technology is in its nascent stage, and its transformation efficiency remains inadequate. Therefore, the development of high-performance electrodes, precise identification of active sites, and strategic construction of the electrolyzer are crucial for future industrial applications.

4.2.4 Perspectives

The integration of the HER with anodic electrooxidation of organics significantly reduces the cell voltage required for water splitting, leading to improved hydrogen production.

Despite these advantages and recent advancements, this coupling technology is in its nascent stage, and its transformation efficiency remains inadequate. To advance hybrid water electrolysis further, several critical aspects must be addressed to realize commercial and large-scale applicationss: 22,79

- (i) Accelerating catalyst discovery: Expediting the discovery of high-performance catalysts is imperative. For this regard, utilizing DFT calculations and machine learning can streamline catalyst design and enhance our comprehension of the structure-performance relationship. This approach holds potential for developing catalysts with superior activity and selectivity.
- (ii) Employing advanced characterization Techniques: Integration of advanced in situ techniques and analytical methods is essential for comprehending the dynamic behavior of catalysts during electrochemical process. Techniques such as X-ray absorption spectroscopy and Raman spectroscopy facilitate real-time monitoring of reaction intermediates and catalyst structure evolution. This deeper understanding can inform the design of high-performance catalysts for efficient hybrid water splitting.
- (iii) Developing bifunctional catalysts: The development of bifunctional catalysts based on earth-abundant elements is crucial for cost-effective and practical applications of hybrid water splitting. These catalysts can simultaneously facilitate multiple oxidation reactions, including biomass and pollutant oxidation, while efficiently harvesting hydrogen with minimal energy consumption. They offer a simplified and economically viable solution for large-scale hydrogen production.
- (iv) Advancing membrane-based systems: Implementation of membrane-based systems is indispensable for practical HWE, enabling the efficient separation of anode and cathode products. Selecting membranes based on the applied electrolyte ensures optimal product separation and overall system performance. These membranebased systems are pivotal for realizing large-scale and commercial application of HWE technology.
- (v) *Integrating with solar systems*: Integrating electrolyzers with solar systems represents a key strategy for further reducing energy costs in hybrid water electrolysis. By leveraging solar energy, the electrolysis process becomes more sustainable and economically viable for large-scale implementation.

4.3 Tandem water electrolysis

The tandem water electrolysis approach addresses challenges in H₂ storage and transportation, ¹⁸ utilizing directly

the in situ generated H2 during the process to produce valuable chemical fuels like methane (CH₄) and ammonia (NH₃) through efficient biological catalysts.⁴ This method, promising for enhancing traditional H2 utilization, was pioneered by Nichols et al.¹¹⁴ Their setup (Figure 6a) involved an airtight two-compartment electrochemical cell with Methanosarcina barkeri (M. barkeri) and CO2 in the cathodic chamber. Sustainable electricity or solar input drives water splitting using inorganic catalysts to produce H₂, consumed by M. barkeri with CO₂ to generate CH₄. GC analysis of the headspace gas products revealed a linear increase in CH₄ production over 11.5 h with applied currents (1.0-7.5 mA) and a Faradaic efficiency above 74 % (Figure 6b). The hybrid system operated robustly over 7 days with a Faradaic efficiency close to 75 % (Figure 6c). Isotope labeling confirmed that the carbon source for CH₄ was the original CO₂. The use of ¹³CO₂ resulted in the detection of only $^{13}\text{CH}_4$ via HRMS (Figure 6d), while the use of $^{12}\text{CO}_2$ led to the observation of only ¹²CH₄. This hybrid system offers significant flexibility in terms of electrocatalysts for HER, a range of abundant and biocompatible inorganic catalysts,

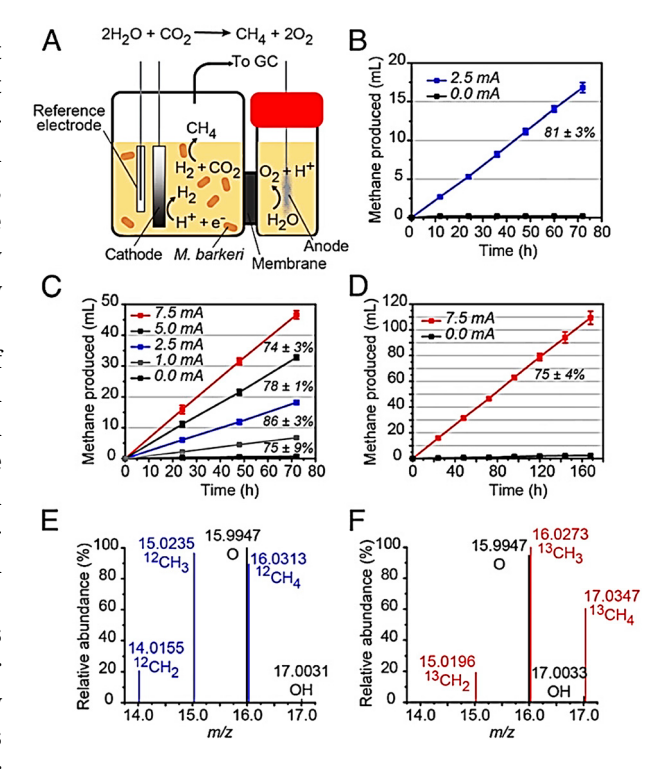


Figure 6: Electrocatalytic reduction of carbon dioxide to methane with a hybrid platinum/M. barkeri platform. (a) Schematic representation of tandem water electrolysis. (b, c) variation of CH₄ production and faradaic efficiency with applied current. (d) Analysis of gas products using highresolution mass spectrometry. (e and f) High-resolution mass spectrometry of headspace gases after electrolysis under an atmosphere of (e) $^{12}CO_2$ and (f) $^{13}CO_2$ in rich media. Error bars represent SD with n = 3 independent experiments in all cases. From. 114

including NiMo and NiS, can be employed. 114 Furthermore, when combined with photoelectrodes, it enables direct conversion of solar energy into chemical compounds, illustrating the potential of this tandem water electrolysis approach.114

Liu et al. 115 showcased a tandem water electrolysis system akin to the one described earlier, but with a twist: converting the generated H₂ into biomass or alcohol fuels with CO₂. In their setup, they employed Co-P as the HER electrocatalyst and Ralstonia eutropha as the biocatalyst. This system exhibited a CO₂ reduction energy efficiency of approximately 50 %, capable of scrubbing 180 g of CO₂ per kW-h of electricity. According to the research, Integration of this hybrid device with existing photovoltaic systems could yield a CO₂ reduction energy efficiency of around 10 %, surpassing that of natural photosynthetic systems.

In another study, Liu et al. 116 introduced a novel tandem water electrolysis system designed to produce NH3 from N_2 and H_2O using autotrophic bacterium Xanthobacter autotrophicus. By harnessing solar energy and renewable electricity to drive water splitting, the approach holds promise as a renewable synthesis platform for the nitrogen reduction reaction (NRR). The researchers demonstrated that the production of NH₃ and X. autotrophicus biofertilizer effectively links atmospheric N_2 to plant biomass. This hybrid inorganic-biological approach for the NRR could potentially serve as a renewable biological and chemical synthesis platform, contingent upon the biomachinery involved in water splitting coupling.

Overall, these innovative tandem water electrolysis systems represent significant strides toward sustainable energy and chemical production, offering promising avenues for addressing environmental challenges and advancing renewable synthesis platforms. However, additional research is needed to optimize these systems for practical applications and to further enhance their efficiency and reliability.

4.4 Microbial electrolysis cells

Microbial electrolysis cells (MECs) represent a bioelectrochemical technology that leverages microbial metabolism to facilitate electrolysis reactions. Unlike microbial fuel cells (MFCs), which primarily generate electricity from microbial activity, MECs are specifically designed for hydrogen production via the electrochemical reduction of protons at the cathode. A schematic diagram illustrating commonly used reactors for MECs, including single- and twochambered configurations, is depicted in Figure 7. 117 Within

these systems, microbial communities oxidize organic matter found in sources such as wastewater or other organic substrates at the anode. This oxidation process releases electrons, protons, CO₂, and other byproducts. ¹¹⁸ While protons migrate to the cathode, electrons travel through an external circuit to reach the cathode. At the cathode, these electrons participate in the reduction of protons derived from water, resulting in the production of hydrogen gas. 119

The anodic oxidation reaction of various organic substrates in an MEC, along with their respective potentials at pH 7, is provided below: 117,120-122

Acetate:
$$CH_3COO^- + 4H_2O \rightarrow 2HCO_3^- + 9H^+ + 8e^-, E = -0.30 \text{ V}$$
(26)

Glucose:
$$C_6H_{12}O_6 + 6H_2O \rightarrow 6CO_2 + 24H^+ + 24e^-, E = -0.43 \text{ V}$$
(27)

Formate:
$$HCOO^- + 2H_2O \rightarrow HCO_3^- + 2H^+ + 2e^-, E = -0.43 \text{ V}$$
(28)

Glecyrol:
$$C_3H_8O_3 + 3H_2O \rightarrow 3CO_2 + 14H^+ + 14e^-$$
 (29)

Lactate:
$$C_3H_6O_3 + 3H_2O \rightarrow 3CO_2 + 12H^+ + 12e^-$$
 (30)

Propionate:
$$C_3H_6O_2 + 4H_2O \rightarrow 3CO_2 + 14H^+ + 14e^-$$
 (31)

Using the cathodic reaction of Eq. (2), the overall MEC reactions for acetate and glucose are given in equations 32 and 33. 117 According to the stoichiometries, MEC enables a theoretical maximum hydrogen yield of 4 mol per mole of acetate. However, a higher theoretical H₂ yield of 12 mol/mol could be achieved using glucose.

$$CH_3COO^- + 4H_2O \rightarrow 2HCO_3^- + H^+ + 4H_2$$
 (32)

$$C_6H_{12}O_6 + 12H_2O \rightarrow 6CO_2 + 12H_2$$
 (33)

The voltage required for HER (-0.412 V) at the cathode is provided through both microbial electrical supply (-0.3 V) and an extra-applied voltage. The additional applied voltage typically amounts to around 0.14 V, as theoretically calculated for acetate $[E_{cathode} - E_{anode} = -0.41 - (-0.3) = 0.14 \text{ V}].$ However, in practice, this voltage often exceeds 0.2 V due to considerations such as electrode overpotentials and ohmic losses. 123 Numerous studies reported a typically applied potential range of 0.5-1.0 V (Table 6), with a minimum requirement of 0.25 V to achieve reasonable current densities and hydrogen generation rates in practical-scale MECs. 124 Nonetheless, this applied potential remains significantly lower than that required for water electrolysis (i.e., oxygen yield, >1.23 V), which remains one of the most important advantages of MECs against other traditional techniques. MECs exhibit the capability to generate

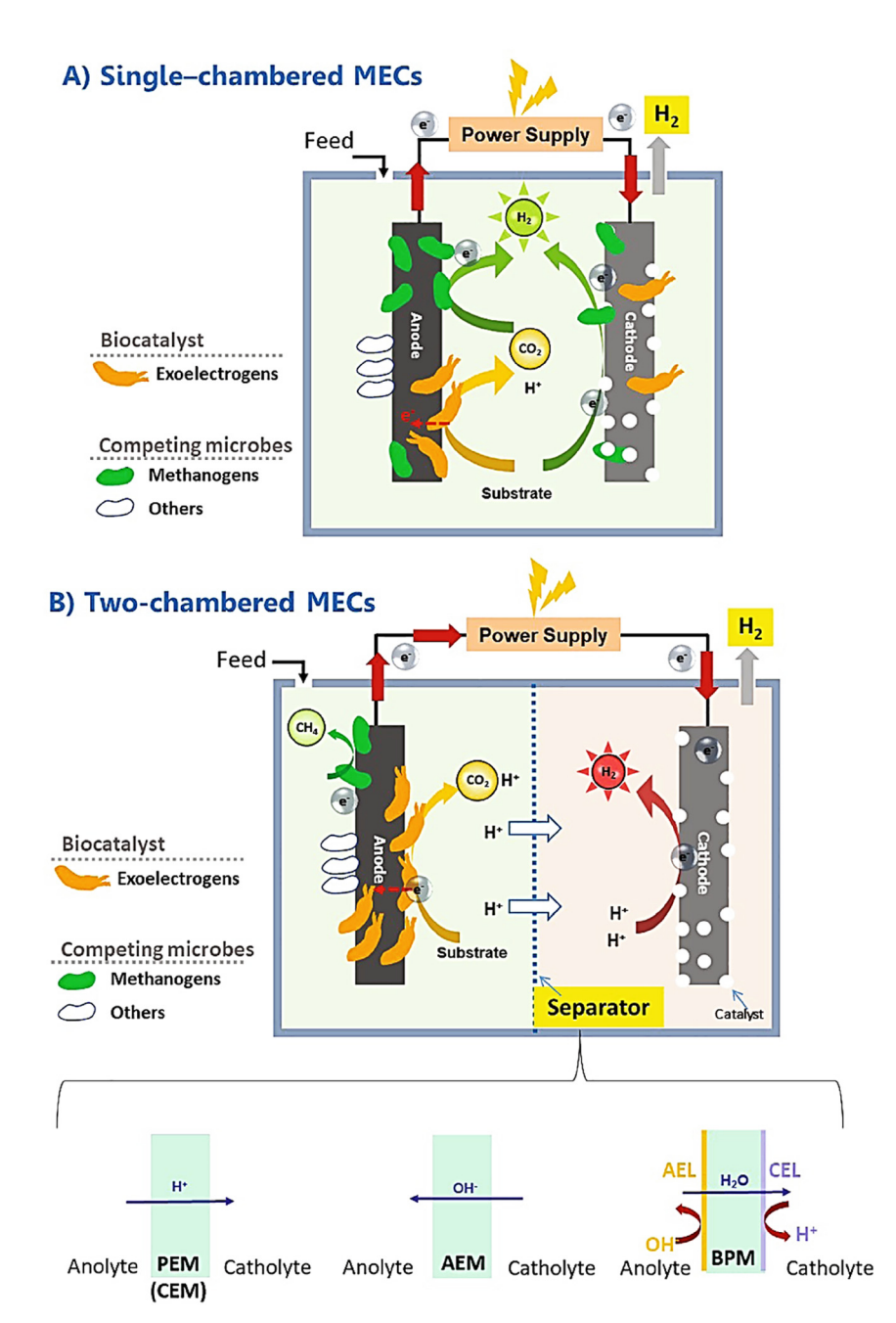


Figure 7: Schematic diagrams illustrating (a) a single-chambered microbial electrolysis cell (MEC) and (b) a two-chambered MEC designed specifically for hydrogen production. From. 117

hydrogen using a diverse range of organic wastewater types as substrates (Table 6), offering the advantage of simultaneous pollutant treatment. Moreover, an array of external power sources, including fuel cells and solar cells, have been harnessed to supply energy to MECs (Figure 7b). Another critical aspect of the electrohydrogenesis process is the internal resistance of the MEC reactor, which is influenced by factors such as electrolyte concentration, construction materials of the MEC, and the presence or absence of ion exchange membranes. The primary objective in hydrogen production is to minimize the internal resistance of the MEC, facilitating efficient electron transfer across the electrodes.

To achieve this goal, various strategies and approaches have been explored and implemented.

4.4.1 Reactor configurations

Diverse reactor configurations and materials have been explored under different operational conditions, with singlechambered and two-chambered setups being the most prevalent (Table 6).²⁵ External voltage necessary for the process can be sourced from conventional power supplies or renewable energy, with solar energy standing out as the most promising, cleanest, efficient, and cost-effective option.

Table 6: Applied potential pf microbial electrolysis cell (MEC) based on using wastewater and pure substrate. 117

MEC configuration	Substrate	Applied voltage (V)	H ₂ production m³/m³/d	Cathodic H ₂ recovery (%)	Ref.
Single chamber	Sludge wastewater	0.9	0.038	15.56–20.05	280
Single chamber	Dairy wastewater	0.7	0.2	_	281
Single chamber	P-glycerol	0.5	0.8	_	122
Dual-chambers	Acetate	1	50	90	282
Dual-chambers	Acetate	0.6	1.1	_	283
Single chamber	Milk	0.8	0.086	91	168
Pilot-scale MEC	Domestic wastewater	0.6	0.015	70	284
Single chamber	Glucose	0.5	0.83	55	122
Single chamber	Proteins	0.6	0.42	87	285
Dual-chambers	Acetate	0.45	0.37	90	126
Dual-chambers	Acetate	0.5	0.02	57	286
Dual-chambers	Domestic wastewater	0.5	0.01	42	166
Single chamber	Acetate	0.8	3.12	96	134,283
Single chamber	Acetate	0.6	0.69	87	132
Dual-chambers	Glycerol	1.2	0.46	85	287
Dual-chambers	Vegetable wastewater	0.8	0.025	11.29	288
Pilot-scale MEC	Urban wastewater	0.5	0.041	90	289
Dual-chambers	Industrial wastewater	1	0.03	38.5	290

When the process is conducted under solar illumination, it is referred to as solar-assisted MECs. 117

Initial research on MECs focused on H-type twochambered configurations, typically constructed from glass or various plastics and separated by a membrane (Figure 7b). 125-127 Commonly used membranes include proton exchange membrane (PEM), anion-exchange membrane (AEM), cation exchange membrane (CEM), and bipolar membranes. 119 In these systems, microorganisms in the anodic chamber, known as exoelectrogens, oxidize organic matter to release electrons. These electrons flow through an external circuit to the cathodic chamber, where hydrogen gas is produced through reduction reactions. The membrane facilitates proton transfer while maintaining gas separation to preserve hydrogen purity. Two-chambered MECs typically achieve around 90 % substrate degradation in the anodic chamber and hydrogen production efficiency ranging from 60 % to 75 %. For instance, an H-type MEC fed with acetate generated 1.19 mmol of hydrogen at 0.540 V, 125 while a solarassisted dual-chambered MEC exhibited faster hydrogen production with a Pt-coated electrode at 0.7 V. 128 Besides, higher H₂ levels of up to 50 m³/m³/d with acetate under certain conditions, have been recorded in dual-chambered MECs (Table 6). Nevertheless, the operation of dualchambered MECs is prone to energy losses attributed to factors like Ohmic loss, activation loss, and concentration loss. 126 Furthermore, the membrane itself contributes to an overpotential. Rozendal et al. 129 found that concentration

energy loss could reach 0.38 V due to differences in concentration and pH gradient between the two chambers. However, hydrogen production using dual-chambered MECs may achieve higher levels, up to 50 m³/m³/d with acetate under certain conditions. The calculated cathodic hydrogen recovery and energy input for different cell designs, substrates, and operating voltages are summarized in Table 6.

In contrast, single-chambered MECs lack a membrane between the anode and cathode (Figure 7a), making them compact and cost-effective. These systems offer lower internal resistance and overpotential due to the absence of a membrane. Stacked systems with anodes surrounding the cathode further minimize resistance. 130,131 However, a major challenge with single-chambered MECs is methane interference from methanogens, compromising hydrogen purity. 129,132 Studies comparing mixed culture and pure culture in single-chambered MECs observed methane co-production in mixed cultures, negatively impacting hydrogen production rates. 132,133 Nevertheless, some studies have demonstrated high hydrogen recovery and production rates in single-chamber systems without membranes. 134 Studies on single-chambered MECs have reported hydrogen production rates up to 3.12 m³/m³/d under different operating conditions and feed compositions (Table 6). Despite achieving higher production rates, single-chambered MECs exhibit lower purity due to methane presence. 134,135 Suppression of methanogens in MEC reactors could enhance hydrogen purity, further improving bio-hydrogen quality. 135

Table 7: Physio-Biological parameters involved in MEC performance.²⁵

Substrate	Chamber	Membrane	Cathode	Anod	Microorganism	Ref.
Dyes	Single	No	Graphite brush	TiO ₂ coated Ni foam	Mixed culture	291
Acetate	Single	Ultrex (cation exchange membrane)	Carbon fbre brush	SiNWs photocathode	Mixed culture	292
Acetate	Dual	AMI7001 (AEM)	Carbon fibers with stainless steel fram	Stainless steel mesh	Mixed culture	293
Acetate	Dual	Nafion 117	Non-wet-proofed carbon paper	Carbon paper coated with Pt –d	Mixed culture	294
Wastewater activated sludge	Single	No	Carbon fiber brushes	Stainless steel mesh	Mixed culture	295
Acetate	Single	No	Graphite plates	Ni mesh	Pure culture geobacter sulfurreducens	156
Cellulose and acetate	Single	No	Carbon brushes	Carbon cloth	Mixed culture	296
Corn stack	Single	No	Graphite felt	Pt coated carbon cloth	Mixed culture	297
Domestic wastewater	Dual	Battery separator, rhinohide	Arbon felt with SS mesh	SS wool/mesh	Mixed culture	179
Industrial wastewater/food processing WW	Single	No	Graphite fibre brushes	Carbon cloth with	Mixed culture	167
Liquid of pressed municipal solid waste	Single	No	Graphite felt	Carbon cloth with Ti/RuO ₂	Mixed culture	298
Sugar industry effluents double	Dual	Yes (PEM Nafion 117)	Graphite	Ni foam, SS mesh 304 and Ni plat	Mixed culture	299
Swine wastewater	Single	No	Graphite brush	Carbon cloth with	Mixed culture	300
Fermentation effluents	Single	No	Graphite brushes	Wet proof air cathode carbon cloth with 0.5 Pt mg/cm ²	Mixed culture	301
Romanian Marine waters	Double	PEM Nafion	Glassy carbon	Graphite rod	Mixed culture	302
Sodium acetate	Double	CEM ralex	Graphite felt	Graphite felt biocathodes (-0.7 V)	Mixed culture	303
Sodium acetate	Single	No	Non-wet-proofed carbon cloth	Pt/C	Mixed culture	304
Glucose + sodium acetate	Single	No	Graphite brush]	MoS2-GO nickel foam (NF) cathode	Mixed culture	145

4.4.2 Electrode materials

The effectiveness of MECs technology relies on the selection of suitable and cost-effective electrode materials, with carbon-based materials being the most common choices. 136 These electrodes could enable microbial organisms (MOs) to form biofilms, facilitating crucial electron transfer from the anode to the cathode for hydrogen production. ^{136,137} Anode materials must meet specific criteria to support biofilm formation and efficient electron transfer. Graphite-based materials like granular graphite beds, granules, graphite felt, and brushes have shown high performance and efficiency due to their porosity and surface area.²⁵ However, maintaining surface area while preventing clogging and biofouling poses a challenge. 137 Various electrode configurations, such as porous and plate types, offer advantages in conductivity, cost, and stability, but increasing their surface

area for improved HER presents difficulties. 138 A list of adopted electrode materials used for MECs is shown in Table 7 and Figure 8. Further details are given in subsequent sections, with additional information can been retrieved in Ref. 25,117,119,123,139,140.

4.4.2.1 Anode

An ideal anode material for MECs requires good biocompatibility, a large specific surface area, high conductivity, and corrosion resistance to support bacterial attachment, growth, and electron transfer. 119 It should also account for factors like cost, practicality, material availability, and stability. 119 Carbon-based materials are the most commonly used in MECs due to their affordability, conductivity, and abundance, 140 including carbon paper, carbon cloth, carbon felt, carbon mesh, graphite felt, reticulated vitrified carbongraphite rod, graphite fiber brush, and graphite.²⁵ While

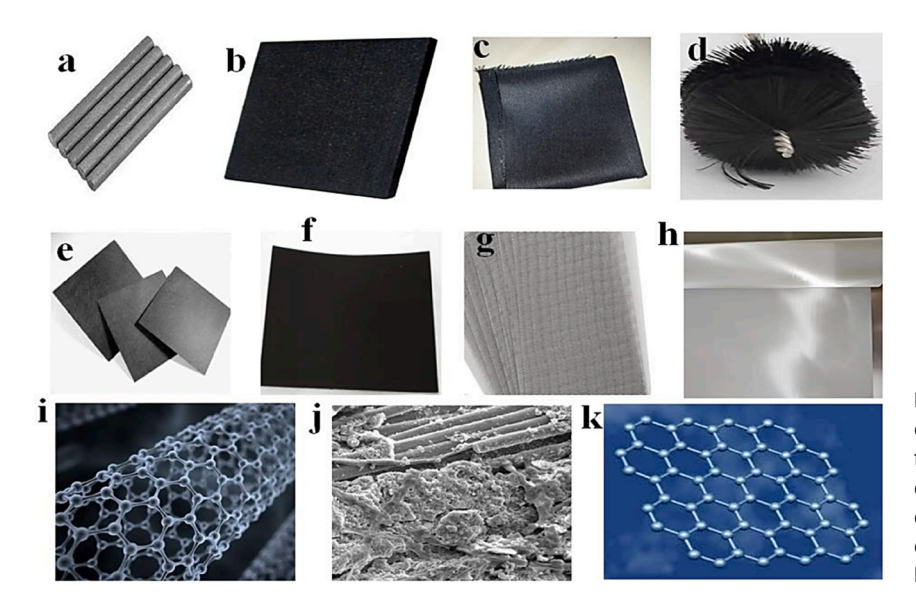


Figure 8: Various conventional and composite electrode types: a) Graphite rods, b) graphite felt, c) carbon cloth, d) carbon fiber brush, e) carbon paper, f) platinized wet-proof carbon cloth, g) stainless steel mesh, h) nickel mesh, i) carbon nanotubes, j) bioanode or biocathode, k) graphene. Adopted from.²⁵

carbon paper, carbon cloth, carbon mesh, and carbon felt are all utilized as standard anode materials in MECs due to their high porosity, each material has its limitations. For example, carbon paper is fragile and lacks durability despite being thin and easily connected to open circuit wires, 28 whereas carbon cloth is more flexible and durable but relatively more expensive.²⁹ Carbon felt has practical properties but suffers from high resistance, ¹⁴¹ and carbon mesh is inexpensive but too thin to maintain structure. 141 Graphitic materials offer better electrical conductivity and stability than ordinary carbon-based materials but come at a higher price. 119 For instance, graphite rod is relatively inexpensive among graphitic materials but limited by low surface area, ¹⁴² while graphite fiber brush is considered a promising future anode material due to its high surface area, low resistance, and market availability. 142

Carbon nanotube (CNT) anodes represent a recent development in MEC research, known for their nanometer size, mechanical stability, lightweight, large surface area, excellent conductivity, and low material cost. Higher electron transfer amplification has been reported with the use of CNTs. Carbon nanotube/polyaniline nanostructure composites and CNTs with gold and palladium nanoparticles are also being established and assessed as anodic materials. However, CNTs can be expensive and may present clogging issues, hindering their widespread application. However, CNTs can be expensive application.

Nanocomposites comprising oxides of titanium (Ti), manganese (Mn), tin (Sn), iron (Fe), among others, combined with carbon-based materials, have also proven effective as anode materials.²⁵ These composite electrodes enhance performance, promote bacterial cell adhesion, and reduce ohmic loss.¹⁴⁷ TiO₂-based electrodes offer biocompatibility

and chemical stability, ¹⁴⁸ while SnO₂-based composite electrodes provide structural stability at a low cost. ¹⁴⁹ Incorporating iron oxide in composite electrodes has shown to enhance extracellular electron transfer, while nickel oxide and manganese oxide are also under investigation. ¹⁴⁸ Conducting polymers like polyaniline (PANI) along with Pt nanoparticles over graphene oxide and PANI, carbon nanotubes on graphite felt, and PEDOT-poly(3,4-ethylenedioxythiophene) over carbon cloth, graphite plate, and graphite felt have been utilized as doping materials to enhance conductivity and anodic performance. ^{150,151} PHBV-poly(3-hydroxybutyrate-co-3-hydroxyvalerate) mixed with carbon nanofibers has also been explored for improved conductivity and cell adhesion. ¹⁵²

4.4.2.2 Cathode

A variety of cathode materials, including carbon-based materials and certain transition metals like stainless steel mesh and titanium, have been explored.²⁵ Cathode materials typically require coupling with a catalyst to enhance the rate of HER. While platinum is the preferred catalyst for HER due to its effectiveness, its high cost and limited availability restrict its widespread use. 119 Moreover, platinum is susceptible to contamination by compounds like sulfide and cyanide, negatively affecting its performance. 153 First-row transition metal compounds are emerging as promising alternatives to platinum-based catalysts for HER due to their abundance, stability, and decent catalytic activity.4 Nickelbased materials and stainless steel are among the extensively studied catalysts due to their natural abundance, stable electrochemical properties, low cost, and high catalytic activity. 119 For instance, Ni-Co-P electrodeposited on stainless steel 316 cathode exhibited superior performance,

achieving the highest coulombic efficiency and an overall energy hydrogen production rate.¹⁵⁴ Further studies have demonstrated the effectiveness of modified cathodes, such as Ni-W and Ni-Mo co-deposited on Ni foam, showing improved corrosion stability and electrocatalytic activity. 155 Phosphorization treatment of stainless-steel cathodes has also been shown to enhance hydrogen production current density. 119 Electroformed Ni mesh cathodes have shown promise as practical alternatives for hydrogen production in MECs, exhibiting comparable performance to Pt/CC cathodes. 156 Overall, the use of catalysts has significantly improved the hydrogen evolution performance of MEC cathodes. The increasing focus on developing Pt-free electrocatalysts for HER water electrolysis underscores the need for continued research in advancing electrocatalysts for hydrogen production in MECs.

4.4.3 Microbial populations: exoelectrogens

Extensive research on exoelectrogens utilized in MECs has been comprehensively reviewed by Kadier et al., 139 Liu et al. 140 and Parkhey and Gupta. 123 Among the exoelectrogenic bacteria for hydrogen production, Shewanella oneidensis and Shewanella putrefaciens from the Gammaproteobacteria family, and Geobacter sulfurreducens from the Deltaproteobacteria family are frequently reported. Additionally, bacteria from other genetic groups such as Ochrobactrum and Rhodopseudomonas from Alphaproteobacteria, Arcobacter from Epsilonproteobacteria, Rhodoferax from Betaproteobacteria, Clostridium from Firmicutes, Propionibacterium from Actinobacteria, and Geothrix from Acidobacteria have also shown anodic respiratory capabilities. 139

These anode-respiring bacteria (ARB) employ one of three mechanisms for extracellular electron transfer: 140,157 (i) a direct contact, where exoelectrogens transfer electrons through their outer membrane directly to the anodecontacting region, 157 (ii) utilizing soluble electron shuttles such as phenazines (e.g., S. oneidensis MR 1), quinones (e.g., S. putrefaciens), and flavins (e.g., Shewanella), 158-160 and (iii) via nanowires or connecting appendages, which is commonly observed in Shewanella and Geobacter. 161 Geobacter species, in particular, have been extensively studied for electron transfer in bioelectrochemical systems, and their dominance in MEC reactors has been well demonstrated. 162,163 The analysis of anodic microbial communities revealed that MEC reactors with predominant populations of the Geobacteraceae family displayed higher power densities than those with varied bacterial communities. 162,163

While pure cultures offer a controlled system for MECs, 139 most MEC reactors utilize mixed consortia of bacteria for H₂ generation. 123 Mixed cultures sourced from wastewaters and sludge present advantages over monocultures, as they are more robust to environmental changes and exhibit higher current densities, leading to enhanced coulombic efficiencies in MEC reactors. 164-167 However, a major drawback of mixed cultures from wastewaters is the potential for cross-contamination with methanogens, which utilize hydrogen gas to produce methane, thereby reducing overall hydrogen yields. 168 Three methods have been proposed to inhibit the growth of methanogens: 169 the first one is adjusting the environmental pH by utilizing a medium solution (pH 5.8) with phosphate buffer. The second is aerating the cathode for 15 min when methane content in the headspace exceeds 5 %. The last one is subjecting the anodes from MFCs to a 15-min boiling process before incorporating them into MECs.

4.4.4 Substrates

Substrates significantly impact hydrogen production in MECs (Figure 9), affecting yield based on their composition, concentration, and type. Various substances, such as acetic acid, lactic acid, butyric acid, glucose, glycerol, cellulose, starch, phenol, methanol, milk, and different types of wastewaters, can feed an MEC for hydrogen production. 25,123,125,126,140,170,171 These substrates are typically categorized into three groups: non-fermentable, fermentable, and various types of wastewaters.²⁵ Different substrates used in MECs are summarized Tables 6 and 7.

Non-fermentable substrates, such as acetic acid, butyric acid, lactic acid, glucose, and propionic acid, are well-suited for MECs. 119,168 Among these, acetate stands out as the most extensively studied feed material. 139 Acetate exhibits promising results, with two-chamber MECs capable of achieving a theoretical hydrogen recovery of 4 mol H₂/mol at an external applied voltage of 1 V. Moreover, single-chamber MECs fed with acetate demonstrate higher hydrogen production quantities due to reduced resistance and lower pH gradients within the system. 172,173

Fermentable organics, such as lignocellulosic biomass, stand out as highly viable feedstock for MECs due to their extensive study and widespread acceptance. 174 Among these, polymeric substrates like hemicellulose, cellulose, and aromatic polymers, including lignin, exhibit remarkable potential for HER.²⁵ Despite their cost-effectiveness and renewability, these substrates require conversion into monosaccharides or low molecular weight compounds to optimize hydrogen yield. For addressing this issue, pretreatment methods are often employed to remove lignin from lignocellulosic biomass, thereby enhancing its

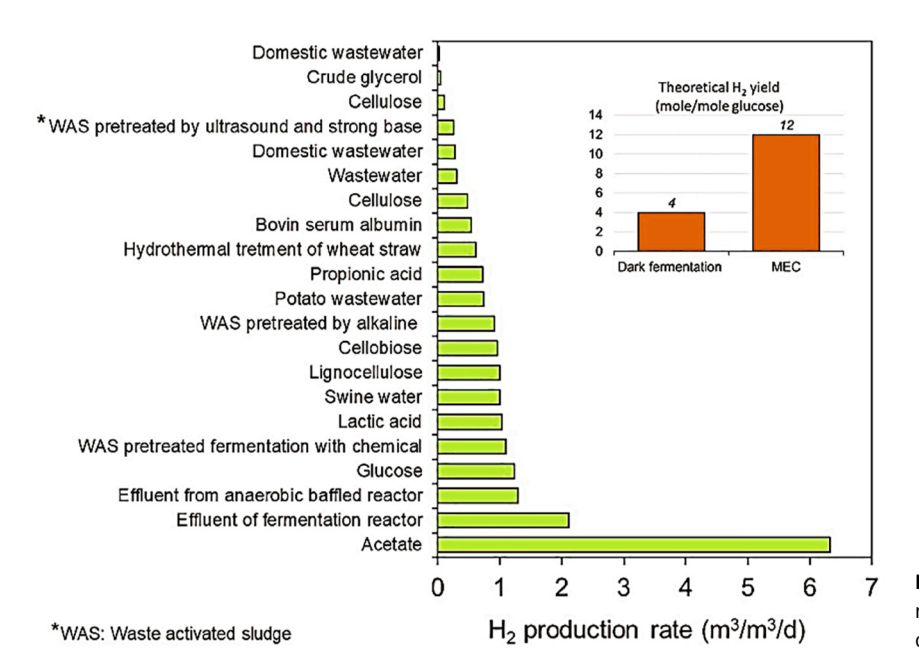


Figure 9: Hydrogen gas production rate of microbial electrolysis cells (MECs) depending on the substrate types. From. ¹¹⁷

digestibility within MECs.^{25,171} A notable approach involves the combined use of dark fermentation and electrohydrogenesis, which has shown promising results in dealing with recalcitrant lignocellulosic materials, leading to increased yields and improved rates of hydrogen production.^{175,176} Comparative analyses have further underscored the advantages of winery wastewater over domestic wastewater as a feedstock for MECs, indicating higher outputs.¹⁶⁵ Effective processing of complex waste substrates involves hydrolysis and fermentation to break down complex macromolecules into simpler compounds, facilitating efficient hydrogen production.^{25,176}

Wastewater is abundant in contaminants and nutrients that require treatment. Additionally, wastewater treatment plants generate large amounts of waste activated sludge (WAS), posing a significant disposal challenge. Both wastewater and WAS can serve as valuable feedstocks for hydrogen production in microbial electrolysis cells (MECs).^{170,177} MECs provide the dual benefit of contaminant removal and energy generation. 170,177 Various types of wastewater, including those rich in cellulose and glucose, as well as domestic and industrial wastewater have been considered in MECs. 165,170,177,178 Therefore, the integration of MECs into wastewater treatment infrastructure represents a step towards a circular economy, where waste products are transformed into valuable resources. By utilizing either WAS or wastewater itself as feedstocks for hydrogen production, MECs contribute to resource recovery and energy independence goals.¹⁷⁷

4.4.5 Challenges and future aspects

In summary, biological hydrogen production in MECs is gaining prominence due to its sustainable nature and low voltage requirements. However, there's a need for improved performance and cost-effectiveness, driving the exploration of new building materials and optimized designs for MECs.²⁵ To enhance efficiency, reducing overpotential and associated losses is crucial. Strategies such as electrode optimization, membrane enhancements, and the use of high surface area electrodes show promise. 119,139 Studies have demonstrated significant overpotential reduction by introducing CO₂ to the cathodic chamber and employing novel catalysts like Ni₂P nanoparticles coated electrodes. Additionally, integrating photocatalysts and exploring bio-cathodes offer avenues for further improvement. 117 Membrane development is also essential, with research focusing on costefficient alternatives to Nafion membranes and strategies to combat biofouling.

On a larger scale, pilot studies have highlighted challenges related to substrate utilization and membrane durability. 178,179 While phosphate buffer solution remains a popular choice for catholytes, further research into electrolytes is warranted. Understanding the role of exoelectrogens like *Shewanella* and *Geobacter* in biofilm formation and electron conduction is critical for optimizing MEC performance. 119,137 Techno-economic assessments and life cycle analyses are essential for evaluating MEC viability. 180

Future efforts should focus on scaling up MECs, utilizing real wastewater, and integrating MECs with other processes like anaerobic digestion for enhanced performance. While a succent review is provided here, a comprehensive overview of MEC technology and its challenges, further research is needed in electrolytes, efficient design, hydrogen storage, and materials to realize successful pilot-scale implementation. Additional reviews addressing these domains would be valuable for advancing MEC technology.

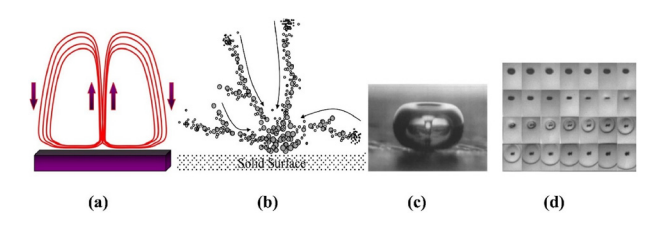


Figure 10: Physical effects of acoustic cavitation, (a) acoustic streaming (oscillator is located at the bottom and liquid surface is at the top), (b) microstreamers, (c) microjet and (d) shockwaves generated by ultrasound and acoustic cavitation. Form. 181

4.5 Application of external stimuli

4.5.1 Ultrasonic field

Ultrasonic irradiation stands as a widely embraced technique among researchers aiming to facilitate the gas bubbles detachment from electrodes. This method capitalizes on the phenomenon of acoustic cavitation, where tiny microbubbles form, expand, and abruptly collapse, inducing micro-agitation and intense microturbulence, known as acoustic streaming, in the vicinity of the electrode surface. 181 Essentially, ultrasonic vibrations cause the medium to oscillate back and forth, leading to a steady streaming away from the piezo location, as illustrated in Figure 10a. This oscillatory flow triggers an acoustic streaming effect, as depicted in Figure 11a, characterized by notable microagitation near the electrode surface and consequential mass transfer effects, fostering intense mixing. Moreover, the interaction between sound waves and gas bubbles gives rise to bubble streamers in an acoustic field, as shown in Figure 10b. 181 These oscillating gas bubble streamers, driven

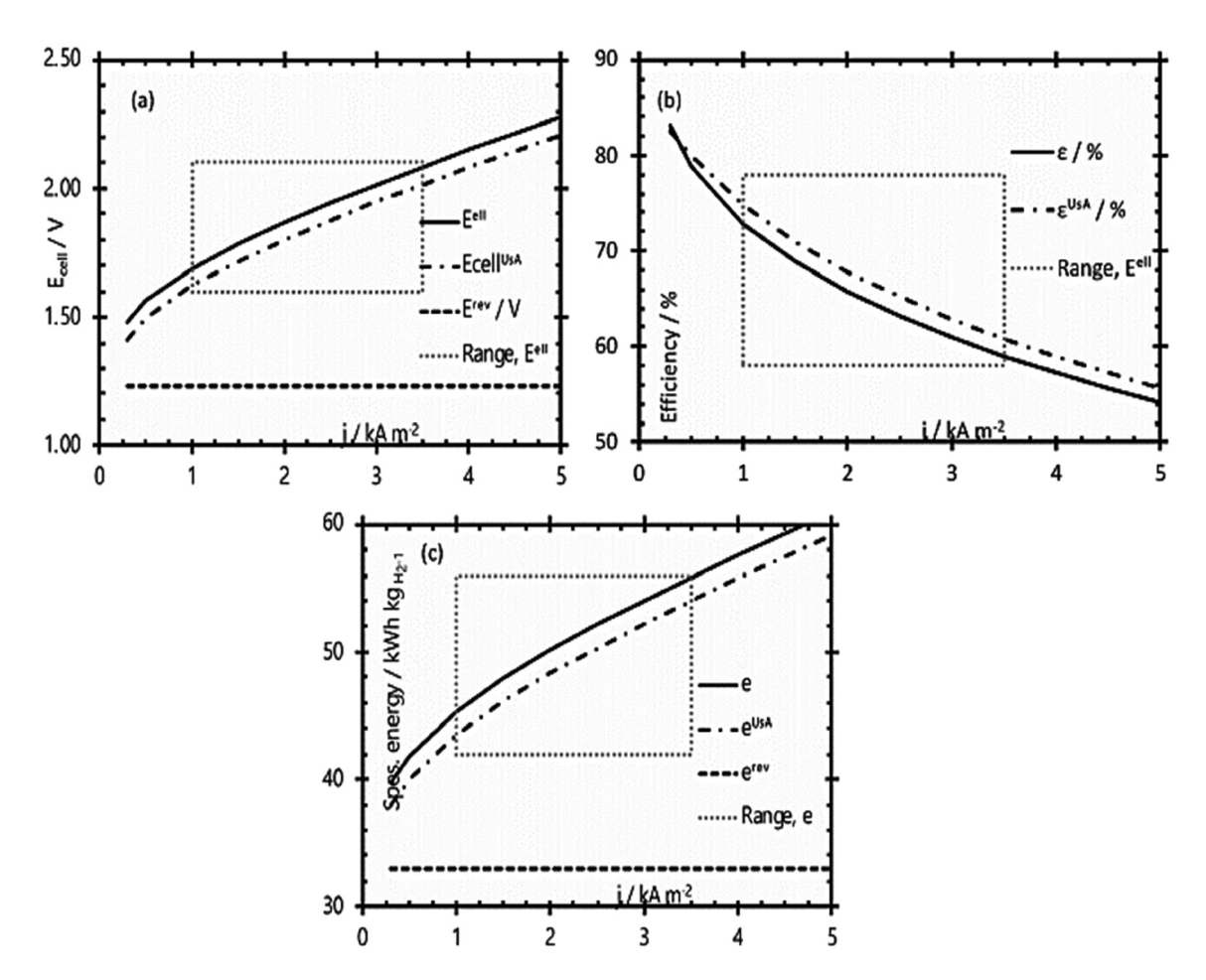
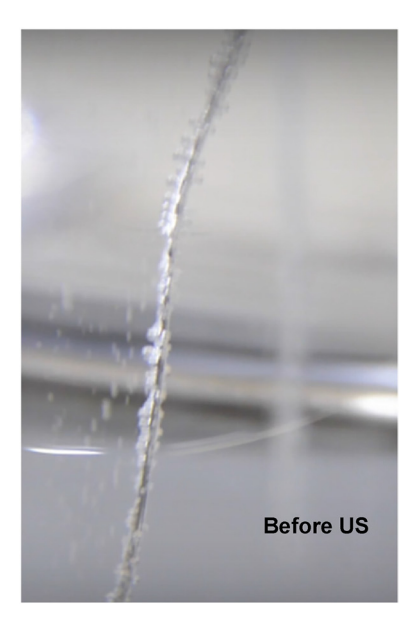


Figure 11: Ultrasonication effect on (a) cell voltage (b) efficiency (ε) and (c) specific energy for hydrogen production (USA: Ultrasound-assisted). From. 182

by primary and secondary Bjerknes forces, propel towards pressure antinodes at high speeds. This microstreaming effect engenders a plethora of physical forces, pivotal in various applications, including expediting the detachment of gas bubbles from the electrode. Among the significant forces generated during acoustic cavitation are microjets (Figure 10c) and shockwaves (Figure 10d). 181 Asymmetric collapse of cavitation bubbles, particularly near a boundary, forms high-speed liquid jets capable of pitting metal surfaces, whereas symmetrical collapse leads to the generation of high-intensity shock waves. Collectively, these ultrasoundinduced actions in the solution effectively cleanse the electrode surface and augment the mass transfer of electrolytes from the solution to the electrode, thereby reducing overpotential through decreased solution and gas resistance. A 2019 review by Islam et al. 182 investigated the potential of power ultrasound to overcome limitations in electrochemical water splitting for hydrogen production. Their findings suggest ultrasound offers several advantages. Firstly, it can clean and activate electrode surfaces, leading to enhanced performance. Secondly, ultrasound promotes increased ions movement within the electrolyte and near the electrode surface, boosting mass transfer and facilitating the reaction. Thirdly, it effectively removes gas bubbles from both the electrolyte and the electrode surface, improving overall efficiency. Islam et al. also observed an increase in electrolytic efficiency (up to 15-20 %) attributed to a combination of factors like higher ion concentration and bubble detachment at the electrode surface, as shown in Figure 11. Photographic visualization of hydrogen bubbles on Pt wire electrode (Figure 12) clearly shown the cleaning effect of sonication.

In the context of water sono-electrolysis, several studies have been done. Li et al. 183 investigated the effect of ultrasonic fields on water electrolysis in alkaline solutions. They observed a significant decrease in cell voltage with the application of an ultrasonic field, particularly at higher current densities and lower electrolyte concentrations. At a constant current density, the reduction in cell voltage under an ultrasonic field decreased with increasing NaOH concentration. The efficiency of H₂ production increased by 5-18 % at higher current densities under an ultrasonic field, with energy savings of up to 10-25 %. Hung et al. 184 studied the combined effect of an ultrasonic field and PVDF-g-G1 BM synthesis membrane for H₂ production. They found that H₂ production efficiency was higher in electrolytic cells with an ultrasonic field compared to those without. Energy saving in H₂ generation using PVDF-g-G1 BM membrane was 15.0-20.0 % and 8.0-12.0 % for cells operated with and without an US field, respectively. Lin and Hourng¹⁸⁵ investigated the impact of a 133 kHz-ultrasonic field with power ranging from 225 to 900 W, in conjunction with varied input voltages, electrolyte concentrations, and electrode gaps. They found that applying a 2.0 V potential along with the US field improved both concentration impedances and activity impedances, while also accelerating the release of hydrogen bubbles. Notably, ultrasonic power, electrolyte concentration, and electrode gap emerged as pivotal factors influencing water electrolysis performance. Under normal temperature conditions, with a 2 mm electrode gap, 4 V potential, and 40 wt% electrolyte concentration, the difference in current density between electrolysis with and without 225 W sonic power was 240 mA/cm². Accounting for the power required for the ultrasonic wave, this resulted in a



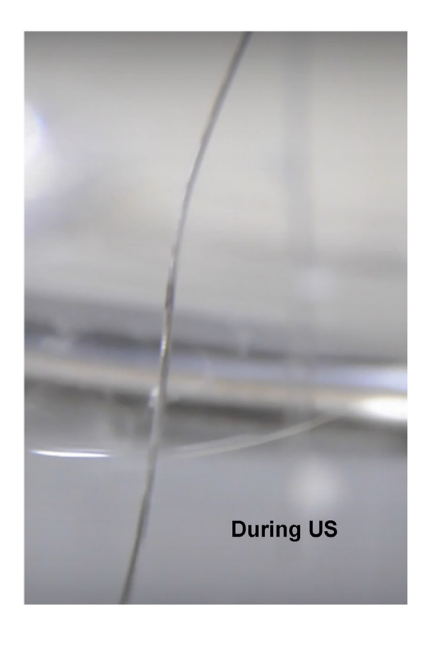


Figure 12: Hydrogen production on Pt wire before and during sonication (US). From. 182

power saving of 3.5 kW and an economic power efficiency of 15%. Additionally, they observed a 20% increase in electrolysis efficiency with a 675 W ultrasonic power, in 10 wt% KOH, with a 5 mm electrode gap, and a specific input power.

Merabet and Kerboua¹⁸⁶ conducted a thorough investigation into alkaline water electrolysis, examining the impact of continuous and pulsed ultrasound under various operational parameters. They found that integrating continuous ultrasound under optimal conditions of KOH electrolyte and nickel foam electrodes led to a 7.78 % increase in cell current, corresponding to 64% decrease in bubbles resistance. Interestingly, the effect of sonication was negligible at 45 °C (the optimal temperature), while room temperature showed better operation performance of the sono-electrolyzer in compared to silent conditions. Continuous mode sonication consistently outperformed pulsed mode, both kinetically and energetically. In a subsequent study, Merabet and Kerboua¹⁸⁷ introduced a membraneless sono-electrolyzer powered by photovoltaics (PV), utilizing alkaline electrolysis and indirect pulsed and continuous 60 kHz sonication. The results showed that indirect continuous sonication achieved the lowest electrode coverage percentage at 37 %, compared to 82% without sonication and 58.3% with pulsed ultrasonication. Furthermore, the bubble resistance decreased significantly from 569.81 m Ω without sonication to 132.54 m Ω with continuous sonication and 273.42 m Ω with pulsed sonication. Indirect continuous sonication evidenced the most effective mode for bubbles subtraction, resulting in a 76 % reduction in bubble resistance compared to no sonication and a 52 % reduction compared to pulsed sonication.

However, it should be noted that prolonged use of sonication must be approached with caution, as it can cause electrode degradation due to the asymmetric collapse of bubbles near solid surfaces, resulting in micro-iets with speeds of up to 100 m/s. 181 While low-frequency sonication (20-100 kHz) is beneficial for physical processes like cleaning and degassing, high-frequency sonication (above 100 kHz) may lead to electrolyte degradation, especially with organic electrolytes or ion liquids. The chemical effects of sonication in aqueous solutions are commonly used for the degradation of organic and inorganic contaminants. 188,189 Therefore, in water electrolysis for hydrogen production, frequency selection should not exceed 100 kHz. It is advisable to use low frequency with higher power to avoid any chemical effects of ultrasound. Additionally, while the power required to generate the ultrasonic field was found to be lower than the power saved from the enhanced efficiency, 183 there's a suggestion that employing an ultrasonic field in water electrolysis might not be economically viable for hydrogen production due to the cost associated with the system required to generate the ultrasonic field. 185 This

includes expenses related to transducers and utilities for measuring the acoustic pressure (e.g., hydrophones). This economic challenge could become more significant as operations scale up to industrial levels.

4.5.2 Magnetic field

Studies examining the impact of magnetic fields on electrolysis efficiency showed predominantly positive outcomes. 190-194 The enhancement effect of magnetic fields on electrochemical reactions primarily stems from magnetohydrodynamic convection induced by the Lorenz force, ^{195,196} which improved bubble detachment. Iida et al. 197 applied a strong magnetic field of 5 T to water electrolysis, resulting in significant reductions in cell voltage, particularly notable in alkaline solutions and at high current densities. Lin et al. 198 observed that this effect becomes more pronounced with decreased electrode spacing. Additionally, materials exhibiting ferromagnetism, like nickel, outperform paramagnetic (e.g., platinum) and diamagnetic (e.g., graphite) materials when subjected to a magnetic field. 198 For instance, using a nickel electrode with a 2 mm inter-electrode distance and a 4 V cell voltage led to a 14.60 % increase in current density. 198 Iida et al. 197 demonstrated improved water electrolysis efficiency through a magnetic field's ability to reduce electrode overpotential [1817]. This effect was observed across various electrolyte conditions, including acidic media (0.05 M H₂SO₄) and alkaline solutions (4.46 M and 0.36 M KOH). Notably, the reduction in OER overpotential was greater compared to the hydrogen evolution reaction HER overpotential under the magnetic field. This difference was attributed to the varying sizes of gas bubbles produced during each process. The researchers proposed that magnetohydrodynamic (MHD) convection plays a crucial role. MHD convection influences bubble detachment from the electrode surface, leading to a significant decrease in the void fraction and the area covered by gas bubbles. This ultimately enhances the overall electrolysis efficiency. Matsushima et al., 199 through measuring supersaturation in the electrode-electrolyte interface and the mass transfer coefficient of dissolved H2 via the current interrupter method, concluded that a magnetic field promotes the mass transfer of dissolved H2, releasing supersaturation near the electrode. In another study, Matsushima et al.²⁰⁰ found that the average bubble layer thickness (δ) on both cathode and anode was reduced by a magnetic field. Wang et al.²⁰¹ expanded on the explanation of magnetic field effects, suggesting that the rotational force applied to H₂O molecules due to the interacting charge and induced charge of the Lorentz force from the induced magnetic field contributed to increased efficiency. They also proposed that the induced magnetic field diminished friction caused by

hydrogen bonding. Consequently, ohmic voltage drops and reaction overpotential are noticeably reduced in the presence of a magnetic field, resulting in lower cell voltage for water electrolysis. Furthermore, it was found that the inclusion of a magnetic field allowed for a reduction in electrolyte concentration, ^{192–194,198} which would be valuable in lowering the overall electrolyte corrosive aspect, thus reducing operating costs associated with electrode corrosion.

4.5.3 Super gravity field

The slow detachment of bubbles in the electrolytic cell, especially at high cell voltages, is a significant issue in water electrolysis. Wang et al. 196 provide an insightful analysis of how a high-gravity field influences bubble detachment. Bubble movement within the cell is primarily controlled by interphase buoyancy, $\Delta \rho g$, where $\Delta \rho$ is the phase density difference and g is the applied acceleration. 196 Buoyancy acts as the driving force for bubble disengagement, causing bubbles to move in the direction of buoyancy during electrolysis. Applying an external force in alignment with the buoyancy direction can significantly enhance bubble disengagement. Consequently, in the context of water electrolysis, this approach can diminish bubble coverage on the electrode surface and reduce bubble dispersion in the electrolyte, particularly in the presence of a super gravity field. As a result, both reaction overpotential and ohmic voltage drop are mitigated, leading to a decrease in cell voltage and energy consumption.

Figure 13a depicts a captured photograph of the electrode surface during hydrogen bubble evolution under normal gravity conditions.²⁰² The image reveals numerous bubbles, each approximately 200 um in diameter, adhering to the electrode surface. In contrast, Figure 13b illustrates the same process under a super gravity field, where only a few bubbles are observed, and their movement is barely discernible. To gain further insight into this phenomenon, let's consider the scenario inverted and operate under microgravity conditions (with gravitational forces weaker than those on Earth). In such conditions, there is a higher intensity of larger bubble coverage on the electrodes, as demonstrated in Figure 13c and 13d. This scenario presents several challenges, including bubble adherence to the electrode and membrane, the accumulation of high gas volume fractions in the electrolyte, and the need to increase electrode spacing to facilitate bubble removal.²⁰³ These factors contribute to increased overpotential and process costs.

Therefore, the enhanced buoyancy force and reduced bubble volume under the super gravity field facilitate the rapid separation of bubbles from the electrolytic cell.²⁰⁴

Consequently, the bubble layer thicknesses (δ_{HG} and δ_{OG}) near both the cathode and anode under the super gravity field (Figure 13f) are expected to be smaller than those ($\delta_{\rm H}$ and δ_0) under normal gravity conditions (Figure 13e). The reduction in bubble layer thickness plays a crucial role in reducing electrolyte resistance and the ohmic voltage drop, primarily due to the diminished dispersion of bubbles within the electrolyte when exposed to the super gravity field. Importantly, the impact of the super gravity field on reducing cell voltage is more pronounced with higher current densities for water electrolysis, as indicated by the relationship between bubble layer thickness (δ) and its effect on cell voltage reduction.²⁰⁴

Cheng et al.²⁰⁵ were the first who demonstrate the effectiveness of a super gravity field in intensifying the water electrolysis process. They achieved a reduction in cell voltage of approximately 0.70 V at 3.0 kA/m² under 190 g (a relative acceleration) compared to normal gravity environments. Similar findings were replicated by Wang et al. ^{202,204} The relationship between the cell voltage of water electrolysis under a super gravity field (U_G) and the gravity coefficient (G) was expressed using the general formula:²⁰⁴

$$U_G = D \log G + U_1 \tag{34}$$

where, U₁ represents the cell voltage under normal gravity conditions (G = 1), D signifies the rate of change of cell voltage with the logarithm of G. The maximum energy saving percentage reaches approximately 17 %. 204 Cheng et al. 205 estimated that the potential energy savings could reach up to 30 kW in a 100 kA electrolytic cell, whereas it was only 2 kW for the super gravity field. The reduction in cell voltage was primarily attributed to a decrease in ohmic voltage drop compared to the reduction in reaction overpotential, particularly at higher current densities and gravity accelerations. 204

Lao et al.²⁰³ also reported the increase of electrohydrogen yield in a centrifugal acceleration field. At normal conditions (7.7 M KOH solution, 348 K), significant reductions in cell voltage were observed at an acceleration of approximately 16 g (~500 rpm of rotational speed). The rotary electrolyzer achieved cell voltages about 0.25-0.5 V lower than equivalent static cells under similar conditions, depending on the current density. These voltages were comparable to those of fully developed pressurized cells in industrial settings, even without an effective electrode catalytic coating. Furthermore, at a higher acceleration of 41 g, the rotary cell sustained a current density of up to 13.5 kA/m² without experiencing gas bubble blinding of the membranes and electrodes. This study demonstrates the potential for intensification compared to typical commercial systems with current densities of about 5 kA/m².

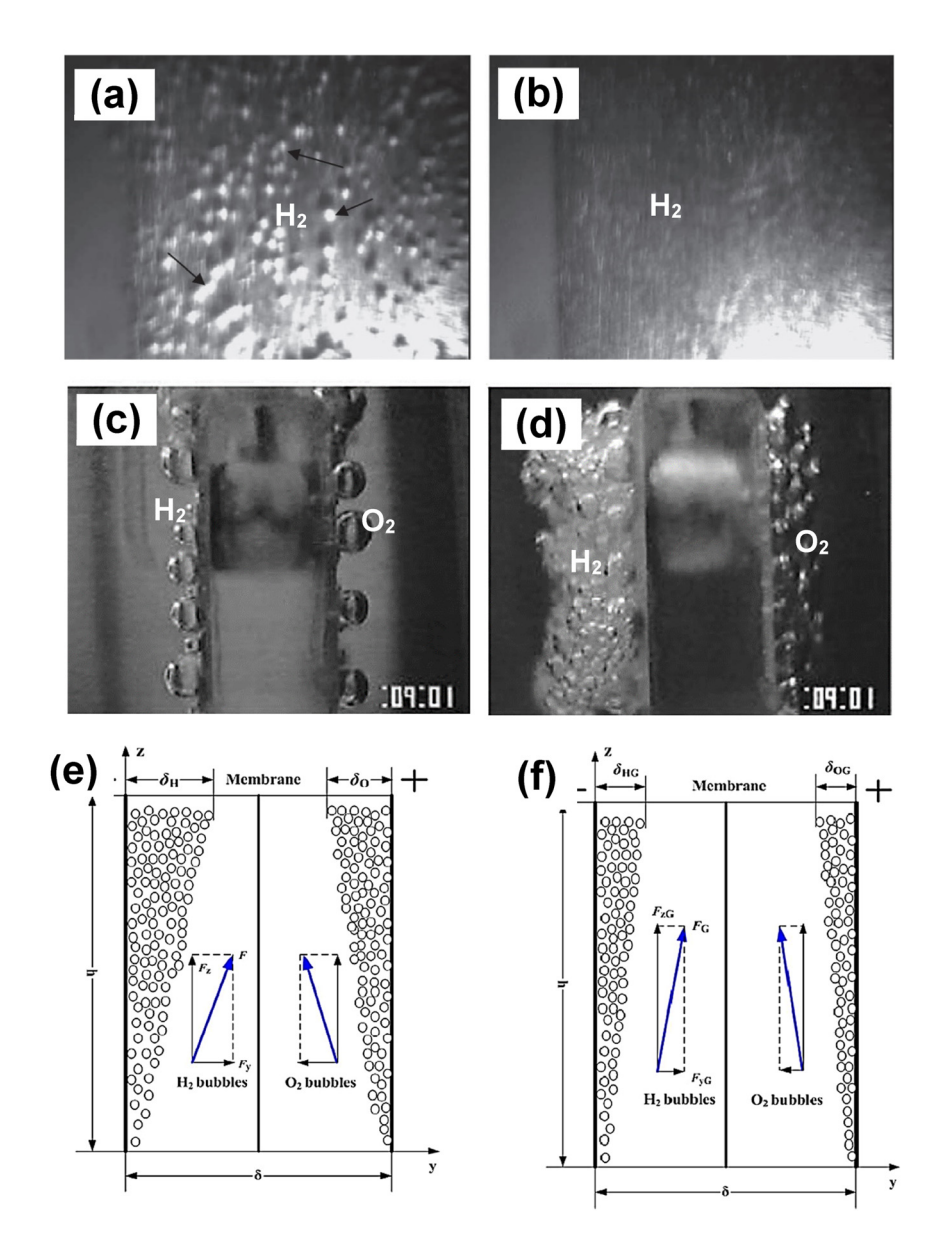


Figure 13: The electrolytic formation of hydrogen and oxygen, (a,b) photographs of cathode surface during hydrogen bubble evolution process at 0.05 A/cm² under (a) normal gravity condition (G = 1) and (b) super gravity field (G = 1 01) in 0.5 M H₂SO₄ aqueous solution. (c,d) gas (H₂, O₂) bubbles evolution in alkaline electrolyte under (c) terrestrial gravity and (d) microgravity conditions, at 8 s after starting water electrolysis using KOH solution. (e,f) Bubbles layer formed in the vicinity of electrodes' surfaces in the absence (e) and under super gravity field (f). [(a, b): From Wang et al. 202 (c,d): From Matsushima et al.305 (e,f): From Wang et al.196

4.6 Seawater electrolysis

Given the vast abundance of seawater, comprising over 96 % of the total water reservoir, and its economically viable potential, the conversion of seawater into hydrogen using renewable electricity represents a promising pathway toward achieving energy sustainability.²⁸ Recent advancements in research have significantly improved our understanding of seawater electrolysis mechanisms, leading to the formulation of design principles such as alkaline design

criteria and the development of chloride blocking layers to enhance catalyst performance.²⁶ Many comprehensive reviews underscored both the significant advancements and the substantial challenges faced in seawater electrocatalysis.²⁶⁻²⁹ In the subsequent sections, we delve into the essential aspects of seawater electrolysis, including challenges and recent advancements in electrode materials. Strategies for developing highly active and selective catalysts for seawater electrolysis, even in the presence of contaminants such as chloride, metal ions, and bio-organisms,

are outlined, along with considerations for electrolyzer design. Additionally, various opportunities for advancing this promising technique are discussed. However, for in-depth analysis, readers are encouraged to refer to the aforementioned article reviews, i.e. ^{26–29}

4.6.1 Challenges of seawater electrolysis

The complexity of seawater poses a significant challenge for seawater electrolysis, primarily due to the diverse range of components present, including microorganisms, sediment, and various ion species. Sediment and microorganisms, which primarily impact the cleanliness of seawater electrolyzers, can be addressed through filtration pretreatment. However, seawater ionic species (i.e., Cl⁻, Br⁻, SO₄²⁻, HCO₃⁻, CO₃²⁻, F⁻, Mg²⁺, Na⁺, Ca²⁺, Cu²⁺, K⁺, Sr²⁺, and Cd²⁺) cannot be easily filtered out, these ions can lead to veritable issues at both the cathode and anode during electrolysis. Therefore, the influence of these species must be carefully considered in seawater electrolysis processes.

At the cathode, the significant challenge for HER arises from the dramatic rise in local pH near the cathode surface as the electrolysis current increases. This pH increase can lead to the formation of precipitates such as Ca(OH)2 and Mg(OH)₂ from seawater cations, consequently blocking HER reactive sites. 44 Currently, two potential solutions are being explored:²⁸ (i) the addition of pH buffers to stabilize pH fluctuations in the seawater electrolysis system, and (ii) the design of suitable seawater electrolyzers to facilitate the separation of sediment from the cathode surface. Furthermore, certain metal ions dissolved in seawater, such as Cu²⁺, Cd²⁺, and Pb²⁺, have a tendency to deposit on the cathode surface at specific potentials. These deposits not only compete with HER but also significantly reduce electrode durability.²⁷ Therefore, catalyst designs should aim to suppress these undesirable electrochemical processes to achieve high selectivity for HER in seawater electrolysis.

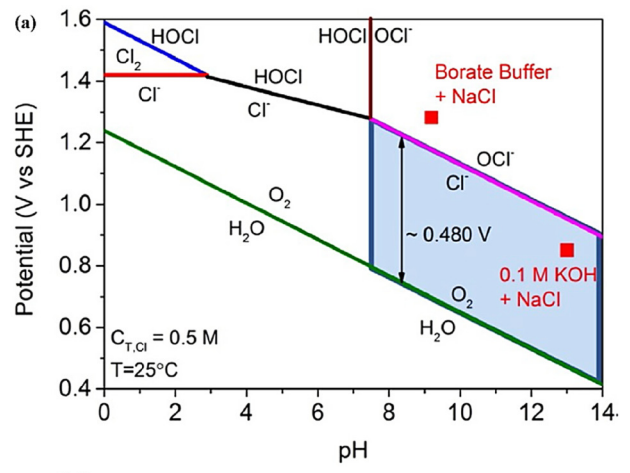
At the anode, the OER is notably influenced by chemically active anions found in seawater. Specifically, chloride (Cl⁻) chemistry is expected to compete with the anodic OER due to its standard redox potential range of 0.9–1.6 V.²⁶ Pourbaix diagram incorporating both the OER and chloride chemistry is shown in Figure 14. This^{29,206} diagram reveals that the chlorine evolution process (ClER) occurs at low pH (<3) (Eq. (35)), while hypochlorite production occurs at high pH (>7.5) (Eq. 336), representing the primary competing reactions for OER at the anode. Consequently, Cl⁻ ions in seawater compete with the OER reaction, and the resulting

 \rm Cl_2 (oxidant) can lead to severe corrosion of the seawater electrolyzer.

$$2Cl^{-} + 2e^{-} \rightarrow Cl_{2}$$
 $E^{0} = 1.36 \text{ V vs. SHE}$ (35)

$$Cl^{-} + 2OH^{-} \rightarrow ClO^{-} + H_{2}O + 2e^{-}$$
 $E^{0} = 0.89 \text{ V vs. SHE}$ (36)

Although thermodynamics favor the OER, both ClER and hypochlorite production (Eqs. (35) and (36)) are two-electron reactions that are kinetically more favorable compared to the four-electron OER. Interestingly, when the electrolyte becomes alkaline, the product of Cl⁻ oxidation transitions



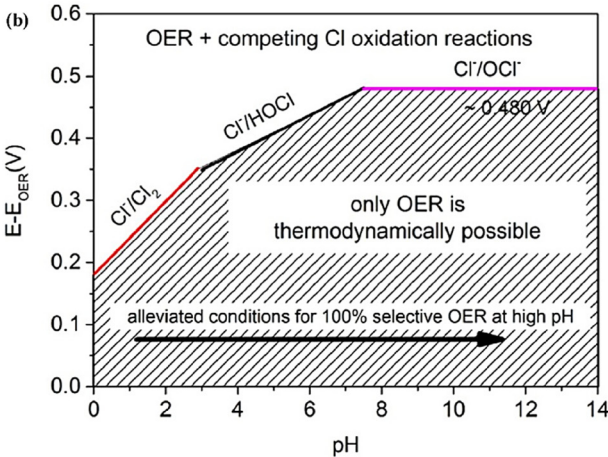


Figure 14: The pourbaix diagram for the OER and the chloride chemistry in aqueous saline electrolyte. 0.5 M NaCl dissolved in this aqueous solution and no other chlorine sources, including the H2O/O2 and the Cl-/ cl₂/HOCl/ClO- redox couples. This figure depicts the potential-pH region where OER and chloride oxidation reactions may occur thermodynamically. The green line represents the thermodynamic equilibrium between H2O and O2. When the electrode potential is more positive than the green line, the OER process becomes thermodynamically possible. The red line shows the competing acidic oxidation of chloride to free gaseous Cl2. The black and purple lines mark the beginning of the oxidation of chloride to HOCl or OCl-. Form.²⁰⁶

from HOCl to OCl⁻, and the thermodynamic overpotential maintains a consistent gap of 480 mV with OER (Figure 14a). Therefore, utilizing a high-performance OER catalyst under alkaline conditions and limiting the overpotential below 480 mV theoretically allows for the complete prevention of Cl⁻ oxidation.²⁷ This principle, known as the 'alkaline design criteria' for seawater electrolysis, has been elucidated by Tong et al.²⁰⁶ and Dionigi et al.²⁹

4.6.2 Electrocatalysts for seawater splitting

Seawater electrolysis presents a big challenge due to the presence of cationic metals and abundant corrosive chloride anions, necessitating robust and efficient electrocatalysts, particularly for the anode. 44 Figure 15 compares the performance of various tested catalysts under diverse testing conditions, including acidic, neutral, basic, simulated seawater, and natural seawater electrolytes.²⁸ Among the tested OER catalysts, in addition to those adopted in pure water, noble metals such as Ir and Ru, as well as transition metal oxides, hydroxides, nitrides, phosphorus-doped complexes, and layered double hydroxides (LDHs), have demonstrated high activity.²⁸ However, when considering only current density and overpotential, the performance differences among various OER catalysts are minimal (Figure 15), as only a portion of the currents is utilized for OER, with additional energy consumed by the oxidation of Cl⁻. Actual seawater electrolysis is even more complex, with many catalysts exhibiting excellent performance in simulated seawater but suffering from performance losses in natural saltwater due to the presence of numerous impurity ions. ⁴⁴ The ClER reaction of Cl⁻ competes with OER, while the deposition of heavy metal ions in seawater affects the catalytic performance of the cathode. ²⁷ Subsequently, we will analyze numerous OER and HER electrocatalysts for seawater electrolysis.

Guided by DFT computation, Hsu et al.207 has engineered an MHCM-z-BCC (MHCM: Transition metal hexacyanometallate; z-BCC: ZIF-67 on the basic cobalt carbonate surface) electrode, demonstrating remarkable selectivity towards the OER in seawater. While Pt^{OER}//Pt^{HER} and IrO₂^{OER}//Pt^{HER} electrolyzers produced 50 and 22 µM of Cl₂, respectively, after 12 h in buffered seawater (pH ~7), the MHCM-z-BCC^{OER}//NiMoS^{HER} electrolyzer exhibited no detectable Cl2 even after 100 h, indicating minimal CIER. Additionally, using the NiMoN@NiFeNOER//NiMoNHER electrolyzer in simulated seawater (1 M KOH with 0.5 M NaCl), only H₂ and O₂ gases were detected with a molar ratio close to 2:1, and a Faradaic efficiency of approximately 97.80 %, ²⁰⁸ demonstrating high selectivity for OER on the anode. Moreover, CoFe LDH displayed a Faradaic efficiency of ~94.0 % at an overpotential (n) of 560 mV.²⁰⁹ Nevertheless, deviations in Faradaic efficiency were observed for both O₂ and H₂ evolution during OER and HER, respectively.

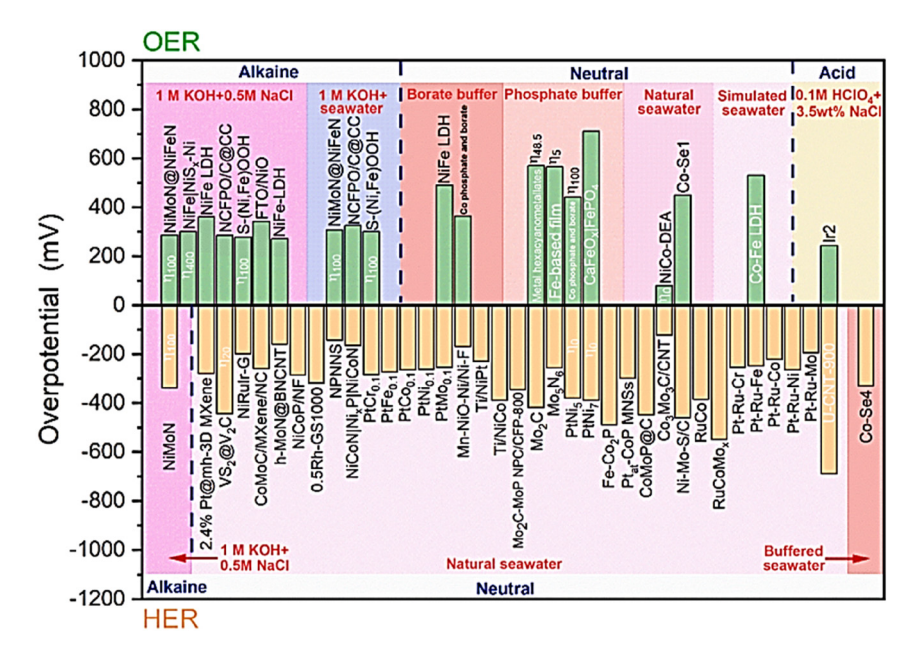


Figure 15: Comparison of the activity of various HER and OER catalysts tested in acidic, neutral, and basic media. Different solutions (natural seawater, simulated seawater or buffered seawater) are distinguished by different color patches. The term overpotential (η) is used to define the overpotential at a certain current density (e.g., 5, 20 and 100 mA/cm², labeled $η_5$, $η_{20}$ and $η_{100}$). If there is no special description, it means that the current density is 10 mA/cm². From.²⁸

NiCoP exhibited approximately 96.5 % Faradaic efficiency for about 60 min, ²¹⁰ while $Ni_5P_4@Ni^{2+} {}^{\delta}O_{\delta}(OH)_{2-\delta}$ displayed nearly 93.0 % Faradaic efficiency with minimal side of CIER reactions during electrolysis (the H2 vield increased linearly). 211 Similarly, Mn-NiO-Ni showed nearly 100 % Faradaic efficiency within 1 h, but deviations occurred after 1h, with approximately 70.0 % Faradaic efficiency observed after 7 h, suggesting the presence of side reactions consuming about 30 % of the total charge. 212 Furthermore, NiRuIr-Graphene exhibited nearly 100% Faradaic efficiency for 2 h during HER in seawater, 213 indicating minimal side reactions.

In more detail, Kuang et al.²¹⁴ demonstrates the effectiveness of dual-layered anode fabrication and subsequent activation in combating chloride corrosion for long-term stability in seawater electrolysis. For instance, their research shows that the NiFe-NiSx-Ni^{#OER}//Ni-NiO-Cr₂O₃^{HER} electrolyzer, equipped with an activated NiFe-NiSx-Ni anode, maintains negligible decay even at high current densities. Specifically, the activated NiFe-NiSx-Ni anode exhibits a low overpotential of ~300 mV at 400 mA/cm² in 1 M KOH with 0.5 M NaCl, significantly lower than the typical of ~480 mV (threshold n). This reduced overpotential indicates its superior resistance to hypochlorite formation, a critical factor for ensuring selective oxygen evolution. Moreover, while the activated NiFe-NiSx-Ni anode remains stable for over 500 h, its counterpart, the activated NiSx-Ni anode, deteriorates rapidly in harsh electrolytes, such as 1 M KOH with 2 M NaCl. These findings underscore the importance of anode activation in achieving high corrosion resistance and OER activity. paving the way for efficient seawater electrolysis.

Yu et al. research²⁰⁸ highlights the benefits of employing a metal nitride anode with a core-shell structure, particularly with a NiFe-based shell, for enhancing OER in seawater electrolysis. This configuration enables the *in situ* formation of thin amorphous layers during OER, improving corrosion resistance against chloride ions. Additionally, the core-shell design allows for electronic structure tuning, increased exposure of active sites, enhanced charge transfer, and improved gas evolution, collectively boosting OER efficiency in seawater. Their study demonstrates that the NiMoN@Ni-FeN^{OER}//NiMoN^{HER} electrolyzer maintains negligible decay even after 100 h of operation at 100 mA cm² in. Furthermore, studies by Ding et al.²¹⁵ demonstrate that cellular stainless steel, characterized by high conductivity and tensile strength, facilitates efficient OER performance by exposing ample active sites and supporting effective charge transfer. Their research shows negligible decay over 110 h at 40 mA/cm². Similarly, the nitrogen-rich, nanostructured Mo₅N₆, atomically thin, as observed by Jin et al., ²¹⁶ enhances HER due to its modified electronic structure and increased active site exposure. Moreover, Lu et al.²¹² find that manganese-doped nickel oxide/nickel heterostructures and nanoarraystructured NiCoP further optimize HER efficiency by facilitating charge transfer and gas evolution processes. Their study reports a significantly high activity with η_{10} of -170 mV in seawater, with reasonable stability maintained for 14 h at η_{10} of -140 mV. These findings underscore the importance of material design and structure in achieving high-performance electrocatalysis for seawater electrolysis.

Lv et al.²¹⁰ discovered that nanoarray structured NiCoP demonstrates high activity with η_{10} of approximately -287 mV in seawater, indicating its effectiveness in the HER. Moreover, it exhibits reasonable stability with η of about -290 mV for 20 h, suggesting its reliability for prolonged operation. Similarly, Huang et al.²¹¹ reveals that the nanostructured Ni₅P₄ with a thin amorphous Ni₅P₄@Ni^{2+ δ}O_δ(OH)_{2-δ} layer displays significantly high activity, with η_{10} of approximately -144 mV in seawater. Furthermore, it exhibits negligible decay even at various current densities over 40 h, indicating its remarkable stability. Sarno et al.²¹³ investigated the performance of the nanostructured NiRuIr alloy anchored on graphene, revealing its substantial stability with approximately 90 % retention over 200 h in seawater. Additionally, Zhou et al. 217 on nanostructured T@Td-ReS2 with Re vacancies highlights enhanced HER performance in seawater. Interestingly, they observed that while the highest conductivity of the electrolyte is observed at approximately 45 °C, the highest hydrogen production rate occurs at about 35 °C. This discrepancy was attributed to the synergy between conductivity and dielectric constant, ultimately leading to the highest hydrogen production rate.

Zheng et al.²¹⁸ found that the PtMo alloy exhibits substantial activity with η_{10} of about -254.6 mV. Moreover, it maintains excellent stability, with 91.13 % retention at n of -800 mV for 173 h. Zhang et al.²¹⁹ compared the HER of nickel (Ni) alloys, including NiCo and NiCu, in seawater. Fabricated on pretreated Ti substrates via the electrodeposition method, NiCu displayed a nanostructure with a feather-like morphology, while NiCo exhibited a loose structure. The nanostructure of these alloys exposed abundant active sites, contributing to their improved HER performance. Specifically, in filtered seawater, NiCo exhibited an overpotential (n) of approximately -1,000 mV at a current density of 111 mA/cm², with negligible decay observed over ~10 h. Similarly, NiCu showed an overpotential of approximately -1,000 mV at a current density of 88 mA/cm², with reasonable stability maintained over ~10 h. Niu et al.²²⁰ conducted a comparative study on the HER activity of RuCoMox alloys with RuCo alloy in filtered seawater. These alloys were deposited on pretreated titanium foil using cyclic voltammetry deposition. The RuCo

alloy features nanoparticles morphology with an average size of approximately 50 nm, while the RuCoMo₇ alloy exhibits a compact structure with cracks. In filtered seawater, RuCo demonstrates higher HER activity against RuCoMo, RuCoMo₂, RuCoMo₃, RuCoMo₅, and RuCoMo₇. Specifically, RuCo exhibits an overpotential η_{10} of approximately -387 mV, with 70 % retention at an overpotential of –1,200 mV over 12 h. Meanwhile, RuCoMox shows an $\eta_{\rm 10}$ of approximately -550 mV, with negligible decay at an overpotential of -1,200 mV over 12 h. Li et al.²²¹ compared the HER performance of various PtRu-based alloys with Pt in seawater. The alloys, including PtRuMo, PtRuCo, PtRuNi, PtRuFe, and PtRuCr, were deposited on Ti mesh using cyclic voltammetry. These alloys exhibited a facecentered-cubic structure similar to Pt. with changes in crystal constants indicating alloying effects. Among the alloys, PtRuMo showed a nanostructure and the lowest charge transfer resistance, indicating enhanced charge transfer. The HER activity followed this order: PtRuMo > PtRuNi > PtRuCo > PtRuFe > PtRuCr > PtRu > Pt. PtRuMo exhibited the highest activity in seawater, with a low η_{10} of -196 mV and excellent stability, retaining 97.9 % efficiency for 172 h. PtRuNi, PtRuCo, PtRuFe, and PtRuCr also showed high activity with reasonable stability in seawater.

The bamboo-like multi-walled carbon nanotubes incorporating carbon-coated cobalt nanoparticles and nitrogen dopants produces a synergistic effect that enhances the performance of the HER. Research by Gao et al.²²² illustrates the remarkable activity and stability of Co/N-C for HER in seawater with a pH around 7. Co/N-C exhibits significantly higher activity in pH-buffered seawater compared to natural seawater, suggesting that neutralizing the seawater pH enhances HER activity. In pH-buffered seawater, Co/N-C achieves an η_{10} of around -250 mV, maintaining reasonable stability for 7 h with η_{10} of approximately -270 mV.

4.6.3 Seawater electrolyzers

Currently, two primary processes exist for producing green hydrogen through seawater electrolysis, with power supplied by renewable sources such as wind, solar, or tidal energy: one-step and two-step processes.²⁸ The one-step technique involves direct electrolysis of seawater to produce hydrogen, utilizing electrolyzers designed to handle seawater as a feedstock. In contrast, the two-step process first involves desalinating seawater to produce ultra-pure water, which is then electrolyzed to generate hydrogen. Advocates of the two-step approach argue that direct seawater splitting research lacks cost-effectiveness.²²³ They contend that, considering the efficiency and costs associated with reverse osmosis technology, the expenses for initial seawater purification are significantly lower than those for seawater electrolysis. 223,224 Therefore, they propose focusing on the two-step method as a more economically viable option for green hydrogen production from seawater.²²⁴

Seawater electrolyzers, on the other hand, are categorized according to their electrolyte type, with three notable technologies:²⁸ Direct Seawater Electrolyzer (DWE), Proton Exchange Membrane Water Electrolyzer (PEMWE), and Anion Exchange Membrane Water Electrolyzer (AEMWE). The characteristics of each type are summarized in Table 8.

Briefly, DWE utilizes seawater as its electrolyte and requires specific electrode materials for corrosion resistance and energy efficiency. It involves a voltage of approximately 4.0 V to achieve 10 mA/cm². The total investment cost exceeds 6,000\$/kW, with estimated annual operation and maintenance (O&M) costs of 4.0-5.0 % of the investment cost.²⁸ PEMWE, on the other hand, relies on highpurity water and a solid polymer electrolyte (e.g., Nafion membrane). It is sensitive to impurities, with magnesium and calcium ions potentially impacting performance via precipitates deposition on the cathode. Investment costs

Table 8: Characteristics of the seawater electrolyzers. 28

Electrolyzer	DWE	PEMWE	AEMWE
Operating temp.	20 °C	50-80°C	40-60 °C
Operating pressure	Standard	<70 bar	<35 bar
Electrolyte	Seawater	Perfluorosulfonic acid membranes	Divinylbenzene polymer support with
			KOH or NaHCO₃
Anode catalyst	/	IrO ₂	Ni or NiFeCo alloys
Cathode catalyst	/	Pt nanoparticles on carbon black	High surface area Ni
Porous transport layer anode	/	Pt coated sintered porous Ti	Nickel foam
Porous transport layer cathode	/	Sintered porous Ti or carbon cloth	Nickel foam or carbon cloth
Bipolar plate anode	/	Pt-coated Ti	Ni-coated stainless steel
Bipolar plate cathode	/	Au-coated Ti	Ni-coated stainless steel

range from 600 to 1,300 €/kW, with estimated annual O&M costs of 3.0–5.0 % of the investment cost. 28 Finally, AEMWE operates in an alkaline environment, allowing for the use of non-precious metal catalysts and less expensive materials. However, the technology is still under development, particularly regarding anionic membranes.²⁸ Anion exchange membranes are crucial to prevent unwanted migration of anions, such as chloride ions, during seawater electrolysis.

4.6.4 Future directions for seawater electrolysis

In summary, despite significant recent efforts in seawater electrolysis, 26-29 there remains ample room for improvement in achieving high-performance hydrogen production. Seawater electrolysis presents unique challenges due to its complex composition compared to freshwater electrolysis. The catalytic activity and stability of reported catalysts often fall short of practical application requirements due to insufficiently low overpotentials. Moreover, most studies utilize artificial saline water rather than real seawater. To enhance seawater electrolysis performance, several key directions for future research are proposed:^{26,44}

- (i) Conducting combined experimental and theoretical analyses to elucidate reaction pathways and active sites of catalysts: Multimetallic compounds and heterostructured catalysts show promise, but their complexity makes understanding reaction pathways and active sites challenging. Systematic research combining experimental data with theoretical analyses can guide the design of materials with desired structures and properties.
- (ii) Employing in situ characterization methods to identify true active sites: Many electrocatalysts undergo surface changes during seawater electrolysis, potentially altering their active sites. In situ characterization techniques, such as Raman, XAS, and Fourier transform infrared spectroscopy, are essential for tracking changes in intermediates during catalytic reactions and guiding the design of high-efficiency catalysts.
- (iii) Developing electrocatalysts with high activity and stability in seawater: Selectivity to hydrogen and oxygen evolution reactions in the presence of multiple cations and chloride anions is crucial. Modulating the electronic structure of active sites through alloying, heteroelement doping, vacancy engineering, and interface engineering can improve catalytic performance. Integration of different active materials into hybrid catalysts is also promising.

(iv) Designing advanced reactors specific to seawater electrolysis: Beyond catalysts, reactor design plays a critical role. Asymmetric reactor designs, with alkaline water in the anode chamber and seawater in the cathode chamber, offer advantages in Cl⁻ diffusion and anode catalyst protection, crucial for seawater electrolysis.

5 Current challenges in electrolysis and electrolyzer development

Recent progress in electrolysis necessitates ongoing investigation to improve efficiency, scalability, and cost-effectiveness in hydrogen production. Table 9 outlines key research endeavors and goals in water electrolysis. Challenges include integrating electrolysis with renewable energy sources and energy grids while maintaining stability.²²⁵ The absence of standardized methodologies in existing data, frequently sourced from commercial entities, underscores the necessity for universal testing protocols.

The advancement of hydrogen production via water electrolysis necessitates a robust regulatory framework to address challenges in standardization, data reliability, performance measurement methodologies. ISO 22734:2019(E) serves as a certification document for alkaline (ALK), proton-exchange membrane (PEM), and anionexchange membrane (AEM) electrolyzers across various applications. 225 The ongoing work of ISO/TC197/WG34 focuses on developing standards for electrolyzer test protocols and safety requirements, emphasizing the need for standardized methods to ensure accurate performance evaluation.²²⁵ As we delve into integrating electrolysis systems with energy grids and renewable sources, scalability becomes a critical issue. This multifaceted inquiry aims to enhance electrolysis capacities while ensuring harmonious integration within broader energy infrastructures, laying pathways for sustainable hydrogen production. Addressing specific challenges of AWE, PEM, and SO electrolysis technologies, such as cross-contamination, costly catalysts, and effective thermal management, can lead to advancements in efficiency and cost reduction.²²⁵ Evaluating the environmental impact of these technologies, particularly in terms of CO₂-equivalent emissions per kg of produced hydrogen, is crucial.²²⁵ Gerloff's comparative lifecycle assessment indicates that SO technology may have the lowest environmental impact, while ALK and PEM electrolysis technologies show similar performance.²²⁶ However, this assessment remains complex and requires further investigation.

Table 9: Key research areas, challenges, potential solutions, and objectives for water electrolysis development.²²⁵

Research Area	Problem	Solution	Objective
Electrode materials	Identifying electrode materials that are both durable and efficient, capable of withstanding the harsh conditions of electrolysis, is paramount. Additionally, these materials must be cost-effective to ensure the economic viability of the electrolysis process.	Platinum, while effective as a catalyst, is prohibitively expensive, underscoring the necessity for alternative materials.	The advancement of electrodes, catalyst development, and material innovations is essential for enhancing electrolysis efficiency and reducing costs.
Electrolyte stability	Electrolyte degradation is a critical factor influencing both the efficiency and ilfespan of electrolysis cells	Research is underway to develop stable and conductive electrolytes, particularly for high-temperature and high-pressure electrolysis amplications.	Investigating coatings, porous, nanostructured of bipolar plates and analyzing degradation mechanisms are essential areas of exploration
Membrane technology	Enhancing proton exchange membranes in PEM electrolysis and ceramic membranes in SO electrolysis is crucial for advancing the technology.	Improving the durability, selectivity, and cost-effectiveness of membranes can significantly enhance the efficiency of electrolyzers.	Improving selectivity, durability, and ion conductivity
Efficiency enhancement	The inefficiency of hydrogen production through electrolysis, which falls far short of theoretical limits, poses a significant barrier to its development, especially considering that hydrogen is primarily used as a carrier.	Achieving an efficiency increase of over 60 % would significantly enhance hydrogen's potential for decarbonization.	Discovering configurations, materials, and operational parameters that optimize hydrogen production while minimizing energy consumption is imperative.
Thermal management	Precise thermal management is vital to prevent overheating, maintain uniform temperature distribution within the electrolyzer cells, and mitigate thermal stress on the materials.	Enhancing thermal management systems is a crucial area of research and innovation, particularly in the realm of solid oxide electrolysis.	Precise thermal management will not only improve efficiency but also enhance durability and overall performance of these devices.
Scale-up and cost reduction Electrolyzer lifespan	Scaling-up electrolysis technology for industrial and commercial applications while simultaneously lowering production costs poses a significant challenge. The operational lifespan of current electrolyzers typically	Economies of scale and advancements in manufacturing processes Extending the lifespan of electrolyzers aims to reduce the	Attaining a global electrolysis capacity capable of contributing to decarbonization, while maintaining a competitive production cost, is the ultimate goal. Researching degradation mechanisms, investigating durable
Hydrogen purity	ranges from approximately 10,000 to 40,000 h, varying based on the specific type and usage patterns. Guaranteeing the purity of the generated hydrogen is paramount, particularly for its utilization in fuel cell applications.	frequency of replacements, thereby mitigating associated costs and environmental impacts. Continuously improving purification methods to effectively eliminate impurities such as oxygen and moisture remains an ongoing challenge.	materials, and improving system design are crucial steps in addressing this challenge. Attain the requisite hydrogen purity is essential for diverse end applications in a sustainable manner.
Dynamic operation	Electrolyzers need to dynamically adjust to fluctuating energy inputs to uphold stability and efficiency.	The fluctuating conditions pose a significant challenge for electrolyzers, especially when integrating with renewable energy sources (RESs), impeding smooth operation.	Efficiently adapting electrolysis systems to manage fluctuating renewable energy inputs is essential for their optimal performance.
Standardization	The absence of defined standards, particularly concerning performance measurement and other parameters, poses a significant challenge.	Creating international standards and regulations for electrolysis technologies, safety protocols, and quality control is imperative.	Developing a comprehensive system of standards and regulations that facilitates the widespread adoption of water electrolysis technology is crucial.
Lifecycle analysis	Conducting comprehensive lifecycle assessments is essential to gain a thorough understanding of the environmental footprint of electrolysis technologies.	Addressing the high lifecycle cost of electrolyzers, stemming from issues such as instability, shortened lifespan, and high initial costs, necessitates the development of innovative and cost-effective solutions.	Assessing the entire lifecycle, encompassing raw material extraction through end-of-life disposal or recycling, is crucial for understanding the environmental impact and sustainability of electrolysis technologies.

6 Conclusions

In this chapter, we have delved into the realm of cutting-edge strategies for low-temperature electrolysis aimed at efficient hydrogen production. Beginning with an introduction to electrochemical water splitting, we explored the fundamental principles underlying this process and the significance of hydrogen as a clean and sustainable energy carrier. Performance indicators were discussed to provide a framework for evaluating the efficiency and effectiveness of electrolysis systems. Moving forward, we delved into emerging strategies for electrochemical water splitting, highlighting innovative approaches such as decoupled, hybrid, and tandem electrolysis systems, as well as microbial electrolysis cells and seawater electrolysis. These strategies offer unique advantages in terms of efficiency, scalability, and environmental impact, paving the way for advancements in hydrogen production technology.

Decoupled water electrolysis presents a promising avenue for improving the overall efficiency of electrolysis systems by separately optimizing the oxygen and hydrogen evolution reactions. Hybrid approaches leverage the synergistic effects of multiple electrolysis techniques, while tandem electrolysis systems enable sequential hydrogen and oxygen production in a single device. Microbial electrolysis cells offer the potential for renewable and sustainable hydrogen production through microbial-driven electrochemical processes. Seawater electrolysis addresses the challenge of freshwater scarcity by utilizing abundant seawater resources for hydrogen production.

The exploration of these cutting-edge strategies underscores the dynamic nature of electrolysis research and development. Despite significant progress, challenges remain, including the need for cost reduction, scalability, and improved catalyst performance. However, with continued innovation and collaboration across interdisciplinary fields, the prospects for low-temperature electrolysis for hydrogen production are promising.

However, while significant strides have been made in the field of low-temperature electrolysis for hydrogen production, several challenges persist. Cost remains a key barrier to widespread adoption, necessitating the development of cost-effective materials and manufacturing processes. Scalability and system integration also pose challenges, particularly for large-scale deployment in industrial settings. Furthermore, catalyst stability and efficiency continue to be areas of active research, with ongoing efforts focused on developing durable and high-performance catalyst materials. Additionally, the integration of renewable energy sources,

such as solar and wind power, into electrolysis systems presents opportunities for sustainable hydrogen production.

Looking ahead, collaboration between academia, industry, and government institutions will be essential for overcoming these challenges and realizing the full potential of low-temperature electrolysis for hydrogen production. By addressing these obstacles and harnessing the innovative strategies discussed in this chapter, we can accelerate the transition to a clean and sustainable hydrogen economy, driving towards a greener and more resilient energy future.

Research ethics: Not applicable. **Informed consent:** Not applicable.

Author contributions: All of the parts of this research were conducted by S. Merouani, A. Dehane, O. Hamdaoui.

Use of Large Language Models, AI and Machine Learning

Tools: None declared.

Conflict of interest: The authors state no conflict of interest.

Research funding: None declared. Data availability: Not applicable.

References

- 1. Rousseau, R.; Etcheverry, L.; Roubaud, E.; Basséguy, R.; Délia, M.L.; Bergel, A. Microbial Electrolysis Cell (MEC): Strengths, Weaknesses and Research Needs from Electrochemical Engineering Standpoint. Appl. Energy 2020, 257, 113938.
- 2. Nikolaidis, P.; Poullikkas, A. A Comparative Overview of Hydrogen Production Processes. Renew. Sustain. Energy Rev. 2017, 67, 597-611.
- 3. Hosseini, S. E.; Wahid, M. A. Hydrogen Production from Renewable and Sustainable Energy Resources: Promising Green Energy Carrier for Clean Development. Renew. Sustain. Energy Rev. 2016, 57, 850-866.
- 4. Li, W.; Tian, H.; Ma, L.; Wang, Y.; Liu, X.; Gao, X. Low-Temperature Water Electrolysis: Fundamentals, Progress, and New Strategies. Mater. Adv. 2022, 3, 5598-5644.
- 5. Arsad, S. R.; Arsad, A. Z.; Ker, P. J.; Hannan, M. A.; Tang, S. G. H. H.; Goh, S. M.; Mahlia, T. M. I. I. Recent Advancement in Water Electrolysis for Hydrogen Production: A Comprehensive Bibliometric Analysis and Technology Updates. Int. J. Hydrogen Energy 2024, 60, 780-801.
- 6. Chi, J.; Yu, H. Water Electrolysis Based on Renewable Energy for Hydrogen Production. Chinese J. Catal. 2018, 39, 390-394.
- 7. Cong, Y.; Yi, B.; Song, Y. Hydrogen Oxidation Reaction in Alkaline Media: From Mechanism to Recent Electrocatalysts. Nano Energy **2018**, *44*, 288–303.
- 8. Chatenet, M.; Pollet, B. G.; Dekel, D. R.; Dionigi, F.; Deseure, J.; Millet, P.; Braatz, R. D.; Bazant, M. Z.; Eikerling, M.; Staffell, I.; Balcombe, P.; Shao-Horn, Y.; Schäfer, H. Water Electrolysis: From Textbook Knowledge to the Latest Scientific Strategies and Industrial Developments. Chem. Soc. Rev. 2022, 51, 4583-4762.
- 9. Vidas, L.; Castro, R. Recent Developments on Hydrogen Production Technologies: State-Of-The-Art Review with a Focus on Green-Electrolysis. Appl. Sci. 2021, 11, 11363.

- 10. Ju, H. K.; Badwal, S.; Giddey, S. A Comprehensive Review of Carbon and Hydrocarbon Assisted Water Electrolysis for Hydrogen Production. Appl. Energy 2018, 231, 502-533.
- 11. Zeng, K.; Zhang, D. Recent Progress in Alkaline Water Electrolysis for Hydrogen Production and Applications. Prog. Energy Combust. Sci. **2010**, *36*, 307–326.
- 12. Xu, Y.; Zhang, B. Recent Advances in Electrochemical Hydrogen Production from Water Assisted by Alternative Oxidation Reactions. ChemElectroChem 2019, 3214-3226; https://doi.org/10.1002/celc. 201900675
- 13. Carmo, M.; Fritz, D. L.; Mergel, J.; Stolten, D. A Comprehensive Review on PEM Water Electrolysis. Int. J. Hydrogen Energy 2013, 38, 4901-4934.
- 14. Liu, G.; Xu, Y.; Yang, T.; Jiang, L. Recent Advances in Electrocatalysts for Seawater Splitting. Nano Mater. Sci. 2023, 5, 101-116.
- 15. Dincer, I.; Acar, C. Review and Evaluation of Hydrogen Production Methods for Better Sustainability. Int. J. Hydrogen Energy 2015, 40, 11094-11111.
- 16. Ren, J. T.; Chen, L.; Wang, H. Y.; Tian, W. W.; Yuan, Z. Y. Water Electrolysis for Hydrogen Production: From Hybrid Systems to Self-Powered/Catalyzed Devices. Energy Environ. Sci. 2023, 17, 49-113.
- 17. Mohanty, B.; Bhanja, P.; Jena, B. K. An Overview on Advances in Design and Development of Materials for Electrochemical Generation of Hydrogen and Oxygen. Mater. Today Energy 2022, 23, 100902.
- 18. You, B.; Sun, Y. Innovative Strategies for Electrocatalytic Water Splitting. Acc. Chem. Res. 2018, 51, 1571-1580.
- 19. Phillips, R.; Edwards, A.; Rome, B.; Jones, D. R.; Dunnill, C. W. Minimising the Ohmic Resistance of an Alkaline Electrolysis Cell through Effective Cell Design. Int. J. Hydrogen Energy 2017, 1-9; https://doi.org/10.1016/j.ijhydene.2017.07.184.
- 20. Contreras, A.; Guirado, R.; Veziroglu, T. N. Design and Simulation of the Power Control System of a Plant for the Generation of Hydrogen via Electrolysis, Using Photovoltaic Solar Energy. Int. J. Hydrogen Energy 2007, 32, 4635-4640.
- 21. McHugh, P. J.; Stergiou, A. D.; Symes, M. D. Decoupled Electrochemical Water Splitting: From Fundamentals to Applications. Adv. Energy Mater. 2020, 10, 1-21.
- 22. Chen, Z.; Wei, W.; Song, L.; Ni, B. J. Hybrid Water Electrolysis: A New Sustainable Avenue for Energy-Saving Hydrogen Production. Sustain. Horizons 2022, 1, 100002.
- 23. Du, L.; Sun, Y.; You, B. Hybrid Water Electrolysis: Replacing Oxygen Evolution Reaction for Energy-Efficient Hydrogen Production and beyond. Mater. Reports Energy 2021, 1, 100004.
- 24. Xu, J.; Amorim, I.; Li, Y.; Li, J.; Yu, Z.; Zhang, B.; Araujo, A.; Zhang, N.; Liu, L. Stable Overall Water Splitting in an Asymmetric Acid/Alkaline Electrolyzer Comprising a Bipolar Membrane Sandwiched by Bifunctional Cobalt-Nickel Phosphide Nanowire Electrodes. Carbon Energy 2020, 2, 646-655.
- 25. Gautam, R.; Nayak, J. K.; Ress, N. V.; Steinberger-Wilckens, R.; Ghosh, U. K. Bio-Hydrogen Production Through Microbial Electrolysis Cell: Structural Components and Influencing Factors. Chem. Eng. J. 2023, *455*, 140535.
- 26. Jiang, S.; Suo, H.; Zhang, T.; Liao, C.; Wang, Y.; Zhao, Q.; Lai, W. Recent Advances in Seawater Electrolysis. Catalysts 2022, 12, 123.
- 27. Mohammed-ibrahim, J.; Moussab, H. Materials Science for Energy Technologies Recent Advances on Hydrogen Production through Seawater Electrolysis. Mater. Sci. Energy Technol. 2020, 3, 780-807.
- 28. Gao, F.; Yu, P.; Gao, M. Seawater Electrolysis Technologies for Green Hydrogen Production: Challenges and Opportunities. Curr. Opin. Chem. Eng. 2022, 36, 100827.

- 29. Dionigi, F.; Reier, T.; Pawolek, Z.; Gliech, M.; Strasser, P. Design Criteria, Operating Conditions, and Nickel-Iron Hydroxide Catalyst Materials for Selective Seawater Electrolysis. ChemSusChem 2016, 9, 962-972.
- 30. Buttler, A.; Spliethoff, H. Current Status of Water Electrolysis for Energy Storage, Grid Balancing and Sector Coupling via Power-To-Gas and Power-To-Liquids: A Review. Renew. Sustain. Energy Rev. 2018, 82, 2440-2454.
- 31. Schmidt, O.; Gambhir, A.; Staffell, I.; Hawkes, A.; Nelson, I.; Few, S. Future Cost and Performance of Water Electrolysis: An Expert Elicitation Study. Int. J. Hydrogen Energy 2017, 42, 30470-30492.
- 32. Lehner, M.; Tichler, R.; Steinmller, H.; Kopper, M.; Steinmüller, H.; Koppe, M. Power-to-Gas: Technology and Business Models; Springer Cham: Switzerland, 2014.
- 33. Zhang, X.; Chan, S. H.; Ho, H. K.; Tan, S.-C.; Li, M.; Li, G.; Li, J.; Feng, Z. Towards a Smart Energy Network: The Roles of Fuel/Electrolysis Cells and Technological Perspectives. Int. J. Hydrogen Energy 2015, 40, 6866-6919.
- 34. Laguna-Bercero, M. A. Recent Advances in High Temperature Electrolysis Using Solid Oxide Fuel Cells: A Review. J. Power Sources 2012, 203, 4-16.
- 35. Schoots, K.; Ferioli, F.; Kramer, G. J.; van der Zwaan, B. C. C. Learning Curves for Hydrogen Production Technology: An Assessment of Observed Cost Reductions. Int. J. Hydrogen Energy 2008, 33, 2630-2645.
- 36. Bertuccioli, L.; Chan, A.; Hart, D.; Lehner, F.; Madden, B.; Standen, E. Development of Water Electrolysis in the European Unione; 2014;
- 37. Hart, D.; Lehner, F.; Rose, R.; Lewis, J.; Klippenstein, M. The Fuel Cell Industry Review 2015; E4Tech: London, 2015.
- 38. Niu, S.; Li, S.; Du, Y.; Han, X.; Xu, P. How to Reliably Report the Overpotential of an Electrocatalyst. ACS Energy Lett. 2020, 5, 1083-1087.
- 39. Wei, C.; Rao, R. R.; Peng, J.; Huang, B.; Stephens, I. E. L.; Risch, M.; Xu, Z. J.; Shao-Horn, Y. Recommended Practices and Benchmark Activity for Hydrogen and Oxygen Electrocatalysis in Water Splitting and Fuel Cells. Adv. Mater. 2019, 31, 1806296.
- 40. Anantharaj, S.; Ede, S. R.; Karthick, K.; Sam Sankar, S.; Sangeetha, K.; Karthik, P. E.; Kundu, S. Precision and Correctness in the Evaluation of Electrocatalytic Water Splitting: Revisiting Activity Parameters with a Critical Assessment. Energy Environ. Sci. 2018, 11, 744-771.
- 41. Song, F.; Li, W.; Yang, J.; Han, G.; Liao, P.; Sun, Y. Interfacing Nickel Nitride and Nickel Boosts Both Electrocatalytic Hydrogen Evolution and Oxidation Reactions. Nat. Commun. 2018, 9; https://doi.org/10. 1038/s41467-018-06728-7.
- 42. Stoerzinger, K. A.; Risch, M.; Han, B.; Shao-Horn, Y. Recent Insights into Manganese Oxides in Catalyzing Oxygen Reduction Kinetics. ACS Catal. 2015, 5, 6021-6031.
- 43. Yu, L.; Sun, S.; Li, H.; Xu, Z. J. Effects of Catalyst Mass Loading on Electrocatalytic Activity: An Example of Oxygen Evolution Reaction. Fundam. Res. 2021, 1, 448-452.
- 44. Mishra, A.; Park, H.; El-Mellouhi, F.; Suk Han, D. Seawater Electrolysis for Hydrogen Production: Technological Advancements and Future Perspectives. Fuel 2024, 361, 130636.
- 45. Cao, B.; Veith, G. M.; Neuefeind, J. C.; Adzic, R. R.; Khalifah, P. G. Mixed Close-Packed Cobalt Molybdenum Nitrides as Non-Noble Metal Electrocatalysts for the Hydrogen Evolution Reaction. J. Am. Chem. Soc. **2013**, *135*, 19186–19192.
- 46. Santos, D. M. F.; Sequeira, C. A. C.; Macciò, D.; Saccone, A.; Figueiredo, J. L. Platinum-Rare Earth Electrodes for Hydrogen Evolution in Alkaline Water Electrolysis. Int. J. Hydrogen Energy 2013, 38, 3137–3145.

- 47. Liang, Z.; Ahn, H. S.; Bard, A. J. A Study of the Mechanism of the Hydrogen Evolution Reaction on Nickel by Surface Interrogation Scanning Electrochemical Microscopy. J. Am. Chem. Soc. 2017, 139, 4854-4858.
- 48. Li, W.; Gao, X.; Xiong, D.; Wei, F.; Song, W.-G.; Xu, J.; Liu, L. Hydrothermal Synthesis of Monolithic Co3Se4 Nanowire Electrodes for Oxygen Evolution and Overall Water Splitting with High Efficiency and Extraordinary Catalytic Stability. Adv. Energy Mater. 2017, 7, 1602579
- 49. Anantharaj, S.; Kundu, S. Do The Evaluation Parameters Reflect Intrinsic Activity of Electrocatalysts in Electrochemical Water Splitting? ACS Energy Lett. 2019, 4, 1260-1264.
- 50. Li, W.; Jiang, N.; Hu, B.; Liu, X.; Song, F.; Han, G.; Jordan, T. J.; Hanson, T. B.; Liu, T. L.; Sun, Y. Electrolyzer Design for Flexible Decoupled Water Splitting and Organic Upgrading with Electron Reservoirs. Chem 2018, 4, 637-649.
- 51. Ghassemzadeh, L.; Kreuer, K.-D.; Maier, J.; Müller, K. Chemical Degradation of Nafion Membranes under Mimic Fuel Cell Conditions as Investigated by Solid-State NMR Spectroscopy. J. Phys. Chem. C 2010, 114, 14635-14645.
- 52. Berger, A.; Segalman, R. A.; Newman, J. Material Requirements for Membrane Separators in a Water-Splitting Photoelectrochemical Cell. Energy Environ. Sci. 2014, 7, 1468-1476.
- 53. Symes, M. D.; Cronin, L. Decoupling Hydrogen and Oxygen Evolution during Electrolytic Water Splitting Using an Electron-Coupled-Proton Buffer. Nat. Chem. 2013, 5, 403-409.
- 54. Paul, A.; Symes, M. D. Decoupled Electrolysis for Water Splitting. Curr. Opin. Green Sustain. Chem. 2021, 29, 100453.
- 55. Ho, A.; Zhou, X.; Han, L.; Sullivan, I.; Karp, C.; Lewis, N. S.; Xiang, C. Decoupling H2(g) and O2(g) Production in Water Splitting by a Solar-Driven V3+/2+(Aq,H2SO4)|KOH(Aq) Cell. ACS Energy Lett. 2019, 4,
- 56. Goodwin, S.; Walsh, D. A. Closed Bipolar Electrodes for Spatial Separation of H2 and O2 Evolution during Water Electrolysis and the Development of High-Voltage Fuel Cells. ACS Appl. Mater. Interfaces 2017. 9. 23654-23661.
- 57. Rausch, B.; Symes, M. D.; Cronin, L. A Bio-Inspired, Small Molecule Electron-Coupled-Proton Buffer for Decoupling the Half-Reactions of Electrolytic Water Splitting. J. Am. Chem. Soc. 2013, 135, 13656-13659.
- 58. Kirkaldy, N.; Chisholm, G.; Chen, J.-J.; Cronin, L. A Practical, Organic-Mediated, Hybrid Electrolyser that Decouples Hydrogen Production at High Current Densities. Chem. Sci. 2018, 9, 1621-1626.
- 59. Zhao, Y.; Ding, C.; Zhu, J.; Qin, W.; Tao, X.; Fan, F.; Li, R.; Li, C. A Hydrogen Farm Strategy for Scalable Solar Hydrogen Production with Particulate Photocatalysts. Angew. Chemie (International Ed. 2020, 59, 9653-9658.
- 60. Chen, L.; Dong, X.; Wang, Y.; Xia, Y. Separating Hydrogen and Oxygen Evolution in Alkaline Water Electrolysis Using Nickel Hydroxide. Nat. Commun. 2016, 7, 1-8.
- 61. Liu, X.; Chi, J.; Dong, B.; Sun, Y. Recent Progress in Decoupled H2 and O2 Production from Electrolytic Water Splitting. ChemElectroChem **2019**, *6*, 2157–2166.
- 62. Wallace, A. G.; Symes, M. D. Decoupling Strategies in Electrochemical Water Splitting and beyond. Joule 2018, 2, 1390–1395.
- 63. MacDonald, L.; McGlynn, J. C.; Irvine, N.; Alshibane, I.; Bloor, L. G.; Rausch, B.; Hargreaves, J. S. J.; Cronin, L. Using Earth Abundant Materials for the Catalytic Evolution of Hydrogen from Electron-Coupled Proton Buffers. Sustain. Energy Fuels 2017, 1, 1782-1787.

- 64. Rausch, B.; Symes, M. D.; Chisholm, G.; Cronin, L. Decoupled Catalytic Hydrogen Evolution from a Molecular Metal Oxide Redox Mediator in Water Splitting. Science (80-.) 2014, 345, 1326-1330.
- 65. Landman, A.; Dotan, H.; Shter, G. E.; Wullenkord, M.; Houaijia, A.; Maljusch, A.; Grader, G. S.; Rothschild, A. Photoelectrochemical Water Splitting in Separate Oxygen and Hydrogen Cells. Nat. Mater. 2017, 16,
- 66. Landman, A.; Halabi, R.; Dias, P.; Dotan, H.; Mehlmann, A.; Shter, G. E.; Halabi, M.; Naseraldeen, O.; Mendes, A.; Grader, G. S.; Rothschild, A. Decoupled Photoelectrochemical Water Splitting System for Centralized Hydrogen Production. Joule 2020, 4, 448-471.
- 67. Ma, Y.; Dong, X.; Wang, Y.; Xia, Y. Decoupling Hydrogen and Oxygen Production in Acidic Water Electrolysis Using a Polytriphenylamine-Based Battery Electrode. Angew. Chemie Int. Ed. 2018, 57, 2904-2908.
- 68. Dotan, H.: Landman, A.: Sheehan, S. W.: Malviva, K. D.: Shter, G. E.: Grave, D. A.; Arzi, Z.; Yehudai, N.; Halabi, M.; Gal, N.; Hadari, N.; Cohen, C.; Rothschild, A.; Grader, G. S. Decoupled Hydrogen and Oxygen Evolution by a Two-step Electrochemical-Chemical Cycle for Efficient Overall Water Splitting. Nat. Energy 2019, 4, 786–795.
- 69. Bienvenu, G. Method for Co-generation of Electric Energy and Hydrogen, US Patent No. 8,617,766, Filed July 27, 2010, and Published December 31 2013.
- 70. You, B.; Liu, X.; Liu, X.; Sun, Y. Efficient H2 Evolution Coupled with Oxidative Refining of Alcohols via A Hierarchically Porous Nickel Bifunctional Electrocatalyst. ACS Catal. 2017, 7, 4564-4570.
- 71. Chen, G.-F.; Luo, Y.; Ding, L.-X.; Wang, H. Low-Voltage Electrolytic Hydrogen Production Derived from Efficient Water and Ethanol Oxidation on Fluorine-Modified FeOOH Anode. ACS Catal. 2018, 8, 526-530.
- 72. Huang, Y.; Chong, X.; Liu, C.; Liang, Y.; Zhang, B. Boosting Hydrogen Production by Anodic Oxidation of Primary Amines over a NiSe Nanorod Electrode. Angew. Chemie Int. Ed. 2018, 57, 13163-13166.
- 73. Liu, W.-J.; Dang, L.; Xu, Z.; Yu, H.-Q.; Jin, S.; Huber, G. W. Electrochemical Oxidation of 5-Hydroxymethylfurfural with NiFe Layered Double Hydroxide (LDH) Nanosheet Catalysts. ACS Catal. **2018**. 8. 5533-5541.
- 74. Babar, P.; Lokhande, A.; Karade, V.; Lee, I. J.; Lee, D.; Pawar, S.; Kim, J. H. Trifunctional Layered Electrodeposited Nickel Iron Hydroxide Electrocatalyst with Enhanced Performance towards the Oxidation of Water, Urea and Hydrazine. J. Colloid Interface Sci. 2019, 557, 10–17.
- 75. Zhang, J.-Y.; Wang, H.; Tian, Y.; Yan, Y.; Xue, Q.; He, T.; Liu, H.; Wang, C.; Chen, Y.; Xia, B. Y. Anodic Hydrazine Oxidation Assists Energy-Efficient Hydrogen Evolution over a Bifunctional Cobalt Perselenide Nanosheet Electrode. Angew. Chemie Int. Ed. 2018, 57, 7649-7653.
- 76. Yu, Z.-Y.; Lang, C.-C.; Gao, M.-R.; Chen, Y.; Fu, Q.-Q.; Duan, Y.; Yu, S.-H. Ni-Mo-O Nanorod-Derived Composite Catalysts for Efficient Alkaline Water-To-Hydrogen Conversion via Urea Electrolysis. Energy Environ. Sci. 2018, 11, 1890-1897.
- 77. Kahlstorf, T.; Hausmann, J. N.; Sontheimer, T.; Menezes, P. W. Challenges for Hybrid Water Electrolysis to Replace the Oxygen Evolution Reaction on an Industrial Scale. Glob. Challenges 2023, 7, 1-11.
- 78. Fan, L.; Wang, D.; Ma, K.; Zhou, C.-A.; Yue, H. Recent Advances in Hydrogen Production from Hybrid Water Electrolysis through Alternative Oxidation Reactions. ChemCatChem 2024, 16, e202301332.
- 79. Wang, Y.; Lu, S.; Yang, M.; Zhang, Z.; Zhang, J. Recent Advances in Anode Catalysts for Waste Valorization through Hybrid Water Electrolysis: Towards Sustainability beyond Hydrogen Production. Mater. Today Sustain. 2024, 25, 100630.

- 80. Zhou, Q.; Shen, Z.; Zhu, C.; Li, J.; Ding, Z.; Wang, P.; Pan, F.; Zhang, Z.; Ma, H.; Wang, S.; Zhang, H. Nitrogen-Doped CoP Electrocatalysts for Coupled Hydrogen Evolution and Sulfur Generation with Low Energy Consumption. Adv. Mater. 2018, 30, 1800140.
- 81. Sun, F.; He, D.; Yang, K.; Qiu, J.; Wang, Z. Hydrogen Production and Water Desalination with On-Demand Electricity Output Enabled by Electrochemical Neutralization Chemistry. Angew. Chemie Int. Ed. 2022, 61, e202203929.
- 82. Tang, C.; Zhang, R.; Lu, W.; Wang, Z.; Liu, D.; Hao, S.; Du, G.; Asiri, A. M.; Sun, X. Energy-Saving Electrolytic Hydrogen Generation: Ni2P Nanoarray as a High-Performance Non-Noble-Metal Electrocatalyst. Angew. Chemie Int. Ed. 2017, 56, 842-846.
- 83. Liu, X.; He, J.; Zhao, S.; Liu, Y.; Zhao, Z.; Luo, J.; Hu, G.; Sun, X.; Ding, Y. Self-Powered H2 Production with Bifunctional Hydrazine as Sole Consumable. Nat. Commun. 2018, 9, 4365.
- 84. Du, M.; Sun, H.; Li, J.; Ye, X.; Yue, F.; Yang, J.; Liu, Y.; Guo, F. Integrative Ni@Pd-Ni Alloy Nanowire Array Electrocatalysts Boost Hydrazine Oxidation Kinetics. ChemElectroChem 2019, 6, 5581–5587.
- 85. Ma, X.; Wang, J.; Liu, D.; Kong, R.; Hao, S.; Du, G.; Asiri, A. M.; Sun, X. Hydrazine-Assisted Electrolytic Hydrogen Production: CoS2 Nanoarray as a Superior Bifunctional Electrocatalyst. New J. Chem. **2017**, *41*, 4754-4757.
- 86. Gao, L.; Xie, J.; Liu, S.; Lou, S.; Wei, Z.; Zhu, X.; Tang, B. Crystalline Cobalt/Amorphous LaCoOx Hybrid Nanoparticles Embedded in Porous Nitrogen-Doped Carbon as Efficient Electrocatalysts for Hydrazine-Assisted Hydrogen Production. ACS Appl. Mater. Interfaces **2020**, 12, 24701-24709.
- 87. Li, Y.; Zhang, J.; Liu, Y.; Qian, Q.; Li, Z.; Zhu, Y.; Zhang, G. Partially Exposed RuP2 Surface in Hybrid Structure Endows its Bifunctionality for Hydrazine Oxidation and Hydrogen Evolution Catalysis. Sci. Adv. **2020**, 6, eabb4197.
- 88. Feng, G.; Kuang, Y.; Li, P.; Han, N.; Sun, M.; Zhang, G.; Sun, X. Single Crystalline Ultrathin Nickel-Cobalt Alloy Nanosheets Array for Direct Hydrazine Fuel Cells. Adv. Sci. 2017, 4, 1600179.
- 89. Peng, W.; Xiao L.; Huang B.; Zhuang L.; Lu J. Inhibition Effect of Surface Oxygenated Species on Ammonia Oxidation Reaction. I. Phys. Chem. **2011**, 115, 23050-23056.
- 90. Hu, S.; Tan, Y.; Feng, C.; Wu, H.; Zhang, J.; Mei, H. Synthesis of N Doped NiZnCu-Layered Double Hydroxides with Reduced Graphene Oxide on Nickel Foam as Versatile Electrocatalysts for Hydrogen Production in Hybrid-Water Electrolysis. J. Power Sources 2020, 453, 227872.
- 91. Huang, J.; Cai, J.; Wang, J. Nanostructured Wire-In-Plate Electrocatalyst for High-Durability Production of Hydrogen and Nitrogen from Alkaline Ammonia Solution. ACS Appl. Energy Mater. **2020**, 3, 4108-4113.
- 92. Xu, W.; Du, D.; Lan, R.; Humphreys, J.; Miller, D. N.; Walker, M.; Wu, Z.; Irvine, J. T. S.; Tao, S. Electrodeposited NiCu Bimetal on Carbon Paper as Stable Non-Noble Anode for Efficient Electrooxidation of Ammonia. Appl. Catal. B Environ. 2018, 237, 1101-1109.
- 93. Dong, B.-X.; Tian, H.; Wu, Y.-C.; Bu, F.-Y.; Liu, W.-L.; Teng, Y.-L.; Diao, G.-W. Improved Electrolysis of Liquid Ammonia for Hydrogen Generation via Ammonium Salt Electrolyte and Pt/Rh/Ir Electrocatalysts. Int. J. Hydrogen Energy 2016, 41, 14507-14518.
- 94. Sun, X.; Ding, R. Recent Progress with Electrocatalysts for Urea Electrolysis in Alkaline Media for Energy-Saving Hydrogen Production. Catal. Sci. Technol. 2020, 10, 1567-1581.
- 95. Chen, S.; Duan, J.; Vasileff, A.; Qiao, S. Z. Size Fractionation of Two-Dimensional Sub-nanometer Thin Manganese Dioxide Crystals Towards Superior Urea Electrocatalytic Conversion. Angew. Chemie Int. Ed. 2016, 55, 3804-3808.

- 96. Zhang, J.-Y.; Tian, X.; He, T.; Zaman, S.; Miao, M.; Yan, Y.; Qi, K.; Dong, Z.; Liu, H.; Xia, B. Y. In Situ Formation of Ni3Se4 Nanorod Arrays as Versatile Electrocatalysts for Electrochemical Oxidation Reactions in Hybrid Water Electrolysis. J. Mater. Chem. A 2018, 6, 15653-15658.
- 97. Zheng, J.; Wu, K.; Lyu, C.; Pan, X.; Zhang, X.; Zhu, Y.; Wang, A.; Lau, W.-M.; Wang, N. Electrocatalyst of Two-Dimensional CoP Nanosheets Embedded by Carbon Nanoparticles for Hydrogen Generation and Urea Oxidation in Alkaline Solution. Appl. Surf. Sci. **2020**, 506, 144977.
- 98. Zhang, B.; Lui, Y. H.; Gaur, A. P. S.; Chen, B.; Tang, X.; Qi, Z.; Hu, S. Hierarchical FeNiP@Ultrathin Carbon Nanoflakes as Alkaline Oxygen Evolution and Acidic Hydrogen Evolution Catalyst for Efficient Water Electrolysis and Organic Decomposition. ACS Appl. Mater. Interfaces 2018. 10. 8739-8748.
- 99. Li, Z.; Li, X.; Zhou, H.; Xu, Y.; Xu, S. M.; Ren, Y.; Yan, Y.; Yang, J.; Ji, K.; Li, L.; Xu, M.; Shao, M.; Kong, X.; Sun, X.; Duan, H. Electrocatalytic Synthesis of Adipic Acid Coupled with H2 Production Enhanced by a Ligand Modification Strategy. Nat. Commun. 2022, 13, 1-12.
- 100. Sauter, W.; Bergmann, O. L.; Schröder, U. Hydroxyacetone: A Glycerol-Based Platform for Electrocatalytic Hydrogenation and Hydrodeoxygenation Processes. ChemSusChem 2017, 10, 3105-3110.
- 101. Fan, L.; Liu, B.; Liu, X.; Senthilkumar, N.; Wang, G.; Wen, Z. Recent Progress in Electrocatalytic Glycerol Oxidation. Energy Technol. 2021, 9, 2000804.
- 102. Gao, T.; Tang, X.; Li, X.; Lan, H.; Yu, S.; Wu, S.; Yue, Q.; Xiao, D. Surface Reconstructing Hierarchical Structures as Robust Sulfion Oxidation Catalysts to Produce Hydrogen with Ultralow Energy Consumption. Inorg. Chem. Front. 2023, 10, 1447-1456.
- 103. Zhang, S.; Zhou, Q.; Shen, Z.; Jin, X.; Zhang, Y.; Shi, M.; Zhou, J.; Liu, J.; Lu, Z.; Zhou, Y.-N.; Zhang, H. Sulfophobic and Vacancy Design Enables Self-Cleaning Electrodes for Efficient Desulfurization and Concurrent Hydrogen Evolution with Low Energy Consumption. Adv. Funct. Mater.
- 104. Zhang, M.; Guan, J.; Tu, Y.; Chen, S.; Wang, Y.; Wang, S.; Yu, L.; Ma, C.; Deng, D.: Bao, X. Highly Efficient H2 Production from H2S via a Robust Graphene-Encapsulated Metal Catalyst. Energy Environ. Sci. 2020, 13,
- 105. Zhang, L.; Wang, Z.; Qiu, J. Energy-Saving Hydrogen Production by Seawater Electrolysis Coupling Sulfion Degradation. Adv. Mater. 2022, 34, 2109321.
- 106. Yi, L.; Ji, Y.; Shao, P.; Chen, J.; Li, J.; Li, H.; Chen, K.; Peng, X.; Wen, Z. Scalable Synthesis of Tungsten Disulfide Nanosheets for Alkali-Acid Electrocatalytic Sulfion Recycling and H2 Generation. Angew. Chemie Int. Ed. 2021, 60, 21550-21557.
- 107. Marshall, A. T.; Haverkamp, R. G. Production of Hydrogen by the Electrochemical Reforming of Glycerol-Water Solutions in a PEM Electrolysis Cell. Int. J. Hydrogen Energy 2008, 33, 4649-4654
- 108. Li, Y.; Wei, X.; Chen, L.; Shi, J.; He, M. Nickel-Molybdenum Nitride Nanoplate Electrocatalysts for Concurrent Electrolytic Hydrogen and Formate Productions. Nat. Commun. 2019, 10, 1-12.
- 109. Zhu, Y.; Qian, Q.; Chen, Y.; He, X.; Shi, X.; Wang, W.; Li, Z.; Feng, Y.; Zhang, G.; Cheng, F. Biphasic Transition Metal Nitride Electrode Promotes Nucleophile Oxidation Reaction for Practicable Hybrid Water Electrocatalysis. Adv. Funct. Mater. 2023, 33, 2300547.
- 110. Tran, G.-S.; Vo, T.-G.; Chiang, C.-Y. Operando Revealing the Crystal Phase Transformation and Electrocatalytic Activity Correlation of MnO2 toward Glycerol Electrooxidation. ACS Appl. Mater. Interfaces **2023**, 15, 22662-22671.

- 111. Zhou, L.; Liang, R.; Ma, Z.; Wu, T.; Wu, Y. Conversion of Cellulose to HMF in Ionic Liquid Catalyzed by Bifunctional Ionic Liquids. Bioresour. Technol. 2013, 129, 450-455.
- 112. Tong, X.; Ma, Y.; Li, Y. Biomass into Chemicals: Conversion of Sugars to Furan Derivatives by Catalytic Processes. Appl. Catal. Gen. 2010, 385,
- 113. Grabowski, G.; Lewkowski, J.; Skowroński, R. The Electrochemical Oxidation of 5-Hydroxymethylfurfural with the Nickel Oxide/ Hydroxide Electrode. Electrochim. Acta 1991, 36, 1995.
- 114. Nichols, E. M.; Gallagher, J. J.; Liu, C.; Su, Y.; Resasco, J.; Yu, Y.; Sun, Y.; Yang, P.; Chang, M. C. Y.; Chang, C. J. Hybrid Bioinorganic Approach to Solar-Tochemical Conversion. Proc. Natl. Acad. Sci. U. S. A. 2015, 112,
- 115. Liu, C.; Colón, B. C.; Ziesack, M.; Silver, P. A.; Daniel, G. Nocera Water Splitting-Biosynthetic System with CO2 Reduction Efficiencies Exceeding Photosynthesis. Science (80-.) 2016, 352, 1210-1213.
- 116. Liu, C.; Sakimoto, K. K.; Colón, B. C.; Silver, P. A.; Nocera, D. G. Ambient Nitrogen Reduction Cycle Using a Hybrid Inorganic-Biological System. Proc. Natl. Acad. Sci. U. S. A. 2017, 114, 6450-6455.
- 117. Yang, E.; Omar Mohamed, H.; Park, S. G.; Obaid, M.; Al-Qaradawi, S. Y.; Castaño, P.; Chon, K.; Chae, K. J. A Review on Self-Sustainable Microbial Electrolysis Cells for Electro-Biohydrogen Production via Coupling with Carbon-Neutral Renewable Energy Technologies. Bioresour. Technol. 2021, 320; https://doi.org/10.1016/j.biortech.2020.124363.
- 118. Zhang, Y.; Angelidaki, I. Microbial Electrolysis Cells Turning to Be Versatile Technology: Recent Advances and Future Challenges. Water Res. 2014, 56, 11-25.
- 119. Xiang, L. J.; Dai, L.; Guo, K. X.; Wen, Z. H.; Ci, S. Q.; Li, J. H. Microbial Electrolysis Cells for Hydrogen Production. Chinese J. Chem. Phys. 2020,
- 120. Oyiwona, G. E.; Ogbonna, J.; Anyanwu, C. U.; Ishizaki, S.; Kimura, Z.; Okabe, S. Oxidation of Glucose by Syntrophic Association between Geobacter and Hydrogenotrophic Methanogens in Microbial Fuel Cell. Biotechnol. Lett. 2017, 39, 253-259.
- 121. Schröder, U. Anodic Electron Transfer Mechanisms in Microbial Fuel Cells and Their Energy Efficiency. Phys. Chem. Chem. Phys. 2007, 9, 2619-2629.
- 122. Selembo, P. A.; Perez, J. M.; Lloyd, W. A.; Logan, B. E. High Hydrogen Production from Glycerol or Glucose by Electrohydrogenesis Using Microbial Electrolysis Cells. Int. J. Hydrogen Energy 2009, 34, 5373-5381.
- 123. Parkhey, P.; Gupta, P. Improvisations in Structural Features of Microbial Electrolytic Cell and Process Parameters of Electrohydrogenesis for Efficient Biohydrogen Production: A Review. Renew. Sustain. Energy Rev. 2017, 69, 1085-1099.
- 124. Ivanov, I.; Ahn, Y.; Poirson, T.; Hickner, M. A.; Logan, B. E. Comparison of Cathode Catalyst Binders for the Hydrogen Evolution Reaction in Microbial Electrolysis Cells. Int. J. Hydrogen Energy 2017, 42, 15739-15744.
- 125. Liu, W.; Wang, A.; Ren, N.; Zhao, X.; Liu, L.; Yu, Z.; Lee, D.-J. Electrochemically Assisted Biohydrogen Production from Acetate. Energy & Fuels 2008, 22, 159-163.
- 126. Liu, H.; Grot, S.; Logan, B. E. Electrochemically Assisted Microbial Production of Hydrogen from Acetate. Environ. Sci. Technol. 2005, 39,
- 127. Jeremiasse, A. W.; Hamelers, H. V. M.; Buisman, C. J. N. Microbial Electrolysis Cell with a Microbial Biocathode. Bioelectrochemistry 2010, 78, 39-43.
- 128. Chae, K.-J.; Choi, M.-J.; Kim, K.-Y.; Ajayi, F. F.; Chang, I.-S.; Kim, I. S. A Solar-Powered Microbial Electrolysis Cell with a Platinum Catalyst-free

- Cathode to Produce Hydrogen. Environ. Sci. Technol. 2009, 43, 9525-9530.
- 129. Rozendal, R. A.; Hamelers, H. V. M.; Molenkamp, R. J.; Buisman, C. J. N. Performance of Single Chamber Biocatalyzed Electrolysis with Different Types of Ion Exchange Membranes. Water Res. 2007, 41, 1984-1994.
- 130. Karthikeyan, R.; Cheng, K. Y.; Selvam, A.; Bose, A.; Wong, J. W. C. Bioelectrohydrogenesis and Inhibition of Methanogenic Activity in Microbial Electrolysis Cells - A Review. Biotechnol. Adv. 2017, 35, 758-771.
- 131. Liang, D.-W.; Peng, S.-K.; Lu, S.-F.; Liu, Y.-Y.; Lan, F.; Xiang, Y. Enhancement of Hydrogen Production in a Single Chamber Microbial Electrolysis Cell through Anode Arrangement Optimization. Bioresour. Technol. 2011, 102, 10881-10885.
- 132. Hu, H.; Fan, Y.; Liu, H. Hydrogen Production Using Single-Chamber Membrane-free Microbial Electrolysis Cells. Water Res. 2008, 42, 4172-4178.
- 133. Ruiz, Y.; Baeza, J. A.; Guisasola, A. Revealing the Proliferation of Hydrogen Scavengers in a Single-Chamber Microbial Electrolysis Cell Using Electron Balances. Int. J. Hydrogen Energy 2013, 38, 15917-15927.
- 134. Call, D.; Logan, B. E. Hydrogen Production in a Single Chamber Microbial Electrolysis Cell Lacking a Membrane. Environ. Sci. Technol. **2008**, *42*, 3401-3406.
- 135. Kadier, A.; Kalil, M. S.; Chandrasekhar, K.; Mohanakrishna, G.; Saratale, G. D.; Saratale, R. G.; Kumar, G.; Pugazhendhi, A.; Sivagurunathan, P. Surpassing the Current Limitations of High Purity H2 Production in Microbial Electrolysis Cell (MECs): Strategies for Inhibiting Growth of Methanogens. Bioelectrochemistry 2018, 119, 211-219
- 136. Guo, K.; Prévoteau, A.; Patil, S. A.; Rabaey, K. Engineering Electrodes for Microbial Electrocatalysis. Curr. Opin. Biotechnol. 2015, 33, 149–156.
- 137. Escapa, A.; Mateos, R.; Martínez, E. J.; Blanes, J. Microbial Electrolysis Cells: An Emerging Technology for Wastewater Treatment and Energy Recovery. From Laboratory to Pilot Plant and beyond. Renew. Sustain. Energy Rev. 2016, 55, 942-956.
- 138. Zhou, M.; Chi, M.; Luo, J.; He, H.; Jin, T. An Overview of Electrode Materials in Microbial Fuel Cells. J. Power Sources 2011, 196, 4427-4435.
- 139. Kadier, A.; Kalil, M. S.; Abdeshahian, P.; Chandrasekhar, K.; Mohamed, A.; Azman, N. F.; Logroño, W.; Simayi, Y.; Hamid, A. A. Recent Advances and Emerging Challenges in Microbial Electrolysis Cells (MECs) for Microbial Production of Hydrogen and Value-Added Chemicals. Renew. Sustain. Energy Rev. 2016, 61, 501-525.
- 140. Liu, H.; Hu, H.; Chignell, J.; Fan, Y. Microbial Electrolysis: Novel Technology for Hydrogen Production from Biomass. Biofuels 2010, 1, 129-142.
- 141. Sun, M.; Zhang, F.; Tong, Z.-H.; Sheng, G.-P.; Chen, Y.-Z.; Zhao, Y.; Chen, Y.-P.; Zhou, S.-Y.; Liu, G.; Tian, Y.-C.; Yu, H. Q. A Gold-Sputtered Carbon Paper as an Anode for Improved Electricity Generation from a Microbial Fuel Cell Inoculated with Shewanella Oneidensis MR-1. Biosens. Bioelectron. 2010, 26, 338-343.
- 142. Lv, Z.; Xie, D.; Yue, X.; Feng, C.; Wei, C. Ruthenium Oxide-Coated Carbon Felt Electrode: A Highly Active Anode for Microbial Fuel Cell Applications. J. Power Sources 2012, 210, 26-31.
- 143. Qiao, Y.; Li, C. M.; Bao, S.-J.; Bao, Q.-L. Carbon Nanotube/Polyaniline Composite as Anode Material for Microbial Fuel Cells. I. Power Sources **2007**, *170*, 79–84.
- 144. Zhang, Y.; Liu, L.; Van der Bruggen, B.; Yang, F. Nanocarbon Based Composite Electrodes and Their Application in Microbial Fuel Cells. J. Mater. Chem. A 2017, 5, 12673-12698.

- 145. Cui, H.-F.; Du, L.; Guo, P.-B.; Zhu, B.; Luong, J. H. T. Controlled Modification of Carbon Nanotubes and Polyaniline on Macroporous Graphite Felt for High-Performance Microbial Fuel Cell Anode. J. Power Sources 2015, 283, 46-53.
- 146. Chen, S.; He, G.; Hu, X.; Xie, M.; Wang, S.; Zeng, D.; Hou, H.; Schröder, U. A Three-Dimensionally Ordered Macroporous Carbon Derived from a Natural Resource as Anode for Microbial Bioelectrochemical Systems. ChemSusChem 2012. 5, 1059-1063.
- 147. Alatraktchi, F. A.; Zhang, Y.; Angelidaki, I. Nanomodification of the Electrodes in Microbial Fuel Cell: Impact of Nanoparticle Density on Electricity Production and Microbial Community. Appl. Energy 2014, 116, 216-222.
- 148. Hindatu, Y.; Annuar, M. S. M.; Gumel, A. M. Mini-Review: Anode Modification for Improved Performance of Microbial Fuel Cell. Renew. Sustain. Energy Rev. 2017, 73, 236-248.
- 149. Wang, Q.; Huang, L.; Yu, H.; Quan, X.; Li, Y.; Fan, G.; Li, L. Assessment of Five Different Cathode Materials for Co(II) Reduction with Simultaneous Hydrogen Evolution in Microbial Electrolysis Cells. Int. J. Hydrogen Energy 2015, 40, 184-196.
- 150. Gnana kumar, G.; Kirubaharan, C. J.; Udhayakumar, S.; Karthikeyan, C.; Nahm, K. S. Conductive Polymer/Graphene Supported Platinum Nanoparticles as Anode Catalysts for the Extended Power Generation of Microbial Fuel Cells. Ind. Eng. Chem. Res. 2014, 53, 16883-16893.
- 151. Kang, Y. L.; Ibrahim, S.; Pichiah, S. Synergetic Effect of Conductive Polymer Poly(3,4-Ethylenedioxythiophene) with Different Structural Configuration of Anode for Microbial Fuel Cell Application. Bioresour. Technol. 2015, 189, 364-369.
- 152. Luckarift, H. R.; Sizemore, S. R.; Farrington, K. E.; Roy, J.; Lau, C.; Atanassov, P. B.; Johnson, G. R. Facile Fabrication of Scalable, Hierarchically Structured Polymer/Carbon Architectures for Bioelectrodes. ACS Appl. Mater. Interfaces 2012, 4, 2082–2087.
- 153. Kadier, A.; Simayi, Y.; Kalil, M. S.; Abdeshahian, P.; Hamid, A. A. A Review of the Substrates Used in Microbial Electrolysis Cells (MECs) for Producing Sustainable and Clean Hydrogen Gas. Renew. Energy 2014, 71, 466-472.
- 154. Chaurasia, A. K.: Goval, H.: Mondal, P. Hydrogen Gas Production with Ni, Ni-Co and Ni-Co-P Electrodeposits as Potential Cathode Catalyst by Microbial Electrolysis Cells. Int. J. Hydrogen Energy 2020, 45, 18250-18265.
- 155. Mitov, M.; Chorbadzhiyska, E.; Nalbandian, L.; Hubenova, Y. Nickel-Based Electrodeposits as Potential Cathode Catalysts for Hydrogen Production by Microbial Electrolysis. J. Power Sources 2017, 356, 467-472.
- 156. Kadier, A.; Simayi, Y.; Chandrasekhar, K.; Ismail, M.; Kalil, M. S. Hydrogen Gas Production with an Electroformed Ni Mesh Cathode Catalysts in a Single-Chamber Microbial Electrolysis Cell (MEC). Int. J. Hydrogen Energy 2015, 40, 14095-14103.
- 157. Torres, C. I.; Marcus, A. K.; Lee, H. S.; Parameswaran, P.; Krajmalnik-Brown, R.; Rittmann, B. E. A Kinetic Perspective on Extracellular Electron Transfer by Anode-Respiring Bacteria. FEMS Microbiol. Rev. **2010**, *34*, 3-17.
- 158. Hernandez, M. E.; Kappler, A.; Newman, D. K. Phenazines and Other Redox-Active Antibiotics Promote Microbial Mineral Reduction. Appl. Environ. Microbiol. 2004, 70, 921-928.
- 159. Newman, D. K.; Kolter, R. A Role for Excreted Quinones in Extracellular Electron Transfer. Nature 2000, 405, 94-97.
- 160. Von Canstein, H.; Ogawa, J.; Shimizu, S.; Lloyd, J. R. Secretion of Flavins by Shewanella Species and Their Role in Extracellular Electron Transfer. Appl. Environ. Microbiol. 2008, 74, 615-623.

- 161. Reguera, G.; McCarthy, K. D.; Mehta, T.; Nicoll, J. S.; Tuominen, M. T.; Lovley, D. R. Extracellular Electron Transfer via Microbial Nanowires. Nature 2005, 435, 1098-1101.
- 162. Kiely, P. D.; Rader, G.; Regan, J. M.; Logan, B. E. Long-Term Cathode Performance and the Microbial Communities that Develop in Microbial Fuel Cells Fed Different Fermentation Endproducts. Bioresour. Technol. 2011, 102, 361-366.
- 163. Kiely, P. D.; Cusick, R.; Call, D. F.; Selembo, P. A.; Regan, J. M.; Logan, B. E. Anode Microbial Communities Produced by Changing from Microbial Fuel Cell to Microbial Electrolysis Cell Operation Using Two Different Wastewaters. Bioresour. Technol. 2011, 102, 388-394.
- 164. Wagner, R. C.; Regan, J. M.; Oh, S.-E.; Zuo, Y.; Logan, B. E. Hydrogen and Methane Production from Swine Wastewater Using Microbial Electrolysis Cells. Water Res. 2009, 43, 1480-1488.
- 165. Cusick, R. D.; Kiely, P. D.; Logan, B. E. A Monetary Comparison of Energy Recovered from Microbial Fuel Cells and Microbial Electrolysis Cells Fed Winery or Domestic Wastewaters. Int. J. Hydrogen Energy **2010**, *35*, 8855–8861.
- 166. Ditzig, J.; Liu, H.; Logan, B. E. Production of Hydrogen from Domestic Wastewater Using a Bioelectrochemically Assisted Microbial Reactor (BEAMR). Int. J. Hydrogen Energy 2007, 32, 2296-2304.
- 167. Tenca, A.; Cusick, R. D.; Schievano, A.; Oberti, R.; Logan, B. E. Evaluation of Low Cost Cathode Materials for Treatment of Industrial and Food Processing Wastewater Using Microbial Electrolysis Cells. Int. J. Hydrogen Energy 2013, 38, 1859-1865.
- 168. Montpart, N.; Rago, L.; Baeza, J. A.; Guisasola, A. Hydrogen Production in Single Chamber Microbial Electrolysis Cells with Different Complex Substrates. Water Res. 2015, 68, 601-615.
- 169. Cebecioglu, R.; Akagunduz, D.; Catal, T. Hydrogen Production in Single-Chamber Microbial Electrolysis Cells Using Ponceau S Dye. 3 Biotech 2021, 11, 27.
- 170. Dange, P.; Pandit, S.; Jadhav, D.; Shanmugam, P.; Gupta, P. K.; Kumar, S.; Kumar, M.; Yang, Y. H.; Bhatia, S. K. Recent Developments in Microbial Electrolysis Cell-Based Biohydrogen Production Utilizing Wastewater as a Feedstock. Sustain 2021, 13, 1-37.
- 171. Aiken, D. C.: Curtis, T. P.: Heidrich, E. S. Avenues to the Financial Viability of Microbial Electrolysis Cells [MEC] for Domestic Wastewater Treatment and Hydrogen Production. Int. J. Hydrogen Energy 2019, 44, 2426-2434.
- 172. Jeremiasse, A. W.; Hamelers, H. V. M.; Croese, E.; Buisman, C. J. N. Acetate Enhances Startup of a H2-Producing Microbial Biocathode. Biotechnol. Bioeng. 2012, 109, 657-664.
- 173. Carmona-Martínez, A. A.; Trably, E.; Milferstedt, K.; Lacroix, R.; Etcheverry, L.; Bernet, N. Long-Term Continuous Production of H2 in a Microbial Electrolysis Cell (MEC) Treating Saline Wastewater. Water Res. 2015, 81, 149-156.
- 174. Cheng, C.-L.; Lo, Y.-C.; Lee, K.-S.; Lee, D.-J.; Lin, C.-Y.; Chang, J.-S. Biohydrogen Production from Lignocellulosic Feedstock. Bioresour. Technol. 2011, 102, 8514-8523.
- 175. Dhar, B. R.; Elbeshbishy, E.; Hafez, H.; Lee, H.-S. Hydrogen Production from Sugar Beet Juice Using an Integrated Biohydrogen Process of Dark Fermentation and Microbial Electrolysis Cell. Bioresour. Technol. **2015**. 198. 223-230.
- 176. Ndayisenga, F.; Yu, Z.; Zheng, J.; Wang, B.; Liang, H.; Phulpoto, I. A.; Habiyakare, T.; Zhou, D. Microbial Electrohydrogenesis Cell and Dark Fermentation Integrated System Enhances Biohydrogen Production from Lignocellulosic Agricultural Wastes: Substrate Pretreatment towards Optimization. Renew. Sustain. Energy Rev. **2021**, *145*, 111078.

- 177. Liu, W.; Huang, S.; Zhou, A.; Zhou, G.; Ren, N.; Wang, A.; Zhuang, G. Hydrogen Generation in Microbial Electrolysis Cell Feeding with Fermentation Liquid of Waste Activated Sludge. Int. J. Hydrogen Energy **2012**, *37*, 13859–13864.
- 178. Heidrich, E. S.; Edwards, S. R.; Dolfing, J.; Cotterill, S. E.; Curtis, T. P. Performance of a Pilot Scale Microbial Electrolysis Cell Fed on Domestic Wastewater at Ambient Temperatures for a 12month Period. Bioresour. Technol. 2014, 173, 87-95.
- 179. Cotterill, S. E.; Dolfing, J.; Curtis, T. P.; Heidrich, E. S. Community Assembly in Wastewater-Fed Pilot-Scale Microbial Electrolysis Cells. Front. Energy Res. 2018, 6, 1-12.
- 180. Savla, N.; Suman; Pandit, S.; Verma, J. P.; Awasthi, A. K.; Sana, S. S.; Prasad, R. Techno-Economical Evaluation and Life Cycle Assessment of Microbial Electrochemical Systems: A Review. Curr. Res. Green Sustain, Chem. 2021, 4, 100111.
- 181. Mohd-Yusof, N. S.; Babgi, B.; Aksu, M.; Madhavan, J.; Ashokkumar, M. Physical and Chemical Effects of Acoustic Cavitation in Selected Ultrasonic Cleaning Applications. *Ultrason. Sonochem.* **2016**, *29*, 568-576.
- 182. Islam, H.; Burheim, O. S.; Pollet, B. G. Sonochemical and Sonoelectrochemical Production of Hydrogen. Ultrason. Sonochem. **2019**, *51*, 533-555.
- 183. Li, S.De; Wang, C. C.; Chen, C. Y. Water Electrolysis in the Presence of an Ultrasonic Field. *Electrochim. Acta* **2009**, *54*, 3877–3883.
- 184. Hung, C. Y.; Li, S.De; Wang, C. C.; Chen, C. Y. Influences of a Bipolar Membrane and an Ultrasonic Field on Alkaline Water Electrolysis. J. Memb. Sci. 2012, 389, 197-204.
- 185. Lin, M. Y.; Hourng, L. W. Ultrasonic Wave Field Effects on Hydrogen Production by Water Electrolysis. J. Chinese Inst. Eng. Trans. Chinese Inst. Eng. A 2014, 37, 1080-1089.
- 186. Merabet, N. H.; Kerboua, K. Membrane Free Alkaline Sono-Electrolysis for Hydrogen Production: An Experimental Approach. Int. J. Hydrogen Energy 2024, 49, 734-753.
- 187. Merabet, N. H.; Kerboua, K. Green Hydrogen from Sono-Electrolysis: A Coupled Numerical and Experimental Study of the Ultrasound Assisted Membraneless Electrolysis of Water Supplied by PV. Fuel **2024**, 356, 129625.
- 188. Pétrier, C. The Use of Power Ultrasound for Water Treatment. In Power ultrasonics: applications of high-intensity ultrasound; Gallego-Juarez, JA; Graff, K., Eds.; Elsevier: The Netherlands, 2015; pp 939-963.
- 189. Merouani, S.; Hamdaoui, O. Sonochemical Treatment of Textile Wastewater. In Water Pollution and Remediation: Photocatalysis; Inamuddin, M.P.; Asiri, A., Eds. Springer-Nature: Switzerland, 2021.
- 190. Koza, J. A.; Mühlenhoff, S.; Zabiński, P.; Nikrityuk, P. A.; Eckert, K.; Uhlemann, M.; Gebert, A.; Weier, T.; Schultz, L.; Odenbach, S. Hydrogen Evolution under the Influence of a Magnetic Field. Electrochim. Acta 2011, 56, 2665-2675.
- 191. Matsushima, H.; Iida, T.; Fukunaka, Y. Gas Bubble Evolution on Transparent Electrode during Water Electrolysis in a Magnetic Field. Electrochim. Acta 2013, 100, 261-264.
- 192. Kaya, M. F.; Demir, N.; Albawabiji, M. S.; Taş, M. Investigation of Alkaline Water Electrolysis Performance for Different Cost Effective Electrodes under Magnetic Field. Int. J. Hydrogen Energy 2017, 42, 17583-17592.
- 193. Lin, M. Y.; Hourng, L. W.; Wu, C. H. The Effectiveness of a Magnetic Field in Increasing Hydrogen Production by Water Electrolysis. Energy Sources, Part A Recover. Util. Environ. Eff. 2017, 39, 140-147.
- 194. Lin, M. Y.; Hourng, L. W.; Hsu, J. S. The Effects of Magnetic Field on the Hydrogen Production by Multielectrode Water Electrolysis. Energy Sources, Part A Recover. Util. Environ. Eff. 2017, 39, 352-357.

- 195. Burton, N. A.; Padilla, R. V.; Rose, A.; Habibullah, H. Increasing the Efficiency of Hydrogen Production from Solar Powered Water Electrolysis. Renew. Sustain. Energy Rev. 2021, 135, 110255.
- 196. Wang, M.; Wang, Z.; Gong, X.; Guo, Z. The Intensification Technologies to Water Electrolysis for Hydrogen Production - A Review. Renew. Sustain. Energy Rev. 2014, 29, 573-588.
- 197. Iida, T.; Matsushima, H.; Fukunaka, Y. Water Electrolysis under a Magnetic Field. J. Electrochem. Soc. 2007, 154, E112.
- 198. Lin, M. Y.; Hourng, L. W.; Kuo, C. W. The Effect of Magnetic Force on Hydrogen Production Efficiency in Water Electrolysis. Int. J. Hydrogen Energy 2012, 37, 1311-1320.
- 199. Matsushima, H.; Kiuchi, D.; Fukunaka, Y. Measurement of Dissolved Hydrogen Supersaturation during Water Electrolysis in a Magnetic Field. Electrochim. Acta 2009, 54, 5858-5862.
- 200. Matsushima, H.; Iida, T.; Fukunaka, Y. Observation of Bubble Layer Formed on Hydrogen and Oxygen Gas-Evolving Electrode in a Magnetic Field. J. Solid State Electrochem. 2012, 16, 617-623.
- 201. Wang, Y.; Zhang, B.; Gong, Z.; Gao, K.; Ou, Y.; Zhang, J. The Effect of a Static Magnetic Field on the Hydrogen Bonding in Water Using Frictional Experiments. J. Mol. Struct. 2013, 1052, 102-104.
- 202. Wang, M.; Wang, Z.; Guo, Z. Understanding of the Intensified Effect of Super Gravity on Hydrogen Evolution Reaction. Int. J. Hydrogen Energy **2009**, *34*, 5311–5317.
- 203. Lao, L.; Ramshaw, C.; Yeung, H. Process Intensification: Water Electrolysis in a Centrifugal Acceleration Field. J. Appl. Electrochem. **2011**, 41, 645-656.
- 204. Wang, M.; Wang, Z.; Guo, Z. Water Electrolysis Enhanced by Super Gravity Field for Hydrogen Production. Int. J. Hydrogen Energy 2010, 35, 3198-3205.
- 205. Cheng, H.; Scott, K.; Ramshaw, C. Intensification of Water Electrolysis in a Centrifugal Field. J. Electrochem. Soc. 2002, 149, D172.
- 206. Tong, W.; Forster, M.; Dionigi, F.; Dresp, S.; Sadeghi Erami, R.; Strasser, P.; Cowan, A. J.; Farràs, P. Electrolysis of Low-Grade and Saline Surface Water. Nat. Energy 2020, 5, 367-377.
- 207. Hsu, S.-H.; Miao, J.; Zhang, L.; Gao, J.; Wang, H.; Tao, H.; Hung, S.-F.; Vasileff, A.: Oiao, S. Z.: Liu, B. An Earth-Abundant Catalyst-Based Seawater Photoelectrolysis System with 17.9% Solar-To-Hydrogen Efficiency. Adv. Mater. 2018, 30, 1707261.
- 208. Yu, L.; Zhu, Q.; Song, S.; McElhenny, B.; Wang, D.; Wu, C.; Qin, Z.; Bao, J.; Yu, Y.; Chen, S.; Ren, Z. Non-Noble Metal-Nitride Based Electrocatalysts for High-Performance Alkaline Seawater Electrolysis. Nat. Commun. 2019, 10, 5106.
- 209. Cheng, F.; Feng, X.; Chen, X.; Lin, W.; Rong, J.; Yang, W. Synergistic Action of Co-fe Layered Double Hydroxide Electrocatalyst and Multiple Ions of Sea Salt for Efficient Seawater Oxidation at Near-Neutral PH. Electrochim. Acta 2017, 251, 336-343.
- 210. Lv, Q.; Han, J.; Tan, X.; Wang, W.; Cao, L.; Dong, B. Featherlike NiCoP Holey Nanoarrys for Efficient and Stable Seawater Splitting. ACS Appl. Energy Mater. 2019, 2, 3910-3917.
- 211. Huang, Y.; Hu, L.; Liu, R.; Hu, Y.; Xiong, T.; Qiu, W.; Balogun, M.-S.; Jie, T.; Pan, A.; Tong, Y. Nitrogen Treatment Generates Tunable Nanohybridization of Ni5P4 Nanosheets with Nickel Hydr(Oxy)Oxides for Efficient Hydrogen Production in Alkaline, Seawater and Acidic Media. Appl. Catal. B Environ. 2019, 251, 181-194.
- 212. Lu, X.; Pan, J.; Lovell, E.; Tan, T. H.; Ng, Y. H.; Amal, R. A Sea-Change: Manganese Doped Nickel/Nickel Oxide Electrocatalysts for Hydrogen Generation from Seawater. Energy Environ. Sci. 2018, 11, 1898-1910.
- 213. Sarno, M.; Ponticorvo, E.; Scarpa, D. Active and Stable Graphene Supporting Trimetallic Alloy-Based Electrocatalyst for Hydrogen

- Evolution by Seawater Splitting. Electrochem. Commun. 2020, 111, 106647.
- 214. Kuang, Y.; Kenney, M. J.; Meng, Y.; Hung, W.-H.; Liu, Y.; Huang, J. E.; Prasanna, R.; Li, P.; Li, Y.; Wang, L.; Lin, M. C.; McGehee, M. D.; Sun, X.; Dai, H. Solar-Driven, Highly Sustained Splitting of Seawater into Hydrogen and Oxygen Fuels. Proc. Natl. Acad. Sci. 2019, 116,
- 215. Huang, X.; Chang, S.; Lee, W. S. V.; Ding, J.; Xue, J. M. Three-Dimensional Printed Cellular Stainless Steel as a High-Activity Catalytic Electrode for Oxygen Evolution. J. Mater. Chem. A 2017, 5, 18176-18182.
- 216. Jin, H.; Liu, X.; Vasileff, A.; Jiao, Y.; Zhao, Y.; Zheng, Y.; Qiao, S.-Z. Single-Crystal Nitrogen-Rich Two-Dimensional Mo5N6 Nanosheets for Efficient and Stable Seawater Splitting. ACS Nano 2018, 12, 12761-12769.
- 217. Zhou, G.; Guo, Z.; Shan, Y.; Wu, S.; Zhang, J.; Yan, K.; Liu, L.; Chu, P. K.; Wu, X. High-Efficiency Hydrogen Evolution from Seawater Using Hetero-Structured T/Td Phase ReS2 Nanosheets with Cationic Vacancies. Nano Energy 2019, 55, 42-48.
- 218. Zheng, J.; Zhao, Y.; Xi, H.; Li, C. Seawater Splitting for Hydrogen Evolution by Robust Electrocatalysts from Secondary M (M = Cr, Fe, Co, Ni, Mo) Incorporated Pt. RSC Adv. 2018, 8, 9423-9429.
- 219. Zhang, Y.; Li, P.; Yang, X.; Fa, W.; Ge, S. High-Efficiency and Stable Alloyed Nickel Based Electrodes for Hydrogen Evolution by Seawater Splitting. J. Alloys Compd. 2018, 732, 248-256.
- 220. Niu, X.; Tang, Q.; He, B.; Yang, P. Robust and Stable Ruthenium Alloy Electrocatalysts for Hydrogen Evolution by Seawater Splitting. Electrochim. Acta 2016, 208, 180-187.
- 221. Li, H.; Tang, Q.; He, B.; Yang, P. Robust Electrocatalysts from an Alloyed Pt-Ru-M (M = Cr, Fe, Co, Ni, Mo)-Decorated Ti Mesh for Hydrogen Evolution by Seawater Splitting. J. Mater. Chem. A 2016, 4, 6513-6520.
- 222. Gao, S.; Li, G.-D.; Liu, Y.; Chen, H.; Feng, L.-L.; Wang, Y.; Yang, M.; Wang, D.; Wang, S.; Zou, X. Electrocatalytic H2 Production from Seawater over Co, N-Codoped Nanocarbons. Nanoscale 2015, 7, 2306-2316.
- 223. Hausmann, I. N.: Schlögl, R.: Menezes, P. W.: Driess, M. Is Direct Seawater Splitting Economically Meaningful? Energy Environ. Sci. 2021, 14, 3679-3685.
- 224. Khan, M. A.; Al-Attas, T.; Roy, S.; Rahman, M. M.; Ghaffour, N.; Thangadurai, V.; Larter, S.; Hu, J.; Ajayan, P. M.; Kibria, M. G. Seawater Electrolysis for Hydrogen Production: A Solution Looking for a Problem? Energy Environ. Sci. 2021, 14, 4831-4839.
- 225. Franco, A.; Giovannini, C. Recent and Future Advances in Water Electrolysis for Green Hydrogen Generation: Critical Analysis and Perspectives. Sustainability 2023, 15, 16917.
- 226. Gerloff, N. Comparative Life-Cycle-Assessment Analysis of Three Major Water Electrolysis Technologies while Applying Various Energy Scenarios for a Greener Hydrogen Production. J. Energy Storage 2021, 43, 102759.
- 227. Lehner, M.; Tichler, R.; Steinmller, H.; Kopper, M. Power-to-Gas: Technology and Business Models; Springer: USA, 2014.
- 228. Kilner, A.; Skinner, S.; Irvine, J.; Edwards, P. Functional Materials for Sustainable Energy Applications; Woodhead Publishing Series in Energy: UK, 2012.
- 229. Crnkovic, F. C.; Machado, S. A. S.; Avaca, L. A. Electrochemical and Morphological Studies of Electrodeposited Ni-Fe-Mo-Zn Alloys Tailored for Water Electrolysis. Int. J. Hydrogen Energy 2004, 29, 249–254.
- 230. Han, Q.; Liu, K.; Chen, J.; Wei, X. Hydrogen Evolution Reaction on Amorphous Ni-S-Co Alloy in Alkaline Medium. Int. J. Hydrogen Energy **2003**, 28, 1345-1352.

- 231. Sheela, G.; Pushpavanam, M.; Pushpavanam, S. Zinc-Nickel Alloy Electrodeposits for Water Electrolysis. Int. J. Hydrogen Energy 2002, 27, 627-633.
- 232. Hu, W. Electrocatalytic Properties of New Electrocatalysts for Hydrogen Evolution in Alkaline Water Electrolysis. Int. J. Hydrogen Energy 2000, 25, 111-118.
- 233. Hu, W.; Lee, I.-Y. Electrocatalytic Properties of Ti2Ni/Ni-Mo Composite Electrodes for Hydrogen Evolution Reaction. Int. J. Hydrogen Energy **1998**, 23, 253-257.
- 234. Los, P.; Rami, A.; Lasia, A. Hydrogen Evolution Reaction on Ni-Al Electrodes. J. Appl. Electrochem. 1993, 23, 135-140.
- 235. Raj, I. A. Nickel-Based, Binary-Composite Electrocatalysts for the Cathodes in the Energy-Efficient Industrial Production of Hydrogen from Alkaline-Water Electrolytic Cells. I. Mater. Sci. 1993, 28, 4375-4382.
- 236. Singh, R. N.; Mishra, D.; Anindita; Sinha, A. S. K.; Singh, A. Novel Electrocatalysts for Generating Oxygen from Alkaline Water Electrolysis. Electrochem. Commun. 2007, 9, 1369-1373.
- 237. El-Deab, M. S.; Awad, M. I.; Mohammad, A. M.; Ohsaka, T. Enhanced Water Electrolysis: Electrocatalytic Generation of Oxygen Gas at Manganese Oxide Nanorods Modified Electrodes. Electrochem. Commun. 2007, 9, 2082-2087.
- 238. Hamdani, M.; Pereira, M. I. S.; Douch, J.; Ait Addi, A.; Berghoute, Y.; Mendonça, M. H. Physicochemical and Electrocatalytic Properties of Li-Co3O4 Anodes Prepared by Chemical Spray Pyrolysis for Application in Alkaline Water Electrolysis. Electrochim. Acta 2004, 49, 1555-1563.
- 239. Wendt, H.; Hofmann, H.; Plzak, V. Materials Research and Development of Electrocatalysts for Alkaline Water Electrolysis. Mater. Chem. Phys. 1989, 22, 27-49.
- 240. Krstajić, N.; Popović, M.; Grgur, B.; Vojnović, M.; Šepa, D. On the Kinetics of the Hydrogen Evolution Reaction on Nickel in Alkaline Solution: Part II. Effect of Temperature. J. Electroanal. Chem. 2001, 512,
- 241. Gennero de Chialvo, M. R.; Chialvo, A. C. Hydrogen Evolution Reaction on a Smooth Iron Electrode in Alkaline Solution at Different Temperatures. Phys. Chem. Chem. Phys. 2001, 3, 3180-3184.
- 242. Science, E. Hydrogen Overpotential on Pure Metals. J. Electrochem. Soc. **1971**, *118*, 1278–1282.
- 243. Correia, A. N.; Machado, S. A. S.; Avaca, L. A. Studies of the Hydrogen Evolution Reaction on Smooth Co and Electrodeposited Ni-Co Ultramicroelectrodes. Electrochem. Commun. 1999, 1, 600-604.
- 244. Jom, B.; BE, C.; E, Y.; RE, W. Comprehensive Treatise of Electrochemistry; Plenum Press: New York; pp 19981.
- 245. Miles, M. H.; Huang, Y. H.; Srinivasan, S. The Oxygen Electrode Reaction in Alkaline Solutions on Oxide Electrodes Prepared by the Thermal Decomposition Method. J. Electrochem. Soc. 1978, 125, 1931.
- 246. Damjanovic, A.; Dey, A.; Bockris, J. O. Electrode Kinetics of Oxygen Evolution and Dissolution on Rh, Ir, and Pt-Rh Alloy Electrodes. I. Electrochem. Soc. 1966, 113, 739.
- 247. Miles, M. H.; Kissel, G.; Lu, P. W. T.; Srinivasan, S. Effect of Temperature on Electrode Kinetic Parameters for Hydrogen and Oxygen Evolution Reactions on Nickel Electrodes in Alkaline Solutions. J. Electrochem. Soc. 1976, 123, 332.
- 248. Bloor, L. G.; Solarska, R.; Bienkowski, K.; Kulesza, P. J.; Augustynski, J.; Symes, M. D.; Cronin, L. Solar-Driven Water Oxidation and Decoupled Hydrogen Production Mediated by an Electron-Coupled-Proton Buffer. J. Am. Chem. Soc. 2016, 138, 6707-6710.
- 249. Li, F.; Yu, F.; Du, J.; Wang, Y.; Zhu, Y.; Li, X.; Sun, L. Water Splitting via Decoupled Photocatalytic Water Oxidation and Electrochemical

- Proton Reduction Mediated by Electron-Coupled-Proton Buffer. Chem. - An Asian J. 2017, 12, 2666-2669.
- 250. Chisholm, G.; Cronin, L.; Symes, M. D. Decoupled Electrolysis Using a Silicotungstic Acid Electron-Coupled-Proton Buffer in a Proton Exchange Membrane Cell. Electrochim. Acta 2020, 331, 135255.
- 251. Chen, K.; Wu, C.-D. Designed Fabrication of Biomimetic Metal-Organic Frameworks for Catalytic Applications. Coord. Chem. Rev. 2019, 378, 445-465.
- 252. Lei, J.; Yang, J.-J.; Liu, T.; Yuan, R.-M.; Deng, D.-R.; Zheng, M.-S.; Chen, J.-J.; Cronin, L.; Dong, Q.-F. Tuning Redox Active Polyoxometalates for Efficient Electron-Coupled Proton-Buffer-Mediated Water Splitting. Chem. - A Eur. J. 2019, 25, 11432-11436.
- 253. Chen, J.-J.; Symes, M. D.; Cronin, L. Highly Reduced and Protonated Agueous Solutions of [P2W18O62]6- for On-Demand Hydrogen Generation and Energy Storage. Nat. Chem. 2018, 10, 1042-1047.
- 254. Amstutz, V.; Toghill, K. E.; Powlesland, F.; Vrubel, H.; Comninellis, C.; Hu, X.; Girault, H. H. Renewable Hydrogen Generation from a Dual-Circuit Redox Flow Battery. Energy Environ. Sci. 2014, 7, 2350–2358.
- 255. Ma, C.; Pei, S.; You, S. Closed Bipolar Electrode for Decoupled Electrochemical Water Decontamination and Hydrogen Recovery. Electrochem. Commun. 2019, 109, 106611.
- 256. Jin, Z.; Li, P.; Xiao, D. A Hydrogen-Evolving Hybrid-Electrolyte Battery with Electrochemical/Photoelectrochemical Charging from Water Oxidation. ChemSusChem 2017, 10, 483-488.
- 257. Choi, B.; Panthi, D.; Nakoji, M.; Kabutomori, T.; Tsutsumi, K.; Tsutsumi, A. A Novel Water-Splitting Electrochemical Cycle for Hydrogen Production Using an Intermediate Electrode. Chem. Eng. Sci. 2017, 157,
- 258. Palumbo, R.; Diver, R. B.; Larson, C.; Coker, E. N.; Miller, J. E.; Guertin, J.; Schoer, J.; Meyer, M.; Siegel, N. P. Solar Thermal Decoupled Water Electrolysis Process I: Proof of Concept. Chem. Eng. Sci. 2012, 84, 372-380.
- 259. Nudehi, S.; Larson, C.; Prusinski, W.; Kotfer, D.; Otto, J.; Beyers, E.; Schoer, J.; Palumbo, R. Solar Thermal Decoupled Water Electrolysis Process II: An Extended Investigation of the Anodic Electrochemical Reaction. Chem. Eng. Sci. 2018, 181, 159-172.
- 260. Ma, Y.; Guo, Z.; Dong, X.; Wang, Y.; Xia, Y. Organic Proton-Buffer Electrode to Separate Hydrogen and Oxygen Evolution in Acid Water Electrolysis. Angew. Chemie Int. Ed. 2019, 58, 4622-4626.
- 261. Wang, J.; Ji, L.; Teng, X.; Liu, Y.; Guo, L.; Chen, Z. Decoupling Half-Reactions of Electrolytic Water Splitting by Integrating a Polyaniline Electrode. J. Mater. Chem. A 2019, 7, 13149-13153.
- 262. Chen, G.; Li, X.; Feng, X. Upgrading Organic Compounds through the Coupling of Electrooxidation with Hydrogen Evolution. Angew. Chemie - Int. Ed. 2022, 61; https://doi.org/10.1002/anie.202209014.
- 263. Xiang, K.; Wu, D.; Deng, X.; Li, M.; Chen, S.; Hao, P.; Guo, X.; Luo, J.-L.; Fu, X.-Z. Boosting H2 Generation Coupled with Selective Oxidation of Methanol into Value-Added Chemical over Cobalt Hydroxide@Hydroxysulfide Nanosheets Electrocatalysts. Adv. Funct. Mater. 2020, 30, 1909610.
- 264. Dai, L.; Qin, Q.; Zhao, X.; Xu, C.; Hu, C.; Mo, S.; Wang, Y. O.; Lin, S.; Tang, Z.; Zheng, N. Electrochemical Partial Reforming of Ethanol into Ethyl Acetate Using Ultrathin Co3O4 Nanosheets as a Highly Selective Anode Catalyst. ACS Cent. Sci. 2016, 2, 538–544.
- 265. Zhao, Y.; Xing, S.; Meng, X.; Zeng, J.; Yin, S.; Li, X.; Chen, Y. Ultrathin Rh Nanosheets as a Highly Efficient Bifunctional Electrocatalyst for Isopropanol-Assisted Overall Water Splitting. Nanoscale 2019, 11, 9319-9326.
- 266. Zheng, J.; Chen, X.; Zhong, X.; Li, S.; Liu, T.; Zhuang, G.; Li, X.; Deng, S.; Mei, D.; Wang, J.-G. Hierarchical Porous NC@CuCo Nitride Nanosheet

- Networks: Highly Efficient Bifunctional Electrocatalyst for Overall Water Splitting and Selective Electrooxidation of Benzyl Alcohol. Adv. Funct. Mater. 2017, 27, 1704169.
- 267. Cui, X.; Chen, M.; Xiong, R.; Sun, J.; Liu, X.; Geng, B. Ultrastable and Efficient H2 Production via Membrane-free Hybrid Water Electrolysis over a Bifunctional Catalyst of Hierarchical Mo-Ni Alloy Nanoparticles. J. Mater. Chem. A 2019, 7, 16501-16507.
- 268. Si, D.; Xiong, B.; Chen, L.; Shi, J. Highly Selective and Efficient Electrocatalytic Synthesis of Glycolic Acid in Coupling with Hydrogen Evolution. Chem Catal. 2021, 1, 941-955.
- 269. Yu, X.; dos Santos, E. C.; White, J.; Salazar-Alvarez, G.; Pettersson, L. G. M.; Cornell, A.; Johnsson, M. Electrocatalytic Glycerol Oxidation with Concurrent Hydrogen Evolution Utilizing an Efficient MoOx/Pt Catalyst. Small 2021, 17, 2104288.
- 270. Lin, C.; Zhang, P.; Wang, S.; Zhou, Q.; Na, B.; Li, H.; Tian, J.; Zhang, Y.; Deng, C.; Meng, L.; Wu, J.; Liu, C.; Hu, J.; Zhang, L. Engineered Porous Co-ni Alloy on Carbon Cloth as an Efficient Bifunctional Electrocatalyst for Glucose Electrolysis in Alkaline Environment. J. Alloys Compd. 2020, 823, 153784.
- 271. You, B.; Liu, X.; Jiang, N.; Sun, Y. A General Strategy for Decoupled Hydrogen Production from Water Splitting by Integrating Oxidative Biomass Valorization. J. Am. Chem. Soc. 2016, 138, 13639-13646.
- 272. Jiang, N.; Liu, X.; Dong, J.; You, B.; Liu, X.; Sun, Y. Electrocatalysis of Furfural Oxidation Coupled with H2 Evolution via Nickel-Based Electrocatalysts in Water. ChemNanoMat 2017, 3, 491-495.
- 273. Kubota, S. R.; Choi, K.-S. Electrochemical Valorization of Furfural to Maleic Acid. ACS Sustain. Chem. Eng. 2018, 6, 9596-9600.
- 274. Yang, G.; Jiao, Y.; Yan, H.; Xie, Y.; Wu, A.; Dong, X.; Guo, D.; Tian, C.; Fu, H. Interfacial Engineering of MoO2-FeP Heterojunction for Highly Efficient Hydrogen Evolution Coupled with Biomass Electrooxidation. Adv. Mater. 2020, 32, 2000455.
- 275. Gu, K.; Wang, D.; Xie, C.; Wang, T.; Huang, G.; Liu, Y.; Zou, Y.; Tao, L.; Wang, S. Defect-Rich High-Entropy Oxide Nanosheets for Efficient 5-Hydroxymethylfurfural Electrooxidation. Angew. Chemie Int. Ed. **2021**, 60, 20253-20258.
- 276. Wang, W.; Wang, Y.; Yang, R.; Wen, Q.; Liu, Y.; Jiang, Z.; Li, H.; Zhai, T. Vacancy-Rich Ni(OH)2 Drives the Electrooxidation of Amino C-N Bonds to Nitrile C≡N Bonds. Angew. Chemie Int. Ed. 2020, 59,
- 277. Chong, X.; Liu, C.; Wang, C.; Yang, R.; Zhang, B. Integrating Hydrogen Production and Transfer Hydrogenation with Selenite Promoted Electrooxidation of α-Nitrotoluenes to E-Nitroethenes. *Angew. Chemie* Int. Ed. 2021, 60, 22010-22016.
- 278. Huang, C.; Huang, Y.; Liu, C.; Yu, Y.; Zhang, B. Integrating Hydrogen Production with Aqueous Selective Semi-dehydrogenation of Tetrahydroisoguinolines over a Ni2P Bifunctional Electrode. Angew. Chemie Int. Ed. 2019, 58, 12014-12017.
- 279. Ma, L.; Zhou, H.; Xu, M.; Hao, P.; Kong, X.; Duan, H. Integrating Hydrogen Production with Anodic Selective Oxidation of Sulfides over a CoFe Layered Double Hydroxide Electrode. Chem. Sci. 2021, 12, 938-945.
- 280. Hu, K.; Xu, L.; Chen, W.; Jia, S.; Wang, W.; Han, F. Degradation of Organics Extracted from Dewatered Sludge by Alkaline Pretreatment in Microbial Electrolysis Cell. Environ. Sci. Pollut. Res. 2018, 25, 8715-8724.
- 281. Hasany, M.; Yaghmaei, S.; Mardanpour, M. M.; Ghasemi Naraghi, Z. Simultaneously Energy Production and Dairy Wastewater Treatment Using Bioelectrochemical Cells: In Different Environmental and Hydrodynamic Modes. Chinese J. Chem. Eng. 2017, 25, 1847–1855.

- 282. Jeremiasse, A. W.; Hamelers, H. V. M.; Saakes, M.; Buisman, C. J. N. Ni Foam Cathode Enables High Volumetric H2 Production in a Microbial Electrolysis Cell. Int. J. Hydrogen Energy 2010, 35, 12716-12723.
- 283. Cheng, S.; Logan, B. E. Sustainable and Efficient Biohydrogen Production via Electrohydrogenesis. Proc. Natl. Acad. Sci. 2007, 104,
- 284. Heidrich, E. S.; Dolfing, J.; Scott, K.; Edwards, S. R.; Jones, C.; Curtis, T. P. Production of Hydrogen from Domestic Wastewater in a Pilot-Scale Microbial Electrolysis Cell. Appl. Microbiol. Biotechnol. 2013, 97,
- 285. Lu, L.; Xing, D.; Xie, T.; Ren, N.; Logan, B. E. Hydrogen Production from Proteins via Electrohydrogenesis in Microbial Electrolysis Cells. Biosens. Bioelectron. 2010, 25, 2690-2695.
- 286. Rozendal, R. A.; Hamelers, H. V. M.; Euverink, G. J. W.; Metz, S. J.; Buisman, C. J. N. Principle and Perspectives of Hydrogen Production through Biocatalyzed Electrolysis. Int. J. Hydrogen Energy 2006, 31, 1632-1640.
- 287. Badia-Fabregat, M.; Rago, L.; Baeza, J. A.; Guisasola, A. Hydrogen Production from Crude Glycerol in an Alkaline Microbial Electrolysis Cell. Int. J. Hydrogen Energy 2019, 44, 17204-17213.
- 288. Zhang, L.; Wang, Y.-Z.; Zhao, T.; Xu, T. Hydrogen Production from Simultaneous Saccharification and Fermentation of Lignocellulosic Materials in a Dual-Chamber Microbial Electrolysis Cell. Int. J. Hydrogen Energy 2019, 44, 30024-30030.
- 289. Chen, J.; Xu, W.; Wu, X.; E, J.; Lu, N.; Wang, T.; Zuo, H. System Development and Environmental Performance Analysis of a Pilot Scale Microbial Electrolysis Cell for Hydrogen Production Using Urban Wastewater. Energy Convers. Manag. 2019, 193, 52-63.
- 290. N, S.; Spurgeon, J.; Matheswaran, M.; Satyavolu, J. Simultaneous Biohydrogen Production with Distillery Wastewater Treatment Using Modified Microbial Electrolysis Cell. Int. J. Hydrogen Energy 2020, 45, 18266-18274.
- 291. Hou, Y.; Zhang, R.; Yu, Z.; Huang, L.; Liu, Y.; Zhou, Z. Accelerated Azo Dye Degradation and Concurrent Hydrogen Production in the Single-Chamber Photocatalytic Microbial Electrolysis Cell. Bioresour. Technol. **2017**, *224*, 63-68.
- 292. Wan, L.-L.; Li, X.-J.; Zang, G.-L.; Wang, X.; Zhang, Y.-Y.; Zhou, Q.-X. A Solar Assisted Microbial Electrolysis Cell for Hydrogen Production Driven by a Microbial Fuel Cell. RSC Adv. 2015, 5, 82276-82281.
- 293. Yang, N.; Hafez, H.; Nakhla, G. Impact of Volatile Fatty Acids on Microbial Electrolysis Cell Performance. Bioresour. Technol. 2015, 193, 449-455.
- 294. Zhang, Y.; Angelidaki, I. Innovative Self-Powered Submersible Microbial Electrolysis Cell (SMEC) for Biohydrogen Production from Anaerobic Reactors. Water Res. 2012, 46, 2727-2736.

- 295. Asztalos, J. R.; Kim, Y. Enhanced Digestion of Waste Activated Sludge Using Microbial Electrolysis Cells at Ambient Temperature. Water Res. **2015**, *87*, 503-512.
- 296. Wang, A.; Sun, D.; Cao, G.; Wang, H.; Ren, N.; Wu, W.-M.; Logan, B. E. Integrated Hydrogen Production Process from Cellulose by Combining Dark Fermentation, Microbial Fuel Cells, and a Microbial Electrolysis Cell. Bioresour. Technol. 2011, 102, 4137-4143.
- 297. Li. X.-H.: Liang, D.-W.: Bai, Y.-X.: Fan, Y.-T.: Hou, H.-W. Enhanced H2 Production from Corn Stalk by Integrating Dark Fermentation and Single Chamber Microbial Electrolysis Cells with Double Anode Arrangement. Int. J. Hydrogen Energy 2014, 39, 8977-8982.
- 298. Zhen, G.; Kobayashi, T.; Lu, X.; Kumar, G.; Hu, Y.; Bakonyi, P.; Rózsenberszki, T.; Koók, L.; Nemestóthy, N.; Bélafi-Bakó, K.; Xu, K. Recovery of Biohydrogen in a Single-Chamber Microbial Electrohydrogenesis Cell Using Liquid Fraction of Pressed Municipal Solid Waste (LPW) as Substrate. Int. J. Hydrogen Energy 2016, 41, 17896-17906.
- 299. Jayabalan, T.; Matheswaran, M.; Naina Mohammed, S. Biohydrogen Production from Sugar Industry Effluents Using Nickel Based Electrode Materials in Microbial Electrolysis Cell. Int. J. Hydrogen Energy 2019, 44, 17381-17388.
- 300. Gunasekaran, M.; Merrylin, J.; Usman, T. M. M.; Kumar, G.; Kim, S.-H.; Banu, J. R. Chapter 30 - Biohydrogen Production from Industrial Wastewater. In Biomass, Biofuels, Biochemicals; Pandey, A.; Larroche, C.; Dussap, C.-G.; Gnansounou, E.; Khanal, S.K.; Ricke, S.B.T.-B.A.F.; C.P. for the P. of L. and G.B., Eds., 2nd ed.; Academic Press: USA, 2019; pp 733-760.
- 301. Lu, L.; Ren, N.; Xing, D.; Logan, B. E. Hydrogen Production with Effluent from an Ethanol-H2-Coproducing Fermentation Reactor Using a Single-Chamber Microbial Electrolysis Cell. Biosens. Bioelectron. 2009, 24, 3055-3060.
- 302. Cucu, A.; Costache, T. A.; Divona, M.; Tiliakos, A.; Stamatin, I.; Ciocanea, A. Microbial Electrolysis Cell: Hydrogen Production Using Microbial Consortia from Romanian Waters. Dig. J. Nanomater. Biostruct. 2013, 8, 1179-1190.
- 303. Croese, E.: Jeremiasse, A. W.: Marshall, I. P. G.: Spormann, A. M.: Euverink, G.-J. W.; Geelhoed, J. S.; Stams, A. J. M.; Plugge, C. M. Influence of Setup and Carbon Source on the Bacterial Community of Biocathodes in Microbial Electrolysis Cells. Enzym. Microb. Technol. **2014**, *61-62*, 67-75.
- 304. Yang, Q.; Jiang, Y.; Xu, Y.; Qiu, Y.; Chen, Y.; Zhu, S.; Shen, S. Hydrogen Production with Polyaniline/Multi-Walled Carbon Nanotube Cathode Catalysts in Microbial Electrolysis Cells. J. Chem. Technol. Biotechnol. 2015, 90, 1263-1269.
- 305. Matsushima, H.; Nishida, T.; Konishi, Y.; Fukunaka, Y.; Ito, Y.; Kuribayashi, K. Water Electrolysis under Microgravity: Part 1. Experimental Technique. Electrochim. Acta 2003, 48, 4119-4125.